CHARACTERIZATION OF THE INTERACTIONS OF THE *DICTYOSTELIUM* 34 KDA ACTIN-BUNDLING PROTEIN WITH ACTIN FILAMENTS AND THE REQUIREMENTS FOR FORMATION OF HIRANO BODIES

by

PAUL ANDREW GRIFFIN

(Under the Direction of Marcus Fechheimer)

ABSTRACT

Hirano bodies are intracytoplasmic structures that are characterized by the presence of paracrystalline arrays of actin filaments. Hirano bodies have been found to be associated with a variety of neurodegenerative diseases; however, most of what is known about Hirano bodies has come from studies using autopsy derived tissue samples. Therefore little is known about the formation of Hirano bodies and their relationship to disease. Recently, a Hirano body cell model system has been developed based on expression of altered forms of the *Dictyostelium* 34 kDa actin-bundling protein. The goals of the studies presented in my dissertation were to: (1) determine the biochemical and structural features required for Hirano body formation; and (2) identify the important intermolecular interactions between 34 kDa protein and actin. In the first study presented, I used F-actin cosedimentation assays to characterize a novel, mutant form of 34 kDa protein, E60K, and I showed that it had calcium-sensitive but activated actin binding. I also showed that E60K protein was able to crosslink and bundle actin filaments *in vitro*. Furthermore, *in vivo* expression of E60K protein in *Dictyostelium* cells resulted in the formation of Hirano bodies. Lastly, I used the F-actin depolymerizing drug, latrunculin B and

demonstrated that actin filaments within the Hirano bodies were resistant to depolymerization. In the second study presented here, I used chemical crosslinking and mass spectrometry to identify the intermolecular interactions involved at the 34 kDa protein-F-actin binding interface. My results show that the full length 34 kDa protein contacts actin at sites within all three previously described actin binding regions (residues 1-123, 193-254, and 279-295). I also identified two distinct 34 kDa protein binding sites on F-actin and show that each of these sites are comprised of at least two actin subunits. Based on the results of my studies, I hypothesize that the formation of Hirano bodies requires both actin filament stabilization and crosslinking of actin filaments into ordered arrays.

INDEX WORDS: Hirano body, 34 kDa actin-bundling protein, crosslinking protein, Actin, chemical crosslinking, mass spectrometry, latrunculin B, F-actin, *Dictyostelium*, point mutation.

CHARACTERIZATION OF THE INTERACTIONS OF THE *DICTYOSTELIUM* 34 KDA ACTIN-BUNDLING PROTEIN WITH ACTIN FILAMENTS AND THE REQUIREMENTS FOR THE FORMATION OF HIRANO BODIES

by

PAUL ANDREW GRIFFIN

B.S., Northern Kentucky University, 1995

A Dissertation Submitted to the Graduate Faculty of The University of Georgia in Partial Fulfillment of the Requirements for the Degree

DOCTOR OF PHILOSOPHY

ATHENS, GEORGIA

2010

CHARACTERIZATION OF THE INTERACTIONS OF THE *DICTYOSTELIUM* 34 KDA ACTIN-BUNDLING PROTEIN WITH ACTIN FILAMENTS AND THE REQUIREMENTS FOR THE FORMATION OF HIRANO BODIES

by

PAUL ANDREW GRIFFIN

Major Professor:	Marcus Fechheimer
Committee:	Claiborne C. V. Glover Edward T. Kipreos Scott T. Dougan

Electronic Version Approved:
Maureen Grasso
Dean of the Graduate School
The University of Georgia
May 2010

DEDICATION

I would like to dedicate my dissertation to my family. The support and encouragement they have given me over the years was invaluable to the completion of my graduate degree. Mom, Dad, Angie, Abbey and Jake…I could not have done this without you all!

I also dedicate this dissertation to my puppies, Nico Donna and Phoebe and to the memory of my bulldog, Rage (1995-2007).

ACKNOWLEDGEMENTS

Wow! Where does one start? I have to start with my Mom and Dad who have been an unbelievable support system for me. They never gave up on me and never told me that I couldn't chase my dreams. I also want to mention my major professor, Dr. Fechheimer, whose patient guidance over the years has helped me to mature into a question driven scientist. Dr. Ruth Furukawa who has been a research mentor, personal advisor, and most importantly a source of comic relief! Of course I can't forget the constructive help I received from my committee members: Dr. Claiborne C. V. Glover, Dr. Edward T. Kipreos, and Dr. Scott T. Dougan. I would like "Thank" Dr. Jon Amster and Lisabeth Hoffman for a productive collaboration. Dr. John Shields for all of his help with everything microscopic and my friend and fellow guitar player, Ryan Brown for everything melodic!

I would like to say "Thanks" to all of my labmates that have helped me along the way, Dr. Dorota Wloga, Dr. Richard Davis, Dr. Sangdeuk Ha, Caelin Cubanas, Cleveland Piggott and Nisha Gupta. Last but not least, I would like to "Thank" an old friend of my mine from my music playing, long hair days, Mr. Ted Brasier! Ted, through your music and lyrics, you taught me to "NEVER GIVE UP" and to always be a "Warrior"…again, "Thanks, Ted…I am a warrior!"

TABLE OF CONTENTS

LIST OF TABLES

Page

LIST OF FIGURES

Page

Chapter 1

INTRODUCTION AND LITERATURE REVIEW

Actin and the cytoskeleton

Actin is an ancient and highly conserved protein that is found in almost all eukaryotic cells. Monomeric actin (G-actin) is assembled into long helical filaments (F-actin) and is the major component of the actin cytoskeleton. The actin cytoskeleton is a dynamic structure that is involved in many different cellular functions such as cell motility, muscle contraction, intracellular transport, cell adhesion, and morphogenesis. The functional roles of actin are dependent on a large number of actin binding proteins that regulate the assembly and disassembly of actin filaments and their combination to form larger subcellular structures (Pollard 2000; dos Remedios 2003; Pollard 2003).

G-actin structure

G-actin is a globular protein composed of 375 amino acids corresponding to a molecular weight of roughly 42 kDa. Mammals express 6 different isoforms of actin: two saromeric (α-skeletal and α-cardiac), two smooth muscle (α and γ), and two cytoskeletal (β and γ). *In vivo*, G-actin contains at least one bound Mg^{2+} ion complexed to either ADP or ATP. Low resolution crystal structures of G-actin suggested that it was "pear-shaped" and comprised of a small domain and a large domain that were separated by a large central "cleft" (Aebi 1981; Curmi 1984). In 1990, Kabsch *et al.* co-crystallized G-actin complexed to DNAse I to obtain the first

atomic resolution structures for ATP- and ADP-G-actin (2.8 Å and 3.0 Å respectively) (Kabsch 1990). X-ray analysis of resulting crystals revealed the presence and position of the "large" and "small" domains, and that the NH_2 and COOH termini were located in close proximity within the small domain. The large domain (residues 145-337) and small domain (residues 1-144 and 338-375) can be further divided into 4 quasi-subdomains (referred to as subdomains 1-4) that share a common repeating structural motif consisting of a multi-strand β-sheet followed by a β-meander and a right-handed β-α-β unit. The large domain is divided into subdomain 3 (residues 145-180 and 270-337) and subdomain 4 (residues 181-269), while the small domain is divided into subdomain 1 (residues 1-32, 70-144, and 338-375) and subdomain 2 (residues 33-69) (Fig. 1.1).

The major contact site of DNAse I binding to G-actin involves a loop comprised of residues 39-50 and Lys61-Ile62 in subdomain 2. Additionally, DNAse I makes some minor contacts involving residues Thr203 and Glu207 within subdomain 4. The carboxyl and amino termini of G-actin are located in subdomain 1.

The Ca^{++} complexed ATP (or ADP) binding site lies in a cleft formed between subdomains 2 and 4. The divalent cation is contained in a hydrophilic pocket that is blocked at the "top" by the di- or tri-phosphate moiety of the nucleotide. The divalent cation is held in the "pocket" through electrostatic interactions involving the charged residues Asp11, Asp154, and Lys18, while Gln137 is contained within the α-helix that links the two subdomains. In the ATP-bound actin monomer, the β-phosphate is bound in a β bend formed by residues Ser14, Gly15, and Leu16 while the γ-phosphate is bound to a subsequent β bend comprised of residues Asp157, Gly158, and Val159. An additional interaction observed in both ADP- and ATP-G-actin forms involves contact of Lys18 with α- and β-phosphate motieties. A hydrophobic pocket formed between subdomains 3 and 4 is the site of adenine binding and involves residues 302-308

(subdomain 3) and residues Lys213 and Glu214 (subdomain 4). Residues 302-308 form the "floor" of the pocket and are contained within a turn that links the second strand of the β-sheet (Asn297-Ser300) to the α-helix 309-320. The upper portion of the hydrophobic pocket is formed by the hydrophobic chain of Glu214 (which is held in place by a salt bridge with Arg210 and a hydrogen bond to the 2'OH group of ribose) and Lys213 (which is held in place by a hydrogen bond to the carbonyl group of Gly182). Finally, the aromatic ring of Tyr306 forms the "back" of the pocket.

Another notable structural feature of G-actin is the presence of two crossover regions allowing the polypeptide chain to cross from small domain to large domain and back. The crossover regions are located around residues 137-144 and residues 336-339 suggesting the possibility of a "hinge" that may allow for conformational change between the two domains. Significantly, the nucleotide binding pocket is also located in this region lying between the two domains.

Since Kabsch *et al.* first described their DNAse I:actin co-crystals, there have been over 30 G-actin crystals described (Aguda 2005). Most of the efforts in obtaining G-actin crystals contain ADP-G-actin. The ADP-G-actin is the form of actin that is found in the actin filament and is hypothesized to be conformationally different than the ATP-G-actin form. The possibility of different conformational states is supported by the finding that ATP hydrolysis occurs after a monomer is incorporated into a filament, and that some actin binding proteins have greater binding affinities for either ATP-G-actin or ADP-G-actin. In addition, differences in the conformational states of ADP and ATP-G-actin are supported by *in vitro* solution studies (Dominguez 2003). Two different models have been proposed based on crystallographic data. The first model involves the "opening" and "closing" of the nucleotide cleft located between

subdomains 2 and 4. In 1996 Chik *et al.* co-crystallized an ADP-G-actin:profilin complex that had the nucleotide binding cleft in the "open" position (Chik 1996). Since all ATP-G-actin crystal structures are in the "closed" state, this lead Sablin *et al.* to propose a model in which ATP hydrolysis after polymerization induces a conformational change that leads to the opening of the nucleotide cleft thus enabling the release of inorganic phosphate (Pi) (Sablin 2002). The second model proposed that the conformational change induced by ATP hydrolysis involved the DNAse I binding loop (D-loop). In 2001, Otterbein *et al.* crystallized an uncomplexed form of ADP-G-actin by labeling G-actin with tetramethylrhodamine (TMR) which prevents G-actin polymerization (Otterbein 2001). Consistent with all other G-actin crystal structures except for the actin:profilin complex (Chik 1996), the ADP bound TMR-actin structure has a "closed" nucleotide cleft but shows a significant "loop-to-helix" transition within the D-loop. Subsequent crystallization of AMPNP-TMR-actin-AMPNP (Graceffa 2003) further supported their model that ATP hydrolysis induces a "loop-to-helix" transition in D-loop of subdomain 2, moving it away from the ATP and allowing release of Pi (Otterbein 2001).

Recently, Rould *et al.* obtained crystals of both ADP and ATP states of monomeric actin using a non-polymerizable actin (Rould 2006). The actin (AP-actin) they used was rendered non-polymerizable by two point mutations within subdomain 4 (A204E/P243K). The ADP bound AP-actin crystal structure also had the nucleotide binding cleft in the "closed" state, but significantly, it showed *no* "loop-to-helix" transitional change in the D-loop as was observed in the ADP bound TMR-actin structure. The structural plasticity of the D-loop from numerous crystal structures makes it difficult to interpret a functional role. For example, D-loop structure has been characterized as either disordered loop (actin:profilin (Schutt 1993) or AP-actin (Rould 2006)), β-sheet (actin:DNAse I (Kabsch 1990)), or α-helix (TMR-actin actin:gelsolin

(McLaughlin 1993; Robinson 1999; Otterbein 2001). However, probably the most important point to be taken from the different actin crystal structures is that all of them represent unpolymerized forms of G-actin, and therefore it is possible that the true state of the nucleotide binding cleft and the D-loop conformation can only be observed within the context of the actin filament.

Actin filament structure

F-actin appears as a two-stranded, right-handed helical polymer with a diameter of 90-95 Å. For each strand along the length of the filament axis there are 13 actin subunits per 6 left-handed turns that repeat every 36 nm. The rotational displacement of successive subunits is 166^{o}, and the axial rise is ~ 27 Å.

The first atomic structural model of F-actin was constructed to about 8 Å resolution by fitting the crystal structure of actin into the filament axis derived from x-ray fiber diffraction patterns of highly oriented F-actin gels (Holmes 1990) (Fig. 1.2). In 1993, the "Holmes Model" was further refined by Lorenz *et al.* using a method known as "directed mutation algorithm" (Lorenz 1993). The refined Holmes Model showed that individual subunits contained within the filament are aligned tangentially to the filament axis. The large domain (subdomains 3 and 4) is at a small radius from the filament axis, and the small domain (subdomains 1 and 2) is at a large radius from the filament axis. Intermolecular contacts between actin subunits are extensive, with each actin subunit in contact with four other subunits within the filament. Fitting the G-actin crystal structure into the filament necessitated only two significant structural changes. However, the sites of the changes did appear important because they were found to be important interaction sites of subunits. One of the changes involved repositioning of the D-loop (residues 40-49)

which was in contact with DNAse I in the actin crystals. When the D-loop was extended to fit into the filament, it made contact with the surface area of the subunit above implicating its importance as an intrastrand contact. The major site of change involved an extension of a hydrophobic "finger-like" projection (residues 264-273) inserted (plugged) into a hydrophobic pocket formed by contacts with helix residues 41-45 and 63-64 of the lower subunit and residues 166, 169, 171, 173, 285, and 289 of the upper subunit.

Recently, a higher resolution F-actin structure was reported using a high magnetic field to orient F-actin gels to obtain a fiber diffraction data to 3.3 Å in the radial and 5.6 Å in the equatorial direction (Oda 2009). The higher resolution F-actin structure revealed many significant structural details. In their model, the G- to F-actin transition induces a ~ 20^{o} relative rotation between the large (inner) and small (outer) domains and a re-orientation of the D-loop (residues 38-49). The rotation between domains is accomplished through dihedral angle rotations of residues 141-142 and 336-337. Significantly, the rotation of the inner and outer domains they observed did not affect the nucleotide binding cleft which remained in the "closed" position. The G- to F-actin "flattening" of the actin causes changes in the intramolecular interactions in the loops that link the inner and outer domains (residues 71-73 "sensor loop" and 108-111). The induced conformational changes within the actin molecule upon polymerization enable it to make extensive contacts with other subunits within the filament. The intrastrand contacts occur primarily between a projection of the upper subunit (residues 283-294) and residues 61-65, 200-208, and 241-247 of the lower subunit.

Interstrand interactions result from two major projections from subdomain 4. The first site of interaction occurs between the α-helix (residues 191-199) of one subunit with the α-helix (residues 110-115) of the subunit in the opposite strand. The second site of interaction involves

the "hydrophobic plug" projection which makes four contacts on three actin monomers and therefore mediates both interstrand and intrastrand contacts. The major sites of interaction occur between the hydrophobic plug (residues 265-271) of one subunit with residues 201-203 and 39-42 of the adjacent lower subunit in the opposite strand and residues 170-174 and 285-286 of the upper subunit in the opposite strand.

It is important to note that the higher resolution F-actin structure identifies a structural feature that may potentially be involved in ATP hydrolysis. *In vitro* studies of human cardiac α-actin mutants have suggested the importance of residue Gln137, which is located deep within the nucleotide binding pocket (Iwasa 2008). In ATP-G-actin crystals, Gln137 is located within the nucleotide binding cleft where it anchors a water molecule that is near the γ-phosphate of the bound ATP. In the Oda F-actin model, domain rotations induced by the "flattening" of the newly polymerized actin molecule reposition Gln137 closer to the γ-phosphate (~4 Å), which may then initiate the hydrolysis of ATP (Oda 2009)

In the Oda F-actin model, the nucleotide binding cleft was found to be in the "closed" state, and the authors describe a new "flat" conformation for G-actin that they believe is associated with polymerization and ATP hydrolysis (Oda 2009). However, even with this new high resolution structure, it is important to remember that data derived from actin crystals, fiber diffraction patterns, and cryo-electron microscopy all represent a static state. The dynamic state of F-actin has been observed in numerous studies (Reisler 2007). In 1982 Egelman *et al.* observed that the axial rise of subunits is relatively fixed (~27 Å) but that relative rotational variability between the subunits is observed (Egelman 1982). Many factors can influence the actin filament, most notably the ligands and actin binding proteins that are bound to it. For example, phalloidin (De La Cruz 1994; De La Cruz 1996), scruin (Schmid 2004), and cofilin

(McGough 1997) all have been shown to affect both the rotation and tilt of subunits within the actin filament. The functional significance(s) of these different F-actin states remains somewhat controversial; however, in one case it has been shown to be important in F-actin depolymerization induced by cofilin (Galkin 2003).

Filament dynamics

Under physiological conditions *in vitro* ATP-G-actin spontaneously polymerizes into a filament. After incorporation into the filament, the ATP is rapidly hydrolyzed to ADP-Pi-actin while the subsequent release of Pi to ADP-actin occurs much more slowly. Additionally, while in the filament, ADP cannot be exchanged for ATP (Carlier 1989). Thus, the net result of polymerization coupled to ATP hydrolysis creates a nonequilibrium polymer that has both structural and functional polarity. The structural polarity of F-actin is also the consequence of the polarity of the actin monomer. All actin subunits in an actin filament are arranged with their nucleotide binding cleft oriented in one direction along the filament axis. This structural polarity of the actin filament was first demonstrated through decoration experiments using the S1 head fragment of myosin II. Examination by transmission electron microscopy of negatively stained S1-decorated F-actin revealed that S1 bound to F-actin in regular orientation producing a series of arrowhead-like projections; and based on this observation, the two ends of the actin filaments were differentiated as "pointed" and "barbed" corresponding to the directionality of the S1 arrowhead projections (Nachmias 1970). *In vitro* studies of the F-actin also showed that polymerization proceeds primarily by addition of ATP-G-actin at the barbed end (Nachmias 1970), while depolymerization occurs primarily by the loss of ADP-G-actin at the pointed end (Wegner 1982; Carlier 1991). Subsequent biochemical analysis was used to measure the rate of

actin polymerization for both ends of the filament and revealed that the rate of ATP-G-actin addition was greater for the barbed end than the pointed end. Furthermore, the rate of subunit addition to either end was dependent on the concentration of ATP-G-actin (Pollard 1986). The minimum concentration of ATP-G-actin (or critical concentration, C_C) required for addition to the barbed and pointed ends were determined to be 0.12 μM and 0.6 μM respectively (Wegner 1983). An important functional property of actin polymerization is the ability of the filaments to reach a "steady state" in which the rate of subunit addition at the barbed end is equal to the rate of subunit dissociation at the pointed end. At steady state, an actin filament undergoes a process called "treadmilling" (Wegner 1976). Treadmilling occurs when the ATP-G-actin concentration is below the C_c for the pointed end but above the C_c for the barbed end resulting in the rate of addition of ATP-G-actin to the barbed end balanced by the dissociation rate of ADP-G-actin from the pointed end (Wegner 1976). Significantly, during treadmilling the filament has polarity with respect to the state of the bound nucleotide of actin because newly polymerizing actin subunits at the barbed end are ATP-G-actin, "older" actin subunits within the filament are mostly ADP-Pi-actin, and finally the actin subunits depolymerizing from the pointed end are ADP-G-actin. Treadmilling *in vivo* enables actin filaments to provide the force necessary to drive cellular processes such as locomotion, intracellular transport, and cell morphology (Pollard 2000).

Actin-binding proteins

A recent review by dos Remedios *et al.* cataloged over 160 separate proteins (excluding synonyms and isoforms) that bind to actin (dos Remedios 2003). Classification of actin-binding proteins (ABPs) is complicated by the numerous cellular roles in which actin is involved.

However, ABPs that are involved in the assembly and disassembly of actin filaments can be classified loosely into 8 major groups (Table 1.1). It is important to note that many of these proteins are not exclusive to one group and may have multiple functional roles.

Actin monomer-binding proteins

Actin monomer-binding proteins function primarily to maintain a pool of unpolymerized G-actin that is readily available for spontaneous filament assembly. Profilin and thymosin-β4 are two common examples of monomer-sequestering proteins (Paavilainen 2004). Thymosin-β4 is the major G-actin sequestering protein found in most eukaryotic non-muscle cells (Safer 1994) and is responsible for the maintenance high concentrations of ATP-G-actin (De La Cruz 2000). Profilin is a small (~15 kDa) protein found in all eukaryotic cells. Profilin binds to both ADP- and ATP-forms of monomeric actin but has a much greater affinity for ATP-G-actin (K_d = 0.1 μM) than ADP-G-actin (K_d = 0.5 μM) (Pollard 2000). Profilin plays a key role in the regulation of actin filament dynamics. One role profilin plays is to "recharge" ADP-G-actin depolymerized from the (-) ends of actin filament by catalyzing the ADP to ATP nucleotide exchange (Goldschmidt-Clermont 1992; Pantaloni 1993). Profilin's other role involves its ability to function as an actin monomer-sequestering protein. In this role, profilin can both inhibit and promote filament assembly depending on the availability of free (+) ends of actin filaments. These seemingly contradictory roles result from the fact that profilin binds at the barbed end of G-actin, thereby inhibiting the ability of G-actin to associate with the (-) end of an actin filament. However, if free (+) ends are available, profilin can increase the rate of filament elongation by providing a "recharged" ATP-G-actin (Pollard 2000; Paavilainen 2004). Lastly, another example of an actin monomer-binding protein is the Srv2/cyclase-associated protein (CAP) family (Paavilainen 2004). Srv2/CAP function is distinct from thymosin-β4 and profilin in that

it promotes filament turnover by binding to recently depolymerized ADF/cofilin-bound actin monomers and re-cycling ADF/cofilin from the actin monomer (Balcer 2003; Bertling 2004).

Filament-depolymerizing proteins

Filament-depolymerizing proteins are important in actin filament dynamics because they can increase filament turnover by accelerating the rate of actin dissociation from the ends (Lappalainen 1997). The best characterized member of this family is ADF/cofilin (Bamburg 1999). ADF/cofilin is able to increase the pointed end dissociation rate 25-fold relative to that observed for purified "treadmilling" actin filaments *in vitro* (Carlier 1997). The mechanism by which ADF/cofilin accelerates subunit dissociation is believed to be the result of a cofilin-induced "twist" in F-actin that could potentially lead to a decrease in the thermodynamic stability of the actin filament (McGough 1997). Although, ADF/cofilin is also able to sever actin filaments, its primary cellular role is believed to be in increasing actin filament turnover by promoting filament depolymerization. Notably, a recent report questions the direct effect of cofilin on the rate constant for dissociation at the minus end and explains the ability of cofilin to speed disassembly as a secondary effect of severing (Andrianantoandro 2006).

Filament-severing proteins

Proteins that sever actin filaments are important in actin filament nucleation. They aid in the creation of new filament nucleation sites by severing pre-existing actin filaments and generating free barbed ends that are available for polymerization. In most eukaryotic cells, the severing of actin filaments is accomplished by gelsolin. In the presence of micromolar Ca^{++}, gelsolin is activated and severs an actin filament, remaining bound to the barbed end (capping) (Kwiatkowski 1999). Rac induced PiP_2 binding to gelsolin, releases it from the barbed end, and leaves the barbed end free for polymerization (Sun 1999). Gelsolin barbed end capping and

severing of actin filaments at the leading edge may also contribute to the generation of actin polymerization-dependent protrusive force in motile cells (Pollard 2000).

Filament-capping proteins

Filament-capping proteins are distinctive from the gelsolin superfamily of proteins in that they "cap" but do not sever actin filaments. Consequently, they do not function as a filament-nucleating protein but instead function in prevention of spontaneous polymerization and filament aging (Wear 2004). The major class of capping proteins is contained in the Capping Protein family which includes Capping Protein (CP), a heterodimeric protein (α- and β-) that binds and caps the barbed end of actin filaments with high affinity and thus prevents both the addition and loss of actin subunits (Cooper 2000). The specialized muscle isoform of CP, CapZ, is responsible for anchoring the filament end in the muscle Z line and preventing polymerization into the neighboring sacromere (Schafer 1995; Papa 1999). Non-muscle CP plays an important part in the dendritic nucleation model that has been recently proposed to account for the protrusive force generated by actin polymerization at the leading edge of the dendrite (Pollard 2003). In this model, CP in the presence of "activated" Arp2/3 complex, increases the amount of filament branching and keeps filaments short by capping longer or "older" filaments (Blanchoin 2000; Pollard 2003).

De novo filament-nucleating proteins

The rate limiting step in the polymerization of actin filaments is nucleation. Polymerization of actin filaments can be nucleated either from pre-existing filaments (via severing and/or uncapping) or *de novo*. Two types of *de novo* filament nucleators are found in most eukaryotic cells, and they function to create two different structural forms of actin filaments. The simplest structural form of actin filaments are long, unbranched filaments. The

protein responsible for the *de novo* formation of unbranched filaments is formin (Pruyne 2002; Sagot 2002). The filaments nucleated by formin are found in contractile rings, stress fibers, and actin bundles (Goode 2007). The other structural form of actin filaments are short, branched filaments that are most commonly observed at the leading edge of motile cells. The Arp2/3 complex is responsible for the nucleation and formation of short, branched actin filaments at the leading edge (Zigmond 1998). The Arp2/3 complex is composed of two actin-related proteins and five novel proteins (Machesky 1994; Mullins 1997). The Arp2/3 complex caps the pointed ends of filaments and nucleates the formation of 70^{o} branches in the barbed end direction (Mullins 1998). The 70^{o} branches nucleated by the Arp2/3 complex are consistent with the filament branch angle observed at the leading edge of fish keratocytes (Svitkina 1997) where the Arp2/3 complex has been localized to branch points (Svitkina 1999).

Filament-stabilizing proteins

The most common filament stabilizing proteins are the tropomyosin family of proteins (Gunning 2005; Kostyukova 2008). Tropomyosins are long α-helical coiled-coil proteins that bind along the length of an actin filament and provide structural stabilization to the filament. In muscle cells, tropomyosin stabilizes the thin filament ensuring the structural integrity of the thin filament. In non-muscle cells, tropomyosin binds to actin filaments and can block or "protect" filament depolymerization by ADF/cofilin (Bernstein 1982; Ono 2002). Additionally, tropomyosin may also block Arp2/3-mediated branching thus preventing new polymerization on existing filaments (Blanchoin 2001).

Motor proteins

Myosin motor proteins are a major group of actin-binding proteins that bind to F-actin and use the energy of ATP hydrolysis to translocate along the axis of an actin filament, produce

force, or maintain tension. Currently, the Myosin Superfamily of proteins is made up of 23 classes and with the exception of myosin VI are all (+) end-directed motors (Foth 2006). The first myosin identified was myosin II which was purified from skeletal muscle (Sellers 2000). Myosin II is a hexameric protein comprised of two heavy chains and two pairs of light chains. The amino-terminal portion of the heavy chain (also referred to as the "head") is the motor domain and contains both the F-actin-binding and catalytic ATPase sites. Myosin II is a "two-headed" myosin held together through the dimerization of the α-helical, coiled-coil rod domain from each of the heavy chains (Sellers 2000). In muscle cells, myosin II is responsible for force generation in muscle contraction, but myosin II is also found in non-muscle cells where its primary function is to provide contractile force for such processes as cytokinesis and contractile rings (Kalhammer 2000; Sellers 2000). The remaining classes of myosins are single-headed motors that perform a wide variety of cellular functions including organelle transport, attachment of cortical actin filaments to the membrane, and endocytosis (Mermall 1998; Kalhammer 2000). The only (-) end-directed myosin is myosin VI, which is responsible for the pointed-end movement of endocytotic vesicles (Kellerman 1992; Hasson 1994) and important in early development (Mermall 1995).

Filament-crosslinking/bundling proteins

The filament-crosslinking proteins are an important group of proteins because they are responsible for the assembly of actin filaments into organized cellular structures. Crosslinking proteins can crosslink actin filaments into meshworks or into highly ordered arrays called bundles (Furukawa 1997). Proteins that crosslink actin filaments are characterized by the requirement of at least two F-actin binding sites that bind simultaneously to two adjacent filaments, and as a general rule a large spatial separation between F-actin binding sites is

characteristic of proteins that crosslink actin filaments while closely spaced F-actin binding sites are common for bundling proteins (Puius 1998). The best characterized family of actin crosslinking proteins is found in the Calponin Homology (CH) domain family of proteins (Gimona 2002). The smallest and simplest CH protein is fimbrin, which is monomeric and has two actin binding sites along the length of its polypeptide chain. Because of its small size, fimbrin cross-links actin filaments into bundles and is localized to filopodia and microvilli (Hartwig 1995). Another example of a CH protein is α-actinin which cross-links and bundles actin filaments in both stress fibers and filopodia (Broderick 2005; Sjöblom 2008). Unlike fimbrin, α-actinin is a homodimer and has one only F-actin binding site per polypeptide chain; therefore, the dimerization of α-actinin is necessary for its cross-linking ability. It is important to note that not all crosslinking proteins are CH proteins. For example, ABP-34 or 34 kDa actin-bundling protein, is an F-actin crosslinking protein found in *Dictyostelium* (Fechheimer 1984; Fechheimer 1987). Interestingly, even though the 34 kDa protein shows no homology to the CH proteins, it does co-localize with α-actinin in filopodia (Fechheimer 1994).

Modular organization of F-actin-binding proteins

Cells have the ability to organize actin filaments into complex macrostructures that are important for cell shape, motility, cell division, and signaling. Actin filaments are organized into higher ordered structures through proteins that are able to crosslink actin filaments. Crosslinking proteins can organize actin filaments into actin gels (meshworks) and highly ordered filament arrays (bundles). Proteins that crosslink and/or bundle actin filaments contain a distinct modular organization that enables them to interact with two separate filaments at the same time. The basic modular organization for an actin crosslinking protein requires a minimum of two distinct

actin binding sites that are separated from each other by a "spacer" region (Matsudaira 1991; Puius 1998). In general, cross-linkers with "long" spacer regions organize actin filaments into meshworks while cross-linkers with "short" spacer regions pack filaments into tight bundles. However, it is important to point out that the length of a spacer region is not the sole determinant of a crosslinker's ability to form meshworks or bundles. Bundle formation can be induced by a high crosslinker:actin filament concentration, as has been demonstrated for filamin, which has a long, flexible spacer region and is normally found in meshworks at the leading edge (Cortese 1990; Hou 1990).

Although several distinct filament-binding motifs have been described (Sjöblom 2008), the best characterized examples of the different F-actin-binding modular arrangements is exhibited by the members of the Calponin Homology (CH) domain proteins (Gimona 2002). Several F-actin crosslinking, bundling, and binding proteins are CH domain proteins such as the spectrin superfamily of proteins (spectrin, α-actinin, dystrophin/utrophin), fimbrin, and filamin (Gimona 2002; Korenbaum 2002). All of these proteins have an actin-binding domain (ABD) module that is composed of two tandem CH domains that span approximately 250 amino acids (Gimona 2002; Sjöblom 2008). CH domain F-actin-crosslinking proteins can be divided into three subclasses based on the structural motif that is responsible for the spatial placement of their ABDs. The first subclass, which includes fimbrin (L-plastin in humans), has the simplest modular arrangement with two ABDs tandemly arranged along a single polypeptide chain. This ABD module arrangement enables fimbrin to form closely packed F-actin bundles. The second subclass is the spectrin superfamily of proteins which use variable numbers of spectrin repeats (a three helix coiled-coil motif) to form dimers and tetramers enabling them to bundle or cross-link actin filaments. The simplest member of this subclass is α-actinin. α-actinin is a homodimer

with one ABD on each polypeptide chain. The two polypeptide chains that make up α-actinin are aligned parallel in a "head-to-tail" arrangement so that one ABD of each chain is at either end, separated from each other by a dimerization interface formed by the spectrin repeats. The last subclass is characterized by the presence of an immunoglobulin-like fold formed from an antiparallel seven-stranded β-barrel structural motif at the dimerization interface and includes filamins and actin-binding protein 120 (ABP-120). Filamins are homodimers and are typified by the prototypical filamin found in *Dictyostelium discoideum* (ddFLN) . The ddFLN modular arrangement of each polypeptide chain is comprised of one ABD and a rod segment composed of six repeats with the last repeat responsible for dimerization (Popowicz 2006).

In addition to sharing a basic modular arrangement, another structural feature inherent to all F-actin-binding proteins known to date is that they simultaneously interact with at least two adjacent actin monomers within the filament (McGough 1994; McGough 1998). This additional structural feature is important in distinguishing between G-actin and F-actin-binding proteins because an "actin binding site" composed of at least two monomers ensures filament binding specificity.

Binding sites on G-actin and F-actin

Many different proteins bind actin and most of them bind either monomeric or filament forms of actin. However, structural studies on G-actin and F-actin bound to proteins and toxins has revealed that most proteins bind to two major "hot spots" on actin (Dominguez 2004). One binding "hot spot" is located in a hydrophobic cleft that is formed between subdomain 1 and sundomain 3 of actin (Dominguez 2004). The hydrophobic cleft is lined with hydrophobic residues from subdomain 1 (Ile341, Ile345, Leu346, Leu349, Thr351, Met355, and possibly the

C-terminus) and subdomain 3 (Tyr143, Ala144, Gly146, Thr148, Gly168) (Kabsch 1990). Proteins bind to this cleft through the hydrophobic side chains of an exposed α-helix, and interestingly there seems to be no consensus sequence amongst helices of proteins from different families. Binding to the hydrophobic cleft is characteristic of proteins and ligands that are actin monomer-specific, including gelsolin, vitamin D-binding protein (DBP), ciboulot (thymosin-β4), profilin, ADF/cofilin, and the marine toxins kabiramide C and jasisamide A (Dominguez 2004).

The hydrophobic cleft is not only a "hot spot" for actin binding proteins and toxins but is also involved in "actin-actin" interactions between subunits contained within a filament. F-actin structural models have shown that the hydrophobic cleft is involved in intrastrand subunit interactions by placing the D-loop (residues 40-48) of a lower subunit into the hydrophobic cleft of the adjacent upper subunit (Leu346 and Phe375) (Holmes 1990; Lorenz 1993; Holmes 2003; Oda 2009). Thus, the localization of a common "binding site" within the hydrophobic cleft of actin may have an important functional role. For example, if nothing is bound to cleft, it might define actin monomer binding specificity by being fully exposed. However, its role may be dependent on "what" is bound to it. In this context, it is possible to predict mechanisms for both inhibiting polymerization and inducing depolymerization of actin filaments. For example, if actin is bound to a monomer-sequestering protein (or toxin) at the hydrophobic cleft, this could prevent polymerization of the actin by blocking important intersubunit interactions for incorporation into the filament. Additionally, in the context of an actin filament, cleft binding by gelsolin or ADF/cofilin may aid in the severing (gelsolin) or depolymerization (cofilin) of F-actin by weakening "actin-actin" interactions between adjacent subunits.

A second actin-binding "hot spot" is found in a "hydrophobic pocket" that is located at the "front" part of the hydrophobic cleft and is mostly contained within subdomain 1 but is also

near the subdomain 3 junction site. This hydrophobic pocket is also present in F-actin where it is near the subdomain 2 of the adjacent lower subunit. In an actin filament, the region around the hydrophobic pocket is a "hot spot" for F-actin-binding proteins, and importantly its spatial proximity enables an F-actin binding protein the opportunity to contact two subunits simultaneously. This is an important structural feature because many if not all F-actin-binding proteins need to contact two successive monomers at the same time (McGough 1994; McGough 1998).

Many different F-actin-binding proteins have been shown to bind at or near the hydrophobic pocket and include gelsolin (McGough 1998; Choe 2002; Burtnick 2004), cofilin (McGough 1997), tropomyosin (Xu 1999), myosin (Rayment 1993; Holmes 2003), α-actinin (McGough 1994), fimbrin (Hanein 1998; Galkin 2008), dystrophin/utrophin (Galkin 2002; Galkin 2003; Sutherland-Smith 2003), cortactin (Pant 2006), vinculin (Janssen 2006), and talin (Gingras 2008). With the exception of gelsolin and other end-capping proteins (discussed later) most of the above proteins are found to interact with some part of the peptide stretches 339-355 of subdomain 1 of the upper subunit and 86-117 of subdomain 1 and/or 43-61 of subdomain 2 of the lower subunit. As mentioned earlier, gelsolin has a slightly different F-actin-binding interface around the hydrophobic pocket (Choe 2002; Burtnick 2004) and is characterized by binding between subdomain 1 and 3 of the upper subunit and subunit 1 of the lower subunit. This slight variation in subdomain contacts may reflect gelsolin's role as a severing protein or end-capping protein. However, it is important to exercise some caution in drawing conclusions about any functional mechanisms because variations in specific contact points may be due to protein binding specificity or an artifact of the low resolution at which the protein binding was characterized (12.5-45 Å).

Villin is an actin crosslinking protein that belongs to the gelsolin superfamily (Bretscher 1980) and is characterized by six gelsolin homology domain repeats (V1-V6) that share 45% amino acid sequence identity to gelsolin's six gelsolin homology domains (G1-G6) (Finidori 1992). Recently, the 3-dimensional structure of villin bound to F-actin was determined by electron tomography (Hampton 2008). Analysis of the 3-dimensional reconstruction of villin crosslinked actin filaments revealed that villin had unique binding sites on F-actin that differed significantly from gelsolin. The gelsolin domain repeat V1-V2 was found to crosslink two filaments simultaneously and to make contact primarily at subdomain 1 and possibly subdomain 4 on each of the adjacent filaments. Additionally, a third contact on F-actin was made by the villin "headpiece" which was originally believed to be the site of actin crosslinking (Glenney 1981). The villin headpiece was shown *not* to contact the hydrophobic pocket but rather to be positioned near a helix from subdomain 3 (residues 308-320) and a helix from subdomain 4 (residues 222-226) within the same actin subunit. When the authors compared their villin-F-actin structure to fimbrin-F-actin structures (Volkmann 2001; Galkin 2008), it was clear that fimbrin and villin binding sites on F-actin were also distinct from one another.

Although the overall global localization on actin for actin-binding proteins seems to be near or around either the hydrophobic cleft or the hydrophobic pocket, the specific residue interactions for each protein differ slightly. This is an intriguing observation given the constraints that the limited number of "hot spots" on actin affords for potential interactions. Even more interesting is that the interaction sites and structural mode of interaction within protein families that share a homologous actin binding domain also differ. This has been shown for several CH domain proteins (Galkin 2006; Galkin 2008) and gelsolin homology domain proteins (Hampton 2008). Further work is needed to identify the precise molecular interactions

of specific actin-binding proteins with actin and the functional implications of the sites of interaction contacted.

34 kDa actin-bundling protein

The 34 kDa actin-bundling protein is one of eleven actin crosslinking proteins in *Dictyostelium* (Furukawa 1997). The 34 kDa protein is dynamic *in vivo*, and its cellular localization often reflects the dynamic behavior of the actin cytoskeleton. Consequently, it localizes to a number of important actin-dependent structures. For example, it can be found at the leading edge (Fechheimer 1987), in filopodia (Fechheimer 1994), at the point of cell-cell contacts (Furukawa 1992), and in phagocytic cups (Okazaki 1995). Clearly, the 34 kDa protein is involved in many diverse functions. This is further supported by genetic studies in which the cellular function of the 34 kDa protein was examined using 34 kDa protein null cells. 34 kDa-deficient *Dictyostelium* cells show modest defects in cell motility, morphology, and growth (Rivero 1996). However, double knockout mutants for α-actinin/34 kDa and ABP-120/34 kDa show even more severe phenotypes suggesting that there is some functional redundancy amongst the actin crosslinking proteins (Rivero 1999). The combinatorial effects of actin crosslinking proteins as illustrated by genetic studies using other actin crosslinking proteins (Fisher 1997; Noegel 2000; Ponte 2000) clearly show that perturbations in the actin crosslinking proteins present in a cell are coupled to modulation of the actin cytoskeleton. Therefore, actin dynamics of *Dictyostelium* are sensitive to perturbations of the normal functions of the actin-binding proteins that regulate it.

Purified 34 kDa protein from the cytosol of *Dictyostelium* is soluble and monomeric in solution (Fechheimer 1984). It is a Ca^{++}-regulated F-actin-binding protein whose ability to

bundle actin filaments is inhibited by micromolar concentrations of Ca^{++} (Fechheimer and Taylor 1984). The cDNA and the gene encoding the 34 kDa protein predict that it is made up of 295 amino acids with a calculated molecular mass of 33,355 Da. The sequence of the protein includes two putative EF hand regions (Ca^{++} binding sites) at residues 84-112 (EF1) and 135-163 (EF2) (Fechheimer 1991). Ca^{++} binding assays reveal that only one mole of Ca^{++} binds per mole of 34 kDa protein, and the site of Ca^{++} binding is restricted to the second EF hand (Furukawa 2003). Molecular dissection of 34 kDa protein using truncated forms of 34 kDa protein identified three regions important for actin binding. The three regions identified were residues 1-123, 193-254, and 278-295 (Lim 1999), with the strongest actin binding correlating with the region encompassing residues 193-254. Subsequent biochemical studies with a C-terminal truncated form of 34 kDa protein, CT (residues 124-295), showed that the CT fragment no longer displayed Ca^{++}-sensitive F-actin binding and had enhanced actin binding possibly caused by the loss of the putative inhibitory N-terminal region (residues 1-70). This observation led to the development of a model that explains possible intramolecular interactions that regulate the 34 kDa protein (Lim 1999). In this model, release of bound Ca^{++} induces a conformational change in the structure of 34 kDa protein so that the N-terminal region (Interaction Zone 1, IZ-1) is no longer able to interact with Interaction Zone 2 (IZ-2) which also contains the strong actin-binding site (residues 193-254). Therefore, it is predicted that in the absence of bound Ca^{++}, the N-terminal region is no longer able to interact with the strong actin binding site thus enabling it to freely bind to F-actin (Fig. 1.3). This model proposes that the activation of actin-binding activity of the CT fragment results from the absence of the N-terminal inhibitory region (residues 1-70) resulting in exposure of the strong actin-binding site (residues 193-254) and an absence of Ca^{++} regulation. Additionally, point mutations in the first EF hand of 34 kDa protein (34 kDa

ΔEF1) can also activate actin binding. Biochemical characterization of purified 34 kDa ΔEF1 protein showed that it had calcium-insensitive activated F-actin binding similar to that for the CT fragment (Maselli 2003). Interestingly, both the CT fragment and the 34 kDa ΔEF1 proteins have been used to develop cultured cell and animal models of actin-rich aggregations that are associated with a variety of disease states (see below).

Actin cytoskeleton and disease

Actin is one of the most conserved proteins. This high level of conservation is likely the result of the low level of mutational tolerance that can be afforded to actin because it is involved in so many important and diverse cellular functions. The cellular importance of functional actin is additionally supported by the observation that most organisms contain multiple actin genes. Consequently, there have been very few reported diseases associated with actin mutations, the exception being mutations involving the skeletal isoform (α-actin). To date, over 60 missense mutations have been described in α-actin, and all of them are linked to congenital myopathies (CM) (Marston 2001; Clarkson 2004). It is remarkable to note that although a large number of α-actin mutations have been identified, the overall conservation between these mutants is still 99% identical. Diseases associated with the actin cytoskeleton are more commonly linked to the proteins that interact with actin. Because there are so many different types of proteins that interact with actin, the list of "actin-associated" diseases is very broad and extensive. They include developmental disorders, diseases of mRNA delivery and translation (Fragile X), diseases based on inclusions (neurodegenerative), musculoskeletal diseases (musclular dystrophy), immune diseases, cancer, inflammation, aging and cell senescence, bacterial invasion, and pathogenesis (Maloney 2008)

The development of cytoplasmic F-actin inclusions is a common pathological hallmark of a broad range of neurodegenerative diseases. Actin inclusions can be classified into three types based on the organizational arrangement of the actin filaments contained within them: irregular aggregates and sheets (inclusions), rod-shaped bundles of filaments (rods), and paracrystalline lattices (Hirano bodies) (Bamburg 2002; Bamburg 2009).

Hirano bodies and disease

Hirano bodies are eosinophilic rod-like structures that were first described by Dr. Asao Hirano in post-mortem brain tissue samples taken from patients affected by a familial form of either Parkinson's disease or Amyotrophic Lateral Sclerosis (ALS) in Guam (Hirano 1968). Since their original description in 1968, Hirano bodies have been found to be associated with a wide variety of disorders including several neurodegenerative diseases (Table 1.2). Most frequently Hirano bodies are found in the pyramidal region of Ammon's horn (CA1) in the hippocampus (Hirano 1994). However, they are not exclusively restricted to neurons and have been found in other cell types such as myofibrils (Tomonaga 1983; Fernandez 1999) and canine testicular interstitial cells (Setoguti 1974).

The structural organization of Hirano bodies as revealed by electron microscopy show that they are composed of parallel filaments arranged in orthogonal sheets that vary in appearance depending on the plane of sectioning through an individual Hirano body (Schochet 1972; Tomonaga 1974). High resolution images of Hirano bodies obtained by freeze-etching electron microscopy further reveal that they are constructed of "paired sheets" of parallel filaments 10-12 nm in diameter with 12 nm spacing between filaments (Izumiyama 1991). Additionally, Izumiyama and colleagues often observed electron dense "crosslinks" between

parallel filaments suggesting that the filaments were linked together by protein-protein interactions.

Immunohistochemical studies of Hirano bodies from post-mortem tissue have shown that they contain F-actin (Goldman 1983; Galloway 1987) and also contain epitopes for actin-associated proteins such as α-actinin, vinculin, ADF/cofilin, and tropomyosin (Galloway 1987; Maciver 1995). Importantly, other proteins not related to the cytoskeleton have also been found to be enriched within Hirano bodies (Table 1.3). The presence of proteins involved in such diverse functions as transcription regulation and cell signaling suggests that Hirano bodies may modulate the pathology of a cell through perturbation of normal cellular processes. For example, the β-amyloid precursor protein (AICD) was found to be enriched in Hirano bodies (Munoz 1993). This is of significance because AICD has been recently shown to be a possible transcription regulator (Cao 2001), and therefore sequestration of AICD in a Hirano body would affect its normal function and more importantly affect cell physiology.

Models for Hirano bodies

Since most work done on Hirano bodies has been in post-mortem tissue, very little is known about the formation and fate of Hirano bodies and the consequences Hirano bodies may have on cell physiology. Fortunately, a cell model system was developed in *Dictyostelium* and mammalian cells that accurately recapitulates the formation of Hirano bodies (Maselli 2002; Maselli 2003; Davis 2008). In *Dictyostelium* cells, Maselli *et al.* found that expression of either a carboxyl-terminal fragment (CT, residues 124-295) or mutated (34 kDa ΔEF1) form of the *Dictyostelium* 34 kDa actin-bundling protein induced the formation of F-actin-enriched structures that were ultrastructurally equivalent to those found in Hirano bodies. Importantly,

expression of CT also induced Hirano body formation in mammalian tissue culture cells, illustrating that Hirano body formation is not a neuron-specific phenomenon (Maselli 2002; Davis 2008; Ha 2010). The CT fragment has also been used to develop a mouse model for Hirano bodies (Ha 2010).

The value of the Hirano body model system has also been demonstrated in two recent studies that address the formation and degradation of Hirano bodies. In 2008, the model system was used to describe the early phases of Hirano body formation (Davis 2008). Using an inducible expression system, Davis *et al.* demonstrated that CT-GFP initially induced the formation of small F-actin aggregations that coalesced into one large aggregate. Then, in 2009, Kim *et al.* showed that degradation of Hirano bodies involves both autophagic and ubiquitin-mediated proteasome pathways (Kim 2009). Their results are consistent with previous studies demonstrating that other intracellular inclusions are also degraded by autophagy and the proteasome (Ravikumar 2002; Webb 2003; Kabuta 2006; Kamimoto 2006).

Goals and scope of the proposed work

The initial goals of this project were to understand the structure, regulation, and mechanism of crosslinking of actin filaments by the 34 kDa actin-bundling protein, and the requirements for induction of the formation of Hirano bodies in cells. A variety of approaches were employed towards these goals. Efforts to elucidate the 3-dimensional structure of the 34 kDa protein by crystallography and X-ray diffraction led to crystals without the required internal order to determine a high resolution structure. Studies of a new mutant form of 34 kDa protein with a mutation in the inhibitory region have shown that this region is essential to regulate actin binding in the full length 34 kDa protein. Further, studies of the interaction of this protein with

actin *in vitro* and in cells show that inhibition of disassembly of actin filaments is a major effect of high affinity binding, and is a property of the actin filaments in Hirano bodies. In addition, chemical crosslinking and mass spectrometry were used to verify that all three of the actin-binding sites identified by Lim *et al*. in truncation fragments do make contacts with actin filaments in the full length protein. Mapping of these interaction sites on a model of the actin filament reveals the structural basis for stabilization of actin filaments and inhibition of disassembly, two key elements required for the formation of Hirano bodies. These findings are reported in the form of two research manuscripts in Chapters 2 and 3 and are further discussed in a summary chapter 4.

References

Aebi, U., Fowler, W. E., Isenberg, G., Pollard, T. D. and Smith, P. R (1981). "Crystalline actin sheets: their structure and polymorphism." J. Cell Biol. **91**(2 Pt 1): 340-51.

Aguda, A. H., Burtnick, L. D. and Robinson, R. C (2005). "The state of the filament." EMBO Rep. **6**(3): 220-6.

Andrianantoandro, E., and Pollard, T. D (2006). "Mechanism of actin filament turnover by severing and nucleation at different concentrations of ADF/cofilin." Mol. Cell **24**(1): 13-23.

Anzil, A. P., Herrlinger, H., Blinzinger, K. and Heldrich, A (1974). "Ultrastructure of brain and nerve biopsy tissue in Wilson disease." Arch. Neurol. **31**(2): 94-100.

Balcer, H. I., Goodman, A. L., Rodal, A. A., Smith, E., Kugler, J., Heuser, J. E. and Goode, B. L (2003). "Coordinated regulation of actin filament turnover by a high-molecular-weight Srv2/CAP complex, cofilin, profilin, and Aip1." Curr. Biol. **13**(24): 2159-69.

Bamburg, J. R. (1999). "Proteins of the ADF/cofilin family: essential regulators of actin dynamics." Annu. Rev. Cell Dev. Biol. **15**: 185-230.

Bamburg, J. R., and Bloom, G. S (2009). "Cytoskeletal pathologies of Alzheimer disease." Cell Motil. Cytoskeleton **66**(8): 635-649.

Bamburg, J. R., and Wiggan, O. P (2002). "ADF/cofilin and actin dynamics in disease." Trends Cell Biol. **12**: 598-605.

Bernstein, B. W., and Bamburg, J. R (1982). "Tropomyosin binding to F-actin protects the F-actin from disassembly by brain actin-depolymerizing factor (ADF)." Cell Motil. **2**(1): 1-8.

Bertling, E., Hotulainen, P., Mattila, P. K., Matilainen, T., Salminen, M. and Lappalainen, P (2004). "Cyclase-associated protein 1 (CAP1) promotes cofilin-induced actin dynamics in mammalian nonmuscle cells." Mol. Biol. Cell **15**(5): 2324-34.

Blanchoin, L., Pollard, T. D. and Hitchcock-DeGregori, S. E (2001). "Inhibition of the Arp2/3 complex-nucleated actin polymerization and branch formation by tropomyosin." Curr. Biol. **11**(16): 1300-4.

Blanchoin, L., Pollard, T. D. and Mullins, R. D (2000). "Interactions of ADF/cofilin, Arp2/3 complex, capping protein and profilin in remodeling of branched actin filament networks." Curr. Biol. **10**(20): 1273-82.

Bretscher, A., and Weber, K (1980). "Villin is a major protein of the microvillus cytoskeleton which binds both G and F actin in a calcium-dependent manner." Cell **20**(3): 839-47.

Broderick, M. J., and Winder, S. J (2005). "Spectrin, alpha-actinin, and dystrophin." Adv. Protein Chem. **70**: 203-46.

Burtnick, L. D., Urosev, D., Irobi, E., Narayan, K. and Robinson, R. C (2004). "Structure of the N-terminal half of gelsolin bound to actin: roles in severing, apoptosis and FAF." EMBO J. **23**(14): 2713-22.

Cao, X., and Sudhof, T. C (2001). "A transcriptively active complex of APP with Fe65 and Histone Acetyltransferase Tip60." Science **293**: 115-120.

Carlier, M. F. (1989). "Role of nucleotide hydrolysis in the dynamics of actin filaments and microtubules." Int. Rev. Cytol. **115**: 139-70.

Carlier, M. F. (1991). "Nucleotide hydrolysis in cytoskeletal assembly." Curr. Opin. Cell Biol. **3**(1): 2-7.

Carlier, M. F., Laurent, V., Santolini, J., Melki, R., Didry, D., Xia, G. X., Hong, Y., Chua, N. H. and Pantaloni, D (1997). "Actin depolymerizing factor (ADF/cofilin) enhances the rate of filament turnover: implication in actin-based motility." J. Cell Biol. **136**(6): 1307-22.

Cartier, L., Gálvez, S. and Gajdusek, D. C (1985). "Familial clustering of the ataxic form of Creutzfeldt-Jakob disease with Hirano bodies." J. Neurol. Neurosurg. Psychiatry **48**(3): 234-8.

Chik, J. K., Lindberg, U. and Schutt, C. E (1996). "The structure of an open state of beta-actin at 2.65 A resolution." J. Mol. Biol. **263**(4): 607-23.

Choe, H., Burtnick, L. D., Mejillano, M., Yin, H. L., Robinson, R. C. and Choe, S (2002). "The calcium activation of gelsolin: insights from the 3A structure of the G4-G6/actin complex." J. Mol. Biol. **324**(4): 691-702.

Clarkson, E., Costa, C. F. and Machesky, L. M (2004). "Congenital myopathies: diseases of the actin cytoskeleton." J. Pathol. **204**(4): 407-17.

Cooper, J. A., and Schafer D. A (2000). "Control of actin assembly and disassembly at filament ends." Curr. Opin. Cell Biol. **12**(1): 97-103.

Cooper, J. A., and Sept, D (2008). "New insights into mechanism and regulation of actin capping protein." Int. Rev. Cell Mol. Biol. **267**: 183-206.

Cortese, J. D., and Frieden, C (1990). "Effect of filamin and controlled linear shear on the microheterogeneity of F-actin/gelsolin gels." Cell Motil. Cytoskeleton **17**(3): 236-49.

Curmi, P. M., Barden, J. A. and dos Remedios, C. G (1984). "Actin tube formation: effects of variations in commonly used solvent conditions." J. Muscle Res. Cell Motil. **5**(4): 423-30.

Davis, R. C., Furukawa, R. and Fechheimer, M (2008). "A cell culture model for investigation of Hirano bodies." Acta Neuropathol. **115**: 205-217.

De La Cruz, E. M., and Pollard, T. D (1994). "Transient kinetic analysis of rhodamine phalloidin binding to actin filaments." Biochemistry **33**(48): 14387-92.

De La Cruz, E. M., and Pollard, T. D (1996). "Kinetics and thermodynamics of phalloidin binding to actin filaments from three divergent species." Biochemistry **35**(45): 14054-61.

De La Cruz , E. M., Ostap, E. M., Brundage, R. A., Reddy, K. S., Sweeney, H. L. and Safer, D (2000). "Thymosin-beta(4) changes the conformation and dynamics of actin monomers." Biophys. J. **78**(5): 2516-27.

Dominguez, R. (2004). "Actin-binding proteins--a unifying hypothesis." Trends Biochem. Sci. **29**(11): 572-8.

Dominguez, R., and Graceffa, P (2003). "Solution properties of TMR-actin: When biochemical and crystal data agree." Biophys. J. **85**: 2073-4.

dos Remedios, C. G., Chhabra, D., Kekic, M., Dedova, I. V., Tsubakihara, M., Berry, D. A. and Noswort, N. J (2003). "Actin binding proteins: regulation of cytoskeletal microfilaments." Physiol. Rev. **83**(2): 433-73.

Egelman, E. H., Francis, N. and DeRosier, D. J (1982). "F-actin is a helix with a random variable twist." Nature (London) **298**: 131-135.

Fechheimer, M. (1987). "The *Dictyostelium discoideum* 30,000-dalton protein is an actin filament-bundling protein that is selectively present in filopodia." J. Cell Biol. **104**: 1539-51.

Fechheimer, M., and Taylor, D. L (1984). "Isolation and characterization of a 30,000-dalton calcium-sensitive actin cross-linking protein from *Dictyostelium discoideum*." J. Biol. Chem. **259**: 4514-20.

Fechheimer, M., Ingalls, H. M., Furukawa, R. and Luna, E. J (1994). "Association of the *Dictyostelium* 30,000 dalton actin bundling protein with contact regions." J. Cell Sci. **107**: 2393-401.

Fechheimer, M., Murdock, D., Carney, M. and Glover, C. V. C (1991). "Isolation and sequencing of CDNA clones encoding the *Dictyostelium discoideum* 30,000 dalton actin bundling protein." J. Biol. Chem. **266**: 2883-9.

Fernandez, R., Fernandez, J. M., Cervera, C., Teijeiro, S., Dominguez, C. and Navarro, C (1999). "Adult glycogenesis II with paracrystalline mitochondrial inclusions and Hirano bodies in skeletal muscle." Neuromuscul. Disord. **9**: 136-43.

Field, E. J., and Narang, H. K (1972). "An electron-microscopic study of scrapie in the rat: further observations on "inclusion bodies" and virus-like particles." J. Neurol. Sci. **17**(3): 347-64.

Field, E. J., Mathews, J. D. and Raine, C. S (1969). "Electron microscopic observations on the cerebellar cortex in kuru." J. Neurol. Sci. **8**(2): 209-24.

Finidori, J., Friederich, E., Kwiatkowski, D. J. and Louvard, D (1992). "*In vivo* analysis of functional domains from villin and gelsolin." J. Cell Biol. **116**(5): 1145-55.

Fischer, R. S., and Fowler, V. M (2003). "Tropomodulins: life at the slow end." Trends Cell Biol. **13**(11): 593-601.

Fisher, E. R., Gonzalez, A. R., Khurana, R. C. and Danowski, T. S (1972). "Unique, concentrically laminated, membranous inclusions in myofibers. ." Am. J. Clin. Pathol. **58**(3): 239-44.

Fisher, P. R., Noegel, A. A., Fechheimer, M., Rivero, F., Prassler, J. and Gerisch, G (1997). "Photosensory and thermosensory responses in *Dictyostelium* slugs are specifically impaired by the absence of the F-actin cross-linking gelation factor (ABP-120)." Curr. Biol. **7**(11): 889-92.

Foth, B. J., Goedecke, M. C. and Soldati, D (2006). "New insights into myosin evolution and classification." Proc. Natl. Acad. Sci. USA **103**(10): 3681-6.

Fu, Y., Ward, J. and Young, H. F (1975). "Unusual, rod-shaped cytoplasmic inclusions (Hirano bodies) in a cerebellar hemangioblastoma." Acta Neuropathol. **31**(2): 129-35.

Furukawa, R., and Fechheimer, M (1997). "The structure, function, and assembly of actin filament bundles." Int. Rev. of Cytol. **175**: 29-90.

Furukawa, R., Butz, S., Fleishmann, E. and Fechheimer, M (1992). "The *Dictyostelium discoideum* 30,000 dalton protein contributes to phagocytosis." Protoplasma **169**: 18-27.

Furukawa, R., Maselli, A. G., Thomson, S. A. M., Lim, R. W.-L., Stokes, J. V. and Fechheimer, M (2003). "Calcium regulation of actin cross-linking is important for function of the actin cytoskeleton in *Dictyostelium*." J. Cell Sci. **116**: 187-96.

Galkin, V. E., Orlova, A., Cherepanova, O., Lebart, M. C. and Egelman, E. H (2008). "High-resolution cryo-EM structure of the F-actin-fimbrin/plastin ABD2 complex." Proc. Natl. Acad. Sci. USA **105**(5): 1494-8.

Galkin, V. E., Orlova, A., Fattoum, A., Walsh, M. P. and Egelman, E. H (2006). "The CH-domain of calponin does not determine the modes of calponin binding to F-actin." J. Mol. Biol. **359**(2): 478-85.

Galkin, V. E., Orlova, A., VanLoock, M. S. and Egelman, E. H (2003). "Do the utrophin tandem calponin homology domains bind F-actin in a compact or extended conformation?" J. Mol. Biol. **331**(5): 967-72.

Galkin, V. E., Orlova, A., VanLoock, M. S., Rybakova, I. N., Ervasti, J. M. and Egelman, E. H (2002). "The utrophin actin-binding domain binds F-actin in two different modes: implications for the spectrin superfamily of proteins." J. Cell Biol. **157**(2): 243-51.

Galkin, V. E., Orlova, A., VanLoock, M. S., Shvetsov, A., Reisler, E. and Egelman, E. H (2003). "ADF/cofilin use an intrinsic mode of F-actin instability to disrupt actin filaments." J. Cell Biol. **163**(5): 1057-66.

Galloway, P. G., Perry, G. and Gambetti, P (1987). "Hirano body filaments contain actin and actin-associated proteins." J. Neuropathol. Exp. Neurol. **46**: 185-99.

Gessaga, E. C., and Anzil, A. P (1975). "Rod-shaped filamentous inclusions and other ultrastructural features in a cerebellar astrocytoma." Acta Neuropathol. **33**(2): 119-27.

Gibson, P. H. (1978). "Light and electron microscopic observations on the relationship between Hirano bodies, neuron and glial perikarya in the human hippocampus." Acta Neuropathol. **42**: 165-71.

Gimona, M., Djinovic-Carugo, K., Kranewitter, W. J. and Winder, S. J (2002). "Functional plasticity of CH domains." FEBS Lett. **513**(1): 98-106.

Gingras, A. R., Bate, N., Goult, B. T., Hazelwood, L., Canestrelli, I., Grossmann, J. G., Liu, H., Putz, N. S., Roberts, G. C., Volkmann, N., Hanein, D., Barsukov, I. L. and Critchley, D. R (2008). "The structure of the C-terminal actin-binding domain of talin." EMBO J. **27**(2): 458-69.

Glenney, J. R. J., Geisler, N., Kaulfus, P. and Weber, K (1981). "Demonstration of at least two different actin-binding sites in villin, a calcium-regulated modulator of F-actin organization." J. Biol. Chem. **256**(15): 8156-61.

Goldman, J. E. (1983). "The association of actin with Hirano bodies." J. Neuropathol. Exp. Neurol. **42**: 146-52.

Goldschmidt-Clermont, P. J., Furman, M. I., Wachsstock, D., Safer, D., Nachmias, V. T. and Pollard, T. D (1992). "The control of actin nucleotide exchange by thymosin beta 4 and

profilin. A potential regulatory mechanism for actin polymerization in cells." Mol. Biol. Cell **3**(9): 1015-24.

Goode, B. L., and Eck, M. J (2007). "Mechanism and function of formins in the control of actin assembly." Annu. Rev. Biochem. **76**: 593-627.

Graceffa, P., and Dominguez, R (2003). "Crystal structure of monomeric actin in the ATP state. Structural basis of the nucleotide-dependent actin dynamics." J. Biol. Chem. **278**: 34172-80.

Gunning, P. W., Schevzov, G., Kee, A. J. and Hardeman, E. C (2005). "Tropomyosin isoforms: divining rods for actin cytoskeleton function." Trends Cell Biol. **15**(6): 333-41.

Ha, S., Furukawa, R. and Fechheimer, M (2010). "Association of AICD and Fe65 with Hirano bodies reduces transcriptional activation and initiation of apoptosis." Neurobiol. Aging.

Ha, S., Furukawa, R., Stramiello, M., Wagner, J. and Fechheimer, M (2010). "Transgenic mouse model for the formation of Hirano bodies." manuscript in preparation.

Hampton, C. M., Liu, J., Taylor, D. W., DeRosier, D. J. and Taylor, K. A (2008). "The 3D structure of villin as an unusual F-Actin crosslinker." Structure **16**(12): 1882-91.

Hanein, D., Volkmann, N., Goldsmith, S., Michon, A. M., Lehman, W., Craig, R., DeRosier, D., Almo, S. and Matsudaira, P (1998). "An atomic model of fimbrin binding to F-actin and its implications for filament crosslinking and regulation." Nat. Struct. Biol. **5**(9): 787-92.

Hartwig, J. H. (1995). "Actin-binding proteins. 1: Spectrin super family." Protein Profile **2**(7): 703-800.

Hasson, T., and Mooseker, M. S (1994). "Porcine myosin-VI: characterization of a new mammalian unconventional myosin." J. Cell Biol. **127**(2): 425-40.

Hirano, A. (1994). "Hirano bodies and related neuronal inclusions." Neuropathol. Appl. Neurobiol. **20**: 3-11.

Hirano, A., Dembitzer, H. M., Kurland, L. T. and Zimmerman, H. M (1968). "The fine structure of some intraganglionic alterations." J. Neuropathol. Exp. Neurol. **27**: 167-82.

Holmes, K. C., Angert, I., Kull, F. J., Jahn, W. and Schröder, R. R (2003). "Electron cryo-microscopy shows how strong binding of myosin to actin releases nucleotide." Nature **425**(6956): 423-7.

Holmes, K. C., Popp, D., Gebhard, W. and Kabsch, W (1990). "Atomic model of the actin filament." Nature (London) **347**: 44-9.

Hou, L., Luby-Phelps, K. and Lanni, F (1990). "Brownian motion of inert tracer macromolecules in polymerized and spontaneously bundled mixtures of actin and filamin." J. Cell Biol. **110**(5): 1645-54.

Iwasa, M., Maeda, K., Narita, A., Maéda, Y. and Oda, T (2008). "Dual roles of Gln137 of actin revealed by recombinant human cardiac muscle alpha-actin mutants." J. Biol. Chem. **283**(30): 21045-53.

Izumiyama, N., Ohtsubo, K., Tachikawa, T. and Nakamura, H (1991). "Elucidation of the three-dimensional ultrastructure of Hirano bodies by the quick-freeze, deep-etch and replica method." Acta Neuropathol. **81**: 248-54.

Janssen, M. E., Kim, E., Liu, H., Fujimoto, L. M., Bobkov, A., Volkmann, N. and Hanein, D (2006). "Three-dimensional structure of vinculin bound to actin filaments." Mol. Cell **21**(2): 271-81.

Jordan-Sciutto, K., Dragich, J., Walcott, D. and Bowser, R (1998). "The presence of FAC1 protein in Hirano bodies." Neuropathol. Appl. Neurobiol. **24**(5): 359-66.

Kabsch, W., Mannherz, H. G., Suck, D., Pai, E. and Holmes, K. C (1990). "Atomic structure of the actin:DNAse I complex." Nature (London) **347**: 37-44.

Kabuta, T., Suzuki, Y. and Wada, K (2006). "Degradation of amyotrophic lateral sclerosis-linked mutant Cu,Zn-superoxide dismutase proteins by macroautophagy and the proteasome." J. Biol. Chem. **281**(41): 30524-33.

Kalhammer, G., and Bähler, M (2000). "Unconventional myosins." Essays Biochem. **35**: 33-42.

Kamimoto, T., Shoji, S., Hidvegi, T., Mizushima, N., Umebayashi, K., Perlmutter, D. H. and Yoshimori, T (2006). "Intracellular inclusions containing mutant alpha1-antitrypsin Z are propagated in the absence of autophagic activity." J. Biol. Chem. **281**(7): 4467-76.

Kellerman, K. A., and Miller, K. G (1992). "An unconventional myosin heavy chain gene from *Drosophila melanogaster*." J. Cell Biol. **119**(4): 823-34.

Kim, D.-H., Davis, R. C., Furukawa, R. and Fechheimer, M (2009). "Autophagy contributes to the degradation of hirano bodies." Autophagy **5**(1): 1-8.

Korenbaum, E., and Rivero, F (2002). "Calponin homology domains at a glance." J. Cell Sci. **115**(Pt 18): 3543-5.

Kostyukova, A. S. (2008). "Tropomodulin/tropomyosin interactions regulate actin pointed end dynamics." Adv. Exp. Med. Biol. **644**: 283-92.

Kwiatkowski, D. J. (1999). "Functions of gelsolin: motility, signaling, apoptosis, cancer." Curr. Opin. Cell Biol. **11**(1): 103-8.

Lappalainen, P., and Drubin, D. G (1997). "Cofilin promotes rapid actin filament turnover *in vivo*." Nature **388**(6637): 78-82.

Lass, R., and Hagel, C (1994). "Hirano bodies and chronic alcoholism." Neuropathol. Appl. Neurobiol. **20**: 12-21.

Lee, H. G., Ueda, M., Miyamoto, Y., Yoneda, Y., Perry, G., Smith, M. A. and Zhu, X (2006). "Aberrant localization of importin alpha1 in hippocampal neurons in Alzheimer disease." Brain Res. **1124**(1): 1-4.

Lee, S. C., Zhao, M. L., Hirano, A. and Dickson, D. W (1999). "Inducible nitric oxide synthase immunoreactivity in the Alzheimer disease hippocampus: association with Hirano bodies, neurofibrillary tangles, and senile plaques." J. Neuropathol. Exp. Neurol. **58**(11): 1163-9.

Lim, R. W. L., Furukawa, R. and Fechheimer, M (1999). "Evidence of intramolecular regulation of the *Dictyostelium discoideum* 34,000 dalton F-actin bundling protein." Biochemistry **38**: 16323-32.

Lim, R. W. L., Furukawa, R., Eagle, S., Cartwright, R. C. and Fechheimer, M (1999). "Three distinct F-actin binding sites in the *Dictyostelium discoideum* 34,000 dalton actin bundling protein." Biochemistry **38**: 800-12.

Liu, J., Taylor, D. W. and Taylor, K. A (2004). "A 3-D reconstruction of smooth muscle alpha-actinin by CryoEm reveals two different conformations at the actin-binding region." J. Mol. Biol. **338**(1): 115-25.

Lorenz, M., Popp, D. and Holmes, K. C (1993). "Refinement of the F-actin model against X-ray fiber diffraction data by the use of a directed mutation algorithm." J. Mol. Biol. **234**(3): 826-36.

Machesky, L. M., Atkinson, S. J., Ampe, C., Vandekerckhove, J. and Pollard, T. D (1994). "Purification of a cortical complex containing two unconventional actins from *Acanthamoeba* by affinity chromatography on profilin-agarose." J. Cell Biol. **127**(1): 107-15.

Maciver, S. K., and Harrington, C. R (1995). "Two actin binding proteins, actin depolymerizing factor and cofilin, are associated with Hirano bodies." Neuroreport **6**: 1985-8.

Maloney, M. T., Kinley, A. W., Pak, C. W. and Bamburg, J. R (2008). ADF/cofilin, Actin Dynamics, and Disease. Actin-Binding Proteins and Disease. New York, Springer New York. **8:** 83-187.

Marston, S. B., and Hodgkinson, J. L (2001). "Cardiac and skeletal myopathies: can genotype explain phenotype?" J. Musc. Res. Cell Motil. **22**(1): 1-4.

Maselli, A. G., Davis, R., Furukawa, R. and Fechheimer, M (2002). "Formation of Hirano bodies in *Dictyostelium* and mammalian cells induced by expression of a modified form of an actin cross-linking protein." J. Cell Sci. **115**: 1939-52.

Maselli, A. G., Furukawa, R., Thomson, S. A. M., Davis, R. C. and Fechheimer, M (2003). "Formation of Hirano bodies induced by the expression of an actin cross-linking protein with a gain of function mutation." Eucaryot. Cell **2**: 778-87.

Matsudaira, P. (1991). "Modular organization of actin crosslinking proteins." Trends Biochem. Sci. **16**(3): 87-92.

McGough, A. (1998). "F-actin binding proteins." Curr. Opin. Struct. Biol. **8**(2): 166-76.

McGough, A., Pope, B., Chiu, W. and Weeds, A (1997). "Cofilin changes the twist of F-actin: implications for actin filament dynamics and cellular function." J. Cell Biol. **138**(4): 771-81.

McGough, A., Way, M. and DeRosier, D (1994). "Determination of the alpha-actinin-binding site on actin filaments by cryoelectron microscopy and image analysis." J. Cell Biol. **126**(2): 433-43.

McLaughlin, P. J., Gooch, J. T., Mannherz, H. G. and Weeds, A. G (1993). "Structure of gelsolin segment 1-actin complex and the mechanism of filament severing." Nature **364**(6439): 685-92.

Mermall, V., and Miller, K. G (1995). "The 95F unconventional myosin is required for proper organization of the *Drosophila* syncytial blastoderm." J. Cell Biol. **129**(6): 1575-88.

Mermall, V., Post, P. L. and Mooseker, M. S (1998). "Unconventional myosins in cell movement, membrane traffic, and signal transduction." Science **279**(5350): 527-33.

Mitake, S., Ojika, K. and Hirano, A (1997). "Hirano bodies and Alzheimer's disease." Kao-Hsiung I Hseuh K'o Tsa Chih **13**: 10-8.

Mori, H., Tomonaga, M., Baba, N. and Kanaya, K (1986). "The structure analysis of Hirano bodies by digital processing on electron micrographs." Acta Neuropathol. **71**(1-2): 32-7.

Mullins, R. D., and Pollard, T. D (1999). "Structure and function of the Arp2/3 complex." Curr. Opin. Struct. Biol. **9**(2): 244-9.

Mullins, R. D., Heuser, J. A. and Pollard, T. D (1998). "The interaction of Arp2/3 complex with actin: nucleation, high affinity pointed end capping, and formation of branching networks of filaments." Proc. Natl. Acad. Sci. USA **95**(11): 6181-6.

Mullins, R. D., Stafford, W. F. and Pollard, T. D (1997). "Structure, subunit topology, and actin-binding activity of the Arp2/3 complex from *Acanthamoeba*." J. Cell Biol. **136**(2): 331-43.

Munoz, D. G., Wang, D. and Greenberg, B. D (1993). "Hirano bodies accumulate C-terminal sequences of beta-amyloid precursor protein (β-APP) epitopes." J. Neuropathol. Exp. Neurol. **52**: 14-21.

Nachmias, V. T., and Huxley, H. E (1970). "Electron microscope observations on actomyosin and actin preparations from *Physarum polycephalum*, and on their interaction with heavy meromyosin subfragment I from muscle myosin." J. Mol. Biol. **50**(1): 83-90.

Nagara, H., Yajima, K. and Suzuki, K (1980). "An ultrastructural study on the cerebellum of the brindled mouse." Acta Neuropathol. **52**(1): 41-50.

Noegel, A. A., and Schleicher, M (2000). "The actin cytoskeleton of *Dictyostelium*: a story told by mutants." J. Cell Sci. **113**: 759-66.

Oda, T., Iwasa, M., Aihara, T., Maéda, Y. and Narita, A (2009). "The nature of the globular- to fibrous-actin transition." Nature **457**(7228): 441-5.

Ogata, J., Budzilovich, G. N. and Cravioto, H (1972). "A study of rod-like structures (Hirano bodies) in 240 normal and pathological brains." Acta Neuropathol. **21**(1): 61-7.

Okamoto, K., Hirai, S. and Hirano, A (1982). "Hirano bodies in myelinated fibers of hepatic encephalopathy." Acta Neuropathol. **58**(4): 307-10.

Okazaki, K., and Yumura, S (1995). "Differential association of three actin-bundling proteins with microfilaments in *Dictyostelium* amoeba." Eur. J. Cell Biol. **66**(1): 75-81.

Ono, S. (2007). "Mechanism of depolymerization and severing of actin filaments and its significance in cytoskeletal dynamics." Int. Rev. Cytol. **258**: 1-82.

Ono, S., and Ono, K (2002). "Tropomyosin inhibits ADF/cofilin-dependent actin filament dynamics." J. Cell Biol. **156**(6): 1065-76.

Otterbein, L. R., Graceffa, P. and Dominguez, R (2001). "The Crystal Structure of Uncomplexed Actin in the ADP State." Science **293**: 708-11.

Paavilainen, V. O., Bertling, E., Falck, S. and Lappalainen, P (2004). "Regulation of cytoskeletal dynamics by actin-monomer-binding proteins." Trends Cell Biol. **14**(7): 386-94.

Pant, K., Chereau, D., Hatch, V., Dominguez, R. and Lehman, W (2006). "Cortactin binding to F-actin revealed by electron microscopy and 3D reconstruction." J. Mol. Biol. **359**(4): 840-7.

Pantaloni, D., and Carlier, M. F (1993). "How profilin promotes actin filament assembly in the presence of thymosin beta 4." Cell **75**(5): 1007-14.

Papa, I., Astier, C., Kwiatek, O., Raynaud, F., Bonnal, C., Lebart, M. C., Roustan, C. and Benyamin, Y (1999). "Alpha actinin-CapZ, an anchoring complex for thin filaments in Z-line." J. Musc. Res. Cell Motil. **20**(2): 187-97.

Peress, N. S., and Perillo, E (1995). "Differential expression of TGF-beta 1, 2 and 3 isotypes in Alzheimer's disease: a comparative immunohistochemical study with cerebral infarction, aged human and mouse control brains." J. Neuropathol. Exp. Neurol. **54**(6): 802-11.

Peterson, C., Kress, Y., Vallee, R., and Goldman, J. E (1988). "High molecular weight microtubule-associated proteins bind to actin lattices (Hirano bodies)." Acta Neuropathol. **77**(2): 168-74.

Peterson, C., Suzuki, K., Kress, Y. and Goldman, J. E (1986). "Abnormalities of dendritic actin organization in the brindled mouse." Brain Res. **382**(2): 205-12.

Pollard, T. D. (1986). "Rate constants for the reactions of ATP- and ADP-actin with the ends of actin filaments." J. Cell Biol. **103**(6 Pt 2): 2747-54.

Pollard, T. D., and Borisy, G. G (2003). "Cellular motility driven by assembly and disassembly of actin filaments." Cell **112**(4): 453-65.

Pollard, T. D., Blanchoin, L. and Mullins, R. D (2000). "Molecular mechanisms controlling actin filament dynamics in nonmuscle cells." Annu. Rev. Biophys. Biomol. Struct. **29**: 545-76.

Ponte, E., Rivero, F., Fechheimer, M., Noegel, A. A. and Bozzaro, S (2000). "Severe develpomental defects in *Dictyostelium* null mutants for actin-binding proteins." Mech. Dev. **91**(1-2): 153-61.

Popowicz, G. M., Schleicher, M., Noegel, A. A. and Holak, T. A (2006). "Filamins: promiscuous organizers of the cytoskeleton." Trends Biochem. Sci. **31**(7): 411-9.

Previll, L. A., Crosby, M. E., Castellani, R. J., Bowser, R., Perry, G., Smith, M. A. and Zhu, X (2007). "Increased expression of p130 in Alzheimer disease." Neurochem. Res. **32**(4-5): 639-44.

Pruyne, D., Evangelista, M., Yang, C., Bi, E., Zigmond, S., Bretscher, A. and Boone, C (2002). "Role of formins in actin assembly: nucleation and barbed-end association." Science **297**(5581): 612-5.

Puius, Y. A., Mahoney, N. M. and Almo, S. C (1998). "The modular structure of actin-regulatory proteins." Curr. Opin. Cell Biol. **10**(1): 23-34.

Ravikumar, B., Duden, R. and Rubinsztein, D. C (2002). "Aggregate-prone proteins with polyglutamine and polyalanine expansions are degraded by autophagy." Hum. Mol. Genet. **11**(9): 1107-17.

Rayment, I., Holden, H. M., Whittaker, M., Yohn, C. B., Lorenz, M., Holmes, K. C. and Milligan, R. A (1993). "Structure of the actin-myosin complex and its implications for muscle contraction." Science **261**(5117): 58-65.

Reisler, E., and Egelman, E. H (2007). "Actin structure and function: What we still do not understand*." J. Biol. Chem. **282**(50): 36133-7.

Renkawek, K., Bosman, G. J. and de Jong, W. W (1994). "Expression of small heat-shock protein hsp 27 in reactive gliosis in Alzheimer disease and other types of dementia." Acta Neuropathol. **87**(5): 511-9.

Rivero, F., Furukawa, R., Noegel, A. A. and Fechheimer, M (1996). "*Dictyostelium discoideum* cells lacking the 34,000 dalton actin binding protein can grow, locomote, and develop, but exhibit defects in regulation of cell structure and movement: a case of partial redundancy." J. Cell Biol. **135**: 965-80.

Rivero, F., Furukawa, R., Noegel, A. A. and Fechheimer, M (1999). "*Dictyostelium* mutants lacking the 34 kDa bundling protein and alpha-actinin or gelation factor." J. Cell Sci. **112**: 2737-51.

Robinson, R. C., Mejillano, M., Le, V. P., Burtnick, L. D., Yin, H. L. and Choe, S (1999). "Domain movement in gelsolin: a calcium-activated switch." Science **286**(5446): 1939-42.

Rossiter, J. P., Anderson, L. L.,Yang, F. and Cole, G. M (2000). "Caspase-cleaved actin (fractin) immunolabelling of Hirano bodies." Neuropathol. Appl. Neurobiol. **26**(4): 342-6.

Rould, M. A., Wan, Q., Joel, P. B., Lowey, S. and Trybus, K. M (2006). "Crystal Structures of Expressed Non-polymerizable Monomeric Actin in the ADP and ATP States*." J. Biol. Chem. **281**(42): 31909-19.

Sablin, E. P., Dawson, J. F., VanLoock, M. S., Spudich, J. A. and Egelman, E. H (2002). "How does ATP hydrolysis control actin's associations?" Proc. Natl. Acad. Sci. USA **99**(17): 10945-7.

Safer, D., and Nachmias V. T (1994). "Beta thymosins as actin binding peptides." Bioessays **16**(7): 473-9.

Sagot, I., Klee, S. K. and Pellman, D (2002). "Yeast formins regulate cell polarity by controlling the assembly of actin cables." Nat. Cell Biol. **4**(1): 42-50.

Santa-Mara, I., Santpere, G., MacDonald, M. J., Gomez de Barreda, E., Hernandez, F., Moreno, F. J., Ferrer, I. and Avila, J (2008). "Coenzyme q induces tau aggregation, tau filaments, and Hirano bodies." J. Neuropathol. Exp. Neurol. **67**(5): 428-34.

Schafer, D. A., Hug, C. and Cooper, J. A (1995). "Inhibition of CapZ during myofibrillogenesis alters assembly of actin filaments." J. Cell Biol. **128**(1-2): 61-70.

Schlüter, K., Jockusch, B. M. and Rothkegel, M (1997). "Profilins as regulators of actin dynamics." Biochim. Biophys. Acta **1359**(2): 97-109.

Schmid, M. F., Sherman, M. B., Matsudaira, P. and Chiu, W (2004). "Structure of the acrosomal bundle." Nature **431**(7004): 104-7.

Schmidt, M. L., Lee, V. M. and Trojanowski, J. Q (1989). "Analysis of epitopes shared by Hirano bodies and neurofilament proteins in normal and Alzheimer's disease hippocampus." Lab. Invest. **60**(4): 513-22.

Schochet, S. S. J., and McCormick, W. F (1972). "Ultrastructure of Hirano bodies." Acta Neuropathol. **21**: 50-60.

Schochet, S. S. J., Lampert, P. W. and Lindenburg, R (1968). "Fine structure of the Pick and Hirano bodies in a case of Pick's disease." Acta Neuropathol. (Berlin) **11**: 330-7.

Schutt, C. E., Myslik, J. C., Rozycki, M. D., Goonesekere, N. C. and Lindberg, U (1993). "The structure of crystalline profilin-beta-actin." Nature **365**(6449): 810-6.

Sellers, J. R. (2000). "Myosins: a diverse superfamily." Biochim. Biophys. Acta. **1496**(1): 3-22.

Setoguti, T., Esumki, H. and Shimizu, T (1974). "Specific organization of intracytoplasmic filaments in the dog testicular interstitial cell." Tiss. Res. **148**: 493-7.

Shao, C. Y., Crary, J. F., Rao, C., Sacktor, T. C. and Mirra, S. S (2006). "Atypical protein kinase C in neurodegenerative disease II: PKCiota/lambda in tauopathies and alpha-synucleinopathies." J. Neuropathol. Exp. Neurol. **65**(4): 327-35.

Silacci, P., Mazzolai, L., Gauci, C., Stergiopulos, N., Yin, H. L. and Hayoz, D (2004). "Gelsolin superfamily proteins: key regulators of cellular functions." Cell Mol. Life Sci. **61**(19-20): 2614-23.

Sima, A. A., and Hinton, D (1983). "Hirano-bodies in the distal symmetric polyneuropathy of the spontaneously diabetic BB-Wistar rat." Acta Neurol. (Scand.) **68**(2): 107-12.

Sjöblom, B., Salmazo, A. and Djinović-Carugo, K (2008). "Alpha-actinin structure and regulation." Cell Mol. Life Sci. **65**(17): 2688-701.

Sun, H. Q., Yamamoto, M., Mejillano, M. and Yin, H. L (1999). "Gelsolin, a multifunctional actin regulatory protein." J. Biol. Chem. **274**(47): 33179-82.

Sutherland-Smith, A. J., Moores, C. A., Norwood, F. L., Hatch, V., Craig, R., Kendrick-Jones, J. and Lehman, W (2003). "An atomic model for actin binding by the CH domains and spectrin-repeat modules of utrophin and dystrophin." J. Mol. Biol. **329**(1): 15-33.

Svitkina, T. M., and Borisy, G. G (1999). "Arp2/3 complex and actin depolymerizing factor/cofilin in dendritic organization and treadmilling of actin filament array in lamellipodia." J. Cell Biol. **145**(5): 1009-26.

Svitkina, T. M., Verkhovsky, A. B., McQuade, K. M. and Borisy, G. G (1997). "Analysis of the actin-myosin II system in fish epidermal keratocytes: mechanism of cell body translocation." J. Cell Biol. **139**(2): 397-415.

Tomonaga, M. (1974). "Ultratructure of Hirano bodies." Acta Neuropathol. **28**: 365-6.

Tomonaga, M. (1983). "Hirano body in extraocular muscle." Acta Neuropathol. **60**((3-4)): 309-13.

Volkmann, N., DeRosier, D., Matsudaira, P. and Hanein, D (2001). "An atomic model of actin filaments cross-linked by fimbrin and its implications for bundle assembly and function." J. Cell Biol. **153**(5): 947-56.

Wear, M. A., and Cooper, J. A (2004). "Capping protein: new insights into mechanism and regulation." Trends Biochem. Sci. **29**(8): 418-28.

Webb, J. L., Ravikumar, B., Atkins, J., Skepper, J. N. and Rubinsztein, D. C (2003). "Alpha-Synuclein is degraded by both autophagy and the proteasome." J. Biol. Chem. **278**(27): 25009-13.

Weeds, A., and Maciver, S (1993). "F-actin capping proteins." Curr. Opin. Cell Biol. **5**(1): 63-9.

Wegner, A. (1976). "Head to tail polymerization of actin." J. Mol. Biol. **108**(1): 139-50.

Wegner, A. (1982). "Treadmilling of actin at physiological salt concentrations. An analysis of the critical concentrations of actin filaments." J. Mol. Biol. **161**(4): 607-15.

Wegner, A., and Isenberg, G (1983). "12-fold difference between the critical monomer concentrations of the two ends of actin filaments in physiological salt conditions." Proc. Natl. Acad. Sci. USA **80**(16): 4922-5.

Xu, C., Craig, R., Tobacman, L., Horowitz, R. and Lehman, W (1999). "Tropomyosin positions in regulated thin filaments revealed by cryoelectron microscopy." Biophys. J. **77**(2): 985-92.

Yamamoto, T., and Hirano, A (1985). "Hirano bodies in the perikaryon of the Purkinje cell in a case of Alzheimer's disease." Acta Neuropathol. **67**(1-2): 167-9.

Zigmond, S. H. (1998). "Actin cytoskeleton: the Arp2/3 complex gets to the point." Curr. Biol. **8**(18): R654-7.

Figure 1.1. G-actin ribbon structure

G-actin ribbon structure based on G-actin:DNAse I crystal structure (Kabsch 1990). The subdomains of G-actin are colored and numbered as follows: subdomain 1 (I-green), subdomain 2 (II-yellow), subdomain 3 (III-orange), and subdomain 4 (IV-blue). The nucleotide bound within the nucleotide binding pocket is ATP (red). Figure adapted from (dos Remedios 2003) (PDB ID code 1ATN (Kabsch 1990)).

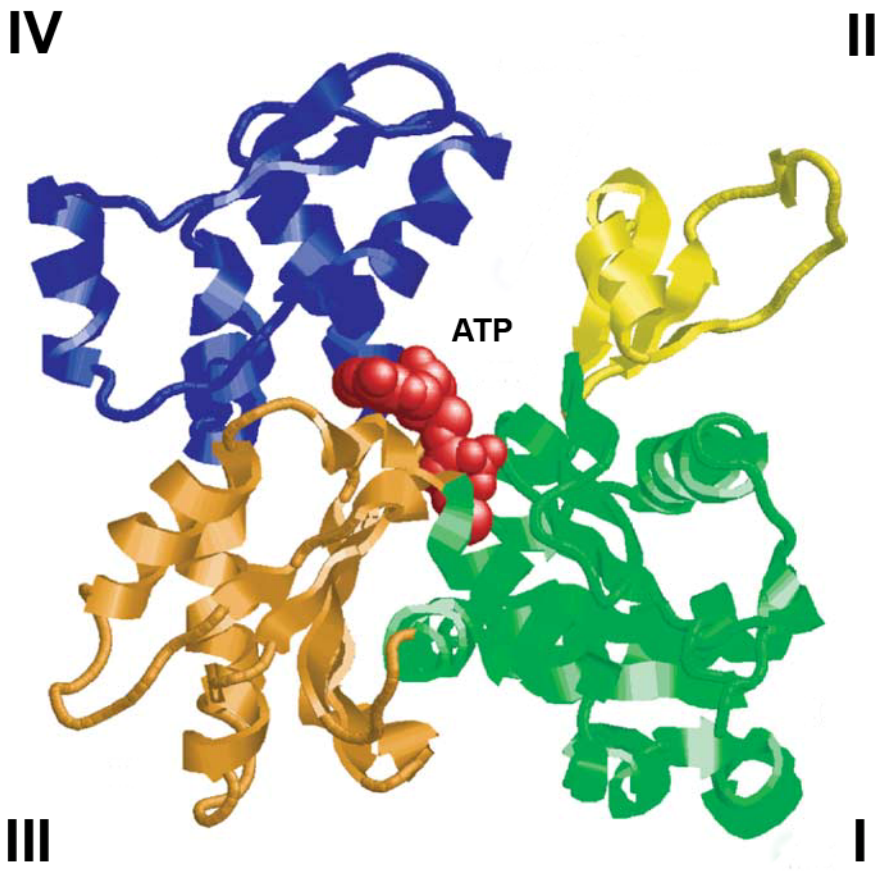
IV
II
ATP
III
I

Figure 1.2. F-actin space-filling model

Space-filling model of an actin filament composed of seven actin subunits. The filament is orientated with the pointed (-) end on top. Each subunit in the filament is colored to distinguish the individual actin monomers in each of the strands (strand one: blue, orange, red, and green; strand two magenta, greenblue, and cyan). The subdomains 1-4 are designated with roman numerals on the orange colored monomer. Figure adapted from Liu *et al*. (PDB ID code 1JSS; original filename: act4polar_fa1.pdb is available via world-wide web at http://www.sb.fsu.edu/~taylor/html/downloads.html) (Liu 2004).

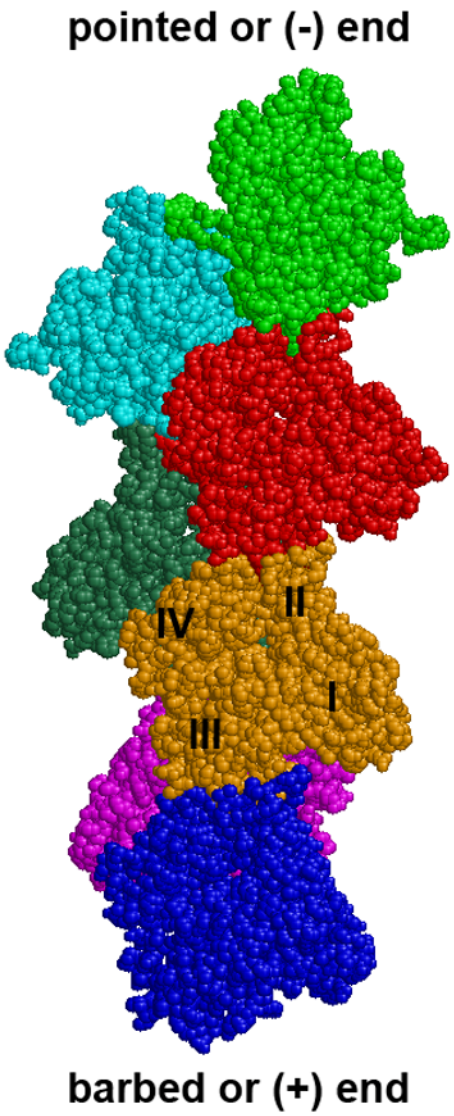
pointed or (-) end
IV
II
I
III
barbed or (+) end

Table 1.1. Actin-binding proteins

Group	Examples	Functional Role	References
Monomer-binding	Profilin	Monomer sequestering, nucleotide exchange	(Schlüter 1997; Paavilainen 2004)
	Thymosin-β4	Monomer sequestering	(Safer 1994; Pollard 2003)
	Srv2/CAP	Recycles ADF/cofilin from G-actin after depolymerization	(Balcer 2003; Paavilainen 2004)
Filament-depolymerizing	ADF/cofilin	Depolymerization of actin filaments/filament turnover	(Bamburg 1999; Ono 2007)
Filament-severing	Gelsolin/ Severin	Severs actin filaments, increases # of (+) ends for polymerization	(Silacci 2004; Ono 2007)
Filament end-binding	CapZ	Binds and caps (+) end of thin filament in muscle	(Weeds 1993; Cooper 2000)
	Tropomodulin	Binds and caps (-) end of thin filament Major (-) end capping-protein in non-muscle cells	(Fischer 2003; Kostyukova 2008)
	Capping Protein (CP)	Major (+) end capping-protein in non-muscle cells	(Wear 2004; Cooper 2008)
De novo filament-nucleation	Arp2/3 complex	Filament side-branching nucleation, crosslinker	(Mullins 1999; Pollard 2003)
	Formin	Nucleation of unbranched, long actin filaments	(Goode 2007)
Motors	Myosin Superfamily	**Currently 23 Classes**	(Foth 2006)
	Myosin I	Single-headed myosin, links filaments to membrane, endocytosis	(Kalhammer 2000)
	Myosin II	Force generation in muscle; non-muscle cells contractile functions	(Sellers 2000)
	Myosin V	(+) end-directed movement of organelles	(Kalhammer 2000)
	Myosin VI	(-) end-directed movement of endocytic vesicles	(Kalhammer 2000; Sellers 2000)
Filament-stabilizing	Tropomysoin	Stabilization/regulates myosin interaction with thin filament	(Gunning 2005; Kostyukova 2008)
Crosslinking/bundling			(Furukawa 1997)
	Fimbrin	Bundles with same polarity/microvilli, filopodia	(Hartwig 1995)
	α-actinin	Crosslinks and bundles/stress fibers, filopodia, muscle Z-line	(Broderick 2005; Sjöblom 2008)
	Spectrin	Links filament networks to plasma membrane	(Hartwig 1995; Broderick 2005)
	Dystrophin	Links cortical actin networks of muscle cells to plasma membrane	(Broderick 2005)
	Filamin	Highly flexible crosslinker/meshworks/leading edge/stress fibers	(Popowicz 2006)
	ABP-34 (34 kDa protein)	Bundles filaments/filopodia/leading edge	(Fechheimer 1987; Fechheimer 1994)

Table 1.2. Hirano bodies and associated diseases

Condition	Cell type/Tissue	References
Alzheimer's disease	Hippocampus CA1, Purkinje cells, Oligodendrocytes	(Gibson 1978; Yamamoto 1985; Mori 1986; Schmidt 1989; Mitake 1997)
Parkinson's disease	Hippocampus CA1	(Hirano 1968)
Pick's disease	Hippocampus CA1	(Schochet 1968)
Amyotrophic lateral sclerosis (ALS)	Hippocampus CA1	(Hirano 1968)
Creutzfeldt-Jakob disease	Hippocampus CA1	(Cartier 1985)
Scrapie and kuru	Cerebellar cortex	(Field 1969; Field 1972)
Hepatic encephalopathy	Hippocampus CA1, Substantia nigra,	(Okamoto 1982)
Chronic alcoholism	Denate nucleus	(Lass 1994)
Neuroblastoma	Stromal cells, Glial cells,	(Fu 1975)
Astrocytoma	Cerebellum	(Gessaga 1975)
Diabetes (rat model)	Peripheral nerves, Oligodendrocytes	(Sima 1983)
Muscle degeneration	Myofibers	(Fisher 1972; Tomonaga 1983; Fernandez 1999)
Brindled mice (Menke's)	Cerebellum, neocortex, cerebral cortex	(Nagara 1980; Peterson 1986)
Wilson's Disease		(Anzil 1974)
General Aging	Hippocampus CA1	(Ogata 1972; Schmidt 1989)

Table 1.3. Hirano body protein components

Protein	Association	References
Actin (F-actin)	Cytoskeleton	(Goldman 1983; Galloway 1987)
α-actinin	F-actin crosslinking protein	(Galloway 1987)
Caspase cleaved actin (Fractin)	Unknown function	(Rossiter 2000)
Coenzyme Q_{10} (Ubiquinine)	Electron transport chain	(Santa-Mara 2008)
Cofilin	Actin-binding protein	(Maciver 1995)
C-terminal fragment of β-APP (AICD)	Transcription regulator	(Munoz 1993; Ha 2010)
FAC1	Transcription repressor	(Jordan-Sciutto 1998)
Hippocampus acetylcholine neurostimulating peptide (HCNP)	Hormone	(Rossiter 2000)
Small heat shock protein 27 (HSP 27)	Stress response	(Renkawek 1994)
Importin α	Cytoplasmic-nuclear transport	(Lee 2006)
Inducible nitric oxide synthase	Stress response	(Lee 1999)
MAPs	Microtubule-binding protein	(Peterson 1988)
Myosin II	Motor protein	(Davis 2008)
Neurofilament subunits L and M	Cytoskeleton	(Schmidt 1989)
P130 (retinoblastoma related protein)	Transcription regulator	(Previll 2007)
Protein Kinase C ι/λ	Cell signaling	(Shao 2006)
Talin	F-actin-crosslinking protein	(Davis 2008)
Transforming growth factor β3	Hormone	(Peress 1995)
Tropomyosin	Actin-binding protein	(Galloway 1987)
Ubiquitin	Protein degradation	(Davis 2008)
Vinculin	Actin-binding protein	(Galloway 1987)
Zyxin	Focal adhesions	(Davis 2008)

Adapted from (Davis 2008)

Figure 1.3. Schematic model of the 34 kDa actin-bundling protein

(A) Cartoon picture of the 34 kDa actin-bundling protein showing the locations of key sites on the 34 kDa protein. They include the N-terminal inhibitory domain (residues 1-70), Interaction Zone 1 (IZ-1, residues 71-123), the calcium binding site (EF2), the strong actin binding site or Interaction Zone 2 (IZ-2), and the C-terminal weak actin binding site (residues 279-295). The NT weak actin-binding site (residues 1-123) is not labeled but is comprised of the N-terminal inhibitory domain and IZ-1. (B) Proposed model for the Ca^{++} regulation of 34 kDa protein. In the absence of a bound calcium ion, IZ-1 forms an intramolecular interaction with IZ-2. The IZ-1/IZ-2 interaction exposes the strong actin-binding site for F-actin binding. Calcium binding at EF2 induces a conformational change within the 34 kDa protein and repositions the N-terminal inhibitory domain in contact with IZ-2, preventing F-actin binding (Lim, 1999b).

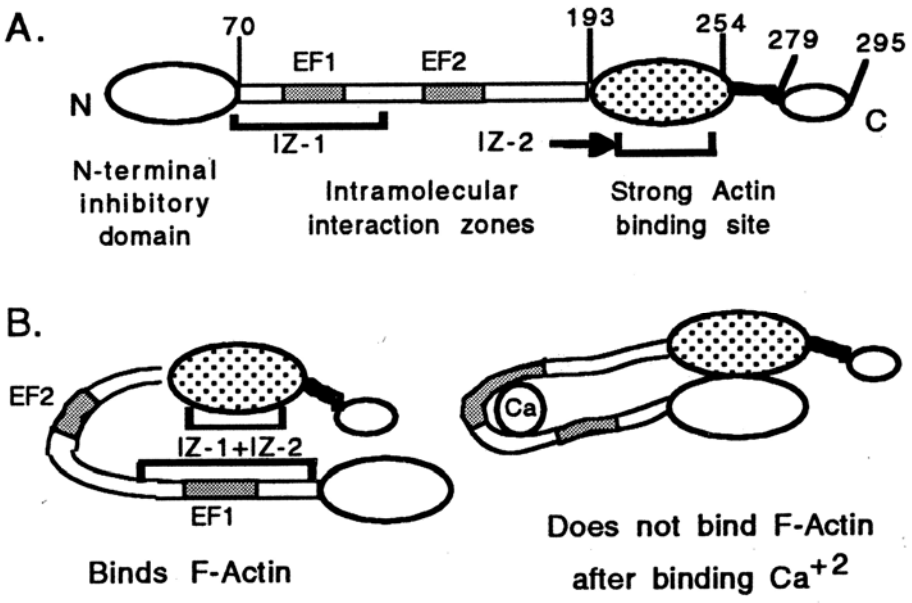
A.
70
193
254
279
295
EF1
EF2
N
C
IZ-1
IZ-2
N-terminal inhibitory domain
Intramolecular interaction zones
Strong Actin binding site
B.
EF2
IZ-1+IZ-2
EF1
Ca
Binds F-Actin
Does not bind F-Actin after binding Ca+2

Chapter 2

THE FORMATION OF HIRANO BODIES REQUIRES BOTH STABILIZATION OF ACTIN FILAMENTS AND CROSSLINKING TO PRODUCE AN ORDERED ARRAY[1]

[1] Paul Griffin, Ruth Furukawa and Marcus Fechheimer. To be submitted to Journal of Cell Science, 2010

Summary

Hirano bodies are paracrystalline F-actin-enriched structures that are defined by their high degree of structural order. However, outside of ultrastructure, not much is known about the biological function of Hirano bodies. Recently, a cell model system for studying Hirano bodies was developed that uses altered forms of the *Dictyostelium* 34 kDa actin-bundling protein that have activated actin binding. In this report, we describe a novel 34 kDa protein mutant, E60K, that has a point mutation at position 60 within the inhibitory domain of 34 kDa protein. We show that (1) E60K protein has actvated F-actin binding but is calcium-regulated, (2) expression of E60K protein in *Dictyostelium* cells leads to the formation of Hirano bodies, (3) both E60K and 34 kDa protein inhibit F-actin depolymerization *in vitro* with E60K protein being more severe, and (4) actin filaments in Hirano bodies are resistant to depolymerization by LatB. Based on our results, we propose that Hirano body formation is the result of both increased actin filament stabilization and actin filament crosslinking.

Introduction

Actin is a major cytoskeletal protein found in all eukaryotic cells. Globular actin or G-actin is a monomeric protein that contains a bound nucleotide. G-actin is able to assemble into large polymers called filamentous actin or F-actin. Both G-actin and F-actin are controlled and regulated by a large number of actin-interacting proteins. A large number of actin-binding proteins modulate the assembly and disassembly of actin filaments (dos Remedios, 2003). For example, unpolymerized actin pools are maintained primarily through G-actin-binding proteins that sequester monomeric actin. By contrast, F-actin-binding proteins help to stabilize F-actin structures. One such class of F-actin-binding protein is characterized by the ability to crosslink

and/or bundle actin filaments into complex structures (Furukawa, 1997). The actin cytoskeleton is involved in many important cellular processes such as cell motility, cell shape, cell signaling, and intracellular trafficking. Thus, the tight regulation of the actin cytoskeleton is important to proper cellular function.

Cytoplasmic aggregations containing actin and actin-binding proteins are associated with a number of neurodegenerative diseases (Bamburg, 2009). One well characterized actin aggregation is Hirano bodies. Hirano bodies are large, F-actin-enriched intracytoplasmic structures that are defined by their paracrystalline filamentous array of F-actin (Goldman, 1983) and actin-binding proteins (Galloway, 1987). Hirano bodies have been described in post-mortem tissues and are found primarily in the CA1 area of Ammons horn of the hippocampus (Hirano, 1968; Schochet, 1968; Wiśniewski, 1970). Hirano bodies have been found to be a associated with a number of different neurodegenerative diseases such as Alzheimer's disease (Gibson, 1977; Mitake, 1997; Schmidt, 1989), Pick's disease (Rewcastle, 1968; Schochet, 1968), amyotrophic lateral sclerosis (ALS) (Hirano, 1968), and Parkinson's Disease (Hirano, 1968). Hirano bodies have also been associated with chronic alcoholism (Lass, 1994) as well as general aging (Hirano, 1994). Despite a large body of literature describing the occurrence of Hirano bodies, the mechanism by which Hirano bodies are formed and their relationship to disease still remains unanswered.

A cellular model system was recently described that enables studies to be done *in vitro* and *in vivo* to shed insight on the formation and cellular consequences of Hirano bodies. Maselli *et al*. reported the development of Hirano body-like structures in the cellular slime mold *Dictyostelium discoideum* and mammalian cells (Maselli, 2002). Hirano bodies were induced to form by the expression of an amino-truncated form of the 34 kDa actin-binding protein (CT)

comprising residues 124-295. The 34 kDa actin-bundling protein is one of eleven actin crosslinking proteins found in *Dictyostelium* (Furukawa, 1997) and has been biochemically characterized as a calcium-sensitive actin-bundling protein (Fechheimer, 1987; Fechheimer, 1993; Fechheimer, 1984). Molecular dissection of recombinant forms of 34 kDa protein have revealed three actin binding sites (residues 1-123, 193-254, and 279-295) as well as an N-terminal inhibitory domain (residues 1-70) that is proposed to regulate 34 kDa protein binding to F-actin (Lim, 1999a; Lim, 1999b). Purified C-terminal fragment (CT; residues 124-295) was characterized *in vitro* and found to possess a calcium-insensitive enhanced F-actin affinity (Lim, 1999a). Therefore, it has been proposed that CT-induced Hirano body formation may be the result of increased F-actin binding and loss of calcium regulation (Maselli, 2002). Further studies using additional mutated forms of 34 kDa protein have revealed that Hirano body formation is not limited to CT but can also be induced by a mutated form of 34 kDa protein called ΔEF1 in which point mutations were used to ablate the x, y, z positions of one of two predicted EF hand motifs (EF1 and EF2) in 34 kDa protein (Maselli, 2003). Biochemical studies with 34 kDa ΔEF1 protein revealed that although it could bind calcium, it also displayed calcium-insensitive increased F-actin binding affinity similar to the CT fragment. Interestingly, studies with another mutant form of 34 kDa protein in which the second EF hand (34 kDa ΔEF2) was mutated resulting in a loss of all calcium binding, revealed that calcium insensitivity did not lead to increased F-actin binding, and furthermore did not induce the formation of Hirano bodies in *Dictyostelium* (Furukawa, 2003).

The goal of this study was to investigate the biochemical or structural features required for induction of the formation of Hirano bodies. We describe a novel mutant form of 34 kDa actin-bundling protein (E60K) that has a point mutation at amino acid position E60 in the

proposed inhibitory domain. Studies of E60K show that although it retains calcium sensitive F-actin binding, it has an almost 3-fold higher F-actin-binding affinity than wild-type 34 kDa protein. We also show that expression of E60K protein in *Dictyostelium* cells leads to the formation of Hirano bodies, which we characterize using both fluorescence microscopy and transmission electron microscopy. Additionally, using the actin depolymerizing drug, latrunculin B (LatB), we demonstrate *in vitro* that depolymerization of filaments cross-linked by either 34 kDa protein or E60K protein is severely inhibited. Finally, we show that the F-actin contained within a Hirano body is resistant to LatB-induced depolymerization. These observations support the hypothesis that both enhanced filament crosslinking and the inhibition of normal actin filament turnover leads to an accumulation of F-actin that is further organized into the highly ordered arrays that comprise the fundamental structure of Hirano bodies.

Materials and methods

Preparation of actin

Actin was prepared and purified from rabbit psoas and leg muscles according to previously established methods (MacLean-Fletcher, 1980; Spudich, 1971). Sephadex G-150 column-purified G-actin was maintained in G-Actin buffer (2 mM Tris-HCl, pH 8.0, 0.2 mM $CaCl_2$, 0.2 mM ATP, 0.2 mM DTT, and 0.02% NaN_3) at 4^{o}C for up to one week with daily dialysis buffer changes. Actin was recycled by polymerization in high salt buffer by bringing final buffer composition to 50 mM KCl, 1 mM ATP, and 1 mM $MgCl_2$. Polymerized actin was spun at 100,000 x g for 2 hours at 4^{o}C. The F-actin pellet was then depolymerized in a small volume of G-actin buffer and maintained as described above.

Generation of bacterial expression vectors

E60K cDNA was sub-cloned from a sequenced pEVII-E60K-EGFP plasmid stock (described below) using PCR and the primer set, LR30K5′ (5′ – TAA **GGA TCC** TTA ACA AGG AGG GTT TTT ACC **ATG** GCA GAA ACA AAA GTT GC -3′) and LR30K3′ (5′ – ACG TA**GGATCC**T TAT TTC TTT TGT GGA CCG T – 3′) into pET-15b (Novagene, USA). PCR with these primers allowed for the insertion of unique *Bam*HI restriction sites on both the 5′ and 3′ end of the coding E60K sequence (*Bam*HI sites highlighted above in bold and underline) as well as removal of EGFP fusion protein. After PCR, the PCR product was digested with *Bam*HI, agarose gel purified using QIAGEN gel extraction system (Qiagen, CA), and ligated into *Bam*HI-digested pET-15b. Ligation mixes were transformed into DH5-α cloning host cells and plated onto ampicillin-selective LB plates. Several clones were picked from selective plates and grown up in LB + ampicillin (100 μg/ml) broth. Plasmid DNA was purified using alkaline lysis method and quantified by Hoescht dye on a Perkin-Elmer flourimeter. Plasmids were sequenced to verify correct E60K nucleotide sequence integrity and orientation at the University of Georgia Molecular Genetics Instrumentation Facility.

Bacterial expression and purification of recombinant proteins

Full-length and mutant forms of 34 kDa actin-bundling protein were expressed in BL21(DE3) cells using the pET-15b expression vector. Bacterial expression of recombinant proteins was induced with 1 mM IPTG for 3 hours. Purification of both recombinant 34 kDa protein and E60K protein was done as previously described (Lim, 1997). After purification, protein concentrations were measured using the BCA assay with bovine albumin as the standard (Smith, 1985). All purified recombinant proteins were dialyzed against 2 mM PIPES pH 7.0, 50 mM KCl, 0.2 mM DTT, 0.03% NaN_3 (34 kDa Storage Buffer) and stored at -80^{o}C.

F-actin co-sedimentation assays

High-speed F-actin co-sedimentation assays were performed as previously described (Fechheimer, 1987; Fechheimer, 1984; Lim, 1997; Maselli, 2003). In order to assess F-actin binding affinity, either 34 kDa protein or E60K protein (3 μM) was mixed with varying concentrations of G-actin (3 μM – 60 μM) under F-actin polymerization conditions (20 mM PIPES, pH 7.0, 50 mM KCl, 1 mM $MgCl_2$, 1 mM ATP, 5 mM EGTA, 0.2 mM DTT). For evaluation of calcium sensitivity, assays were performed in the same buffer above with the addition or omission of 4.5 mM $CaCl_2$ while keeping either 34 kDa protein or E60K protein concentration (3 μM) and actin concentration (3 μM) constant. All co-sedimentation samples were mixed and allowed to polymerize for 2 hours at room temperature. F-actin binding was assessed by centrifugation in a Beckman airfuge at 23 psi (115,000 x g) for 30 minutes. After centrifugation was complete, supernatant and pellet fractions were prepared for analysis by SDS-PAGE, stained with Coomassie blue, and analyzed by scanning densitometry using a Molecular Dynamics Laser Scanning Densitometer.

***Dictyostelium* culture growth and transformation**

Dictyostelium 34-kDa-null cells$^-$ (Rivero, 1996) were grown and maintained as axenic cultures in HL-5 medium supplemented with 10 μg/ml hygromycin at 20^{o}C and 150 rpm (Loomis, 1971). Cell cultures were counted on a hemacytometer and passed continuously to keep cell density below 2.0 x 10^6 cells/ml.

Protein expression of E60K-EGFP and 34kDa-EGFP protein in *Dictyostelium* cells employed an inducible expression vector, pVEII (Blusch, 1992). Protein expression in the pVEII vector is under control of a discoidin promoter that is repressed in the presence of folate. The expression vector used for this study was constructed to express 34 kDa protein fused to a

carboxyl terminal EGFP taken from pEGFP-N1 (Clontech, Palo Alto, California). pEVII-E60K-EGFP was serendipitously generated and found in clone screens during the construction of 34 kDa-EGFP-pVEII for a previously published study (Kim, 2009). Transformation of plasmids pVEII-E60K-EGFP and pVEII-34 kDa-EGFP into 34-kDa-null cells was done by electroporation (Mann, 1998) and transformed cells were plated and allowed to recover for 24 hours in 100 mm petri dishes containing HL5 medium and 1 mM folate. Clone selection was done with 3 μg/mL G418. Once control plates were cleared, remaining clones were selected, grown axenically to cell density of 7.5 x 10^5 cells/ml, and frozen stocks were made in HL5 medium supplemented with 5% DMSO and stored at −80°C. All experiments conducted in this study used fresh cell cultures that were never maintained for > 4 weeks. Cells carrying the pVEII expression vector were not allowed to reach cell densities of greater than 1.0 x 10^6 cells/ml in HL5/G418 medium with 1 mM folate. This was done to ensure that expression from the discoidin promoter in the pVEII vector was repressed. To induce expression, cell cultures were grown to 1.0 x 10^6 cells/ml and harvested by centrifugation (800 x g, 5 minutes, room temperature). Pelleted cells were washed two times with 17 mM phosphate buffer (pH 6.1) and resuspended at 5 x 10^5 cells/ml in HL5/G418 medium. 10 ml of cell suspension was used to inoculate 100 mm petri dishes. Plates were incubated at 20°C. It was empirically determined that maximal expression from the pVEII system was obtained after 16-20 hours after plating. Under these growth conditions, >80% of E60K-EGFP cells contained at least one Hirano body (data not shown).

Fluorescence microscopy

Cells were prepared in 100 mm petri dishes and grown for 16-20 hours for induction of Hirano bodies as described above. The cells were resuspended, counted, pelleted, and resuspended in 17 mM phosphate buffer (pH 6.1) to a final density of 1.0 x 10^6 cells/ml.

Approximately 1.0 x 10^5 total cells were applied to a coverslip and allowed to adhere for 30 minutes at 20^{o}C. Cells on coverslips were fixed for 25 minutes in 3.7% formaldehyde, 17 mM phosphate buffer (pH 6.1) and subsequently permeabilized in acetone at -20^{o}C for 2 minutes (Fechheimer, 1987). TRITC-phalloidin (Sigma, USA) was used to stain F-actin. Fixed and stained coverslips were examined on a Zeiss LSM 510 VIS/META confocal microscope. Images were prepared as described in previous studies (Davis, 2008; Fechheimer, 1987).

Transmission electron microscopy

Negative-stain transmission electron microscopy was used to compare F-actin structures formed by 34 kDa protein and E60K protein. In order to examine the bundling abilities of E60K and 34 kDa protein, 10 μM G-actin was induced to polymerize in 20 mM PIPES pH 7.0, 50 mM KCl, 1 mM $MgCl_2$, 1 mM ATP, 5 mM EGTA, 0.2 mM DTT at 4^{o}C overnight. F-actin polymerized overnight was gently added to either 34 kDa protein or E60K protein to give final concentrations of 5 μM and 2.5 μM, respectively. Actin-only samples were also done in parallel as a control. F-actin structures were deposited onto carbon coated-formvar 400 mesh copper grids by incubating the grid on a small drop of polymerized protein solution. Grids were then briefly washed by incubating on a fresh drop of polymerization buffer, stained for 30 seconds on a drop of 1% uranyl acetate/H_2O, and allowed to air dry. Resulting grids were examined on a JOEL 100 CXII transmission electron microscope operating at 80 kV. Images were photographed on film and scanned at 2,400 dpi for subsequent analysis using ImageJ 1.37. Negatives were prepared using Adobe Photoshop.

E60K-EGFP *Dictyostelium* cells used for transmission electron microscopy were prepared as previously described (Maselli, 2002; Novak, 1995). Epon 812-embedded cells were sectioned on a RMC 5,000 ultramicrotome (Tuscon, AZ), stained with 1 % uranyl acetate/H_2O

for 5 minutes and 4% lead citrate for 30 minutes at room temperature and allowed to air dry. Sections were then examined on a JOEL 100 CXII transmission microscope and recorded on film. Resulting negatives were scanned at 2,400 dpi and prepared for publication using Adobe Photoshop.

Latrunculin B-induced F-actin depolymerization

Latrunculin B (Sigma; a kind gift from Dr. M. Kandasamy and Dr. R. B. Meagher, University of Georgia) was used to *probe* the dynamics and stability of F-actin. These studies were done first *in vitro* by co-sedimentation assays. LatB co-sedimentation assays were done by polymerizing 3 μM actin alone (control), 3 μM E60K + 3 μM actin, and 3 μM 34 kDa protein + 3 μM actin for 2 hours at room temperature. After polymerization, LatB was added to a final concentration of 4.5 μM. LatB treatment was allowed to progress for 2 hours or 24 hours before high-speed centrifugation to pellet F-actin. After 30 minute centrifugation, pellet and supernatant samples were prepared for SDS-PAGE analysis. Resulting gels were analyzed using ImageJ 1.37. Data presented represent three independent trials done in triplicate.

LatB treatment of E60K-EGFP and 34 kDa-EGFP *Dictyostelium* cells was done on 16-20 hour plated cells. Cells were harvested from plates and pelleted by centrifugation at 800 x g for 5 minutes. Cell pellets were re-suspended to a final cell density of 1.0×10^6 cells/ml in 17 mM phosphate buffer (pH 6.1). 99 μM of resuspended cells (1.0×10^6 cells/ml) were deposited onto a cover slip and allowed to adhere for 30 minutes at 20°C. Then 1 μL of either 1 mM LatB in 20% DMSO, 17 mM phosphate buffer pH 6.1(final [LatB] = 10 μM) or 20% DMSO, 17 mM phosphate buffer (control) was added and allowed to mix by diffusion. After 2 hour incubation at 20°C, cells were fixed and stained with TRITC-phalloidin as described above. Coverslips were examined on a Zeiss LSM 510 VIS/META confocal microscope. In order to allow

quantitative fluorescence comparisons to be done, the red channel gain settings for E60K-EGFP and 34 kDa-EGFP *Dictyostelium* cells were set using the "No Lat B"-treated controls for each and held constant for recording of LatB treated cells. Quantitative analysis of changes in TRITC fluorescence was done using ImageJ 1.37.

Results

The availability of a new mutant form of the 34 kDa protein with a single codon change in the inhibitory region of the protein provides a new tool for investigation of the structural and biochemical requirements for formation of Hirano bodies. The E60K mutant form of 34 kDa actin-bundling protein was generated serendipitously during construction of pEVII-34 kDa-EGFP used for a previous study (Kim, 2009). Figure 2.1 shows the nucleotide and corresponding amino acid sequences flanking the amino acid 60 position for wild-type 34 kDa and E60K mutant. A single nucleotide change (G to A) in the codon at position 60 changes the amino acid from a negatively charged glutamate (E) to a positive charged lysine (K). The E60K change occurs in the putative inhibitory region of the 34 kDa protein which spans residues 1–70 (Lim, 1999a). Because truncated forms of the 34 kDa protein lacking the inhibitory region showed activated F-actin binding and an absence of calcium sensitivity, Lim *et al.* proposed that the amino terminal portion of 34 kDa protein (residues 1-70) interacted with the strong actin binding site (residues 193-254) in the presence of micromolar calcium and thereby prevented exposure of the strong site and subsequent binding to F-actin (Lim, 1999a). Hereafter, the 34 kDa protein with the E60K mutation is abbreviated as E60K. The E60K cDNA was subcloned as a non-fusion protein, and both recombinant 34 kDa protein and E60K protein were expressed and purified as previously described (Lim, 1997).

Biochemical characterization of E60K protein *in vitro*

The purified E60K protein was monomeric in solution and was not distinguishable in this regard from the wild-type 34 kDa protein (data not shown) (Fechheimer, 1987). In order to explore what effect the E to K change may have on the F-actin binding affinity of E60K protein, F-actin co-sedimentation assays were used. The binding to F-actin of both 34 kDa protein and E60K protein either in the presence or absence of micromolar calcium was first assessed in mixtures of 3 μM actin and 3 μM 34 kDa protein or E60K protein. In the absence of calcium, the binding of E60K protein was nearly 2.5 times higher than that of 34 kDa protein (1.74 μM E60K and 0.74 μM 34 kDa protein co-sedimented with F-actin, respectively) (Fig. 2.2A). In the presence of micromolar calcium, binding to F-actin by 34 kDa protein was reduced by 40% compared to a 50% reduction in E60K binding (Fig.2.2A). Thus, the E60K protein showed a stronger binding to F-actin at low calcium, and a similar sensitivity to the presence of micromolar calcium (Fig. 2.2A). While these studies showed a difference in the binding of 34 kDa protein and E60K protein to F-actin at a single actin concentration, careful study of the relative F-actin affinity of E60K protein and 34 kDa protein to F-actin required investigation of the binding as a function of actin concentration. Co-sedimentation was studied in solutions containing 3 μM E60K or 34 kDa protein and increasing concentrations of actin from 3 μM to 60 μM under same polymerizing conditions as used in calcium studies. At equimolar actin to 34 kDa protein concentration (3 μM), approximately 1 mole of 34 kDa protein bound to every 5 moles of actin. By comparison, at that same molar ratio, E60K protein bound to actin at 0.65 to 1. Increasing the total actin concentration to 6 μM resulted in nearly all of the E60K protein being bound (2.62 μM), but had only a modest effect on the total amount of 34 kDa protein bound (0.76 μM). Even at very high actin to 34 kDa protein concentrations (20:1), the binding

of the 34 kDa protein to F-actin reached only 2.01 μM, and the saturation of the binding of 34 kDa protein to F-actin was not achieved under the conditions employed. These results confirm a substantially higher affinity of the binding of E60K protein to F-actin as compared to wild-type 34 kDa protein with little or no difference in calcium sensitivity between the two forms.

E60K protein crosslinks and bundles F-actin

Both native and recombinant 34 kDa protein are able to crosslink and bundle F-actin (Fechheimer, 1987; Fechheimer, 1984; Lim, 1997). Therefore, the ability of E60K protein to crosslink and bundle actin filaments was examined by negative stain transmission electron microscopy. Control actin filaments incubated overnight did not form bundles and instead were randomly dispersed (Fig. 2.3A). The 34 kDa protein crosslinked and bundled F-actin, and the bundles varied in width depending on the number of actin filaments contained in them (Fig. 2.3B). The E60K protein also was able to crosslink actin filaments into bundles (Fig. 2.3C). 34 kDa protein bundled actin filaments into arrays that most often resembled "train tracks" with a regular filament spacing of 10-12 nm (Fig. 2.3D). In contrast, bundles that resulted from E60K protein appeared to be "knobby" or "decorated" and their overall filament organization appeared less well ordered than filaments observed in 34 kDa actin bundles (Fig. 2.3E). In addition to actin filament organizational differences, actin bundles formed after co-polymerization overnight in the presence of 34 kDa protein (Fig. 2.4A) were shorter than those observed the presence of E60K protein (Fig. 2.4B). The average length of E60K bundles was 3.98 microns compared to 2.25 microns for 34 kDa protein (Fig. 2.4C). The differences in the binding and bundling of 34 kDa protein and E60K protein to F-actin *in vitro* prompted our study of their physiological effects *in vivo* described below.

E60K protein expression leads to Hirano body formation

Previous studies conducted in our laboratory have demonstrated that specific mutant forms of 34 kDa protein can lead to the formation of Hirano body-like structures when expressed in either *Dictyostelium* or mammalian cells (Davis, 2008; Kim, 2009; Maselli, 2002; Maselli, 2003). The formation of Hirano bodies by mutant 34 kDa proteins is believed to be the result of increased F-actin affinity and loss of calcium sensitivity. Since we determined that E60K protein has an increased F-actin affinity *in vitro* but a normal calcium sensitivity, we explored the possibility that E60K expression could also lead to Hirano body formation in *Dictyostelium*. For this study we transformed the 34 kDa knockout strain, 34-kDa-null *Dictyostelium* (Rivero, 1996) with an EGFP fused at the carboxy-terminus to either 34 kDa protein or E60K protein. The EGFP fusion proteins enabled us to easily visualize the localization of the expressed proteins within the *Dictyostelium* cells. To induce maximum expression of both 34 kDa-EGFP and E60K-EGFP the cells were plated in folate-free HL5/G418 medium overnight at 20^{o}C. Under these growth conditions, > 80% of *Dictyostelium* cells expressing E60K-EGFP contained either one large Hirano body or numerous smaller ones of various sizes. The 34 kDa-EGFP-expressing *Dictyostelium* cells displayed 34 kDa-EGFP protein localization along the cortex of the cell and was enriched in filopodia as previously described (Fig. 2.5A Panel 2) (Fechheimer, 1987; Fechheimer, 1994; Maselli, 2003). Additionally, TRITC-phalloidin staining of the F-actin in these cells showed a co-localization of 34 kDa-EGFP and F-actin (Fig. 2.5A Panels 2 and 3) that has consistently been observed for 34 kDa protein and F-actin. E60K-EGFP-expressing *Dictyostelium* cells had E60K-EGFP localized in oval, punctate structures located within the cytoplasm (Fig. 2.5B Panel 2). Many of these E60K-EGFP structures appeared large and encompassed much of the cytoplasm. TRITC-phalloidin staining revealed that these structures

co-localized with F-actin (Fig. 2.5B Panel 3). The co-localization of E60K-EGFP and F-actin within the oval structures is consistent with the presence of Hirano bodies seen in previous studies done with other mutant forms of 34 kDa protein (Maselli, 2002; Maselli, 2003). However, since F-actin-rich structures must reveal a high level of order to be classified as Hirano bodies, electron microscopy was employed to examine the E60K/F-actin structures.

Ultrastructure of E60K-induced Hirano bodies in *Dictyostelium*

Transmission electron microscopy was used to examine E60K-EGFP-expressing *Dictyostelium* cells. Cells used for this study were checked by fluorescence microscopy to confirm the presence of putative Hirano bodies and then fixed and embedded in resin for thin sectioning. Figure 2.6A is a cross-section through a E60K-EGFP *Dictyostelium* cell. Within the cytoplasm of this cell, there are two inclusions that appear as distinct, electron-dense structures (Fig. 2.6A labeled "HB"). Enlarged images of these inclusions are shown in Figure 2.6B and C. It is important to note that these inclusions differ from the electron-dense nucleolus material contained within the nucleoplasm of the cell (Fig. 2.6A labeled "Nuc"). The nucleolus material is clearly bound within a double nuclear membrane thus delineating it from the cytoplasm. In contrast, the "HB" inclusions are not surrounded by a membrane as can be easily seen compared to the numerous membrane-bound organelles seen around them (Fig. 2.6B, C). Instead, the "HB" inclusions are contained in the cytoplasm consistent with previous reports characterizing Hirano body structures in *Dictyostelium* and mammalian cells (Hirano, 1994; Maselli, 2002). When these inclusions are examined at higher magnification they displayed different patterns of ordered structures. Figure 2.6D-E shows a panel of Hirano bodies with typically observed actin filament packing arrays all of which are characteristic of Hirano body ultrastructural features previously described (Hirano, 1994). Specifically, actin filaments are arranged parallel to one

another with center-to-center filament spacing of 10-12 nm (Fig. 2.6D, E). In addition, two parallel sheets of actin filaments are superimposed on each other at oblique angles thus giving the Hirano body a "cross-hatched" appearance (Fig. 2.6F, G). These morphologies are both characteristic of Hirano bodies as varying patterns of filament arrangement are obtained from different planes of section through these paracrystalline inclusions (Maselli, 2002; Schochet, 1972).

Latrunculin B-induced depolymerization of F-actin

Full-length and truncated forms of 34 kDa protein have been previously shown to affect F-actin depolymerization in a concentration-dependent manner (Lim, 1999b; Zigmond, 1992). It is believed to do so by affecting the "off" rate of actin monomers from the ends of actin filaments and not by capping since the critical concentration is not altered (Zigmond, 1992). The observation that the E60K protein had an increased affinity for F-actin compared to wild-type 34 kDa protein led us to explore the possibility that it may also have an effect on F-actin depolymerization. Solutions containing 3 μM actin, or 3 μM actin plus either 3 μM 34 kDa protein or E60K protein were allowed to co-polymerize overnight. Depolymerization of F-actin was induced by the addition of LatB to a final concentration of 4.5 μM at room temperature for 2 and 24 hours. Co-sedimentation assays were used to determine the amount of F-actin remaining after LatB treatment and compared to control samples that received no LatB. In the absence of LatB, actin-only samples contained 2.34 μM F-actin (Fig. 2.7). Similarly, F-actin concentrations for both 34 kDa protein/actin and E60K/actin solutions were 2.38 μM and 2.52 μM, respectively (Fig. 2.7). LatB decreased the F-actin concentration of the actin-only control to 0.53 μM (Fig. 2.7). In contrast, LatB depolymerization of F-actin was inhibited by the presence of either 34 kDa protein or E60K protein. The F-actin concentration of 34 kDa/actin solutions incubated

with LatB contained 1.53 μM F-actin, while E60K/actin solutions with LatB contained 2.60 μM F-actin (Fig. 2.7). Similar results were observed for 24 hour LatB treatment as well (data not shown). The extent of inhibition of depolymerization was more severe for E60K protein than for 34 kDa protein (2.60 μM vs. 1.53 μM, respectively) and may therefore reflect the increased F-actin-binding affinity of E60K protein described above.

Hirano bodies are resistant to Latrunculin B drug treatment

LatB treatment of *Dictyostelium* induces the depolymerization of the actin cytoskeleton and has been used in numerous studies to examine actin′s role in such cell processes as endocytosis, cell motility, and regulation of contractile vacuoles (Drengk, 2003; Gerisch, 2004; Malchow, 2006). Because Hirano bodies are composed primarily of F-actin (Galloway, 1987; Hirano, 1994), we examined the effect LatB treatment would have on their presence in E60K-EGFP-expressing *Dictyostelium* cells. For this study, both 34 kDa-EGFP and E60K-EGFP *Dictyostelium* were incubated overnight in 100 mm plates to ensure maximum pVEII-induced protein expression and formation of large Hirano bodies in E60K cells. Cells were incubated for 2 hours in the presence or absence of 10 μM LatB, and then fixed and stained for fluorescence microscopy. The 34 kDa-EGFP cells with no LatB treatment had normal cortical 34 kDa protein localization as visualized by GFP fluorescence (Fig. 2.8A). Additionally, TRITC-phalloidin staining revealed that they had a robust F-actin content that also co-localized with 34 kDa-EGFP (Fig. 2.8B). As expected, the E60K-EGFP cells without LatB contained large Hirano bodies that were enriched in E60K-EGFP (Fig. 2.8E) and F-actin (Fig. 2.8F). LatB treatment of 34 kDa-EGFP cells caused a drastic decrease in F-actin content as seen by a loss of TRITC-phalloidin staining (Fig. 2.8D). The 34 kDa-EGFP fluorescence levels remain high, but the cellular distribution of the 34 kDa protein appears to be evenly distributed in the cytoplasm indicating

that it is no longer localized in the cell by the actin cytoskeleton (Fig. 2.8C vs. A). In contrast, E60K-EGFP cells in the presence of LatB had similar E60K-EGFP localization as observed for no LatB E60K-EGFP cells (Fig. 2.8E vs. G). TRITC-phalloidin staining of LatB E60K-EGFP cells shows an overall decrease in cytoplasmic F-actin consistent with that observed in LatB treated 34 kDa-EGFP cells (Fig. 2.8H vs. G) but significantly, the F-actin contained within the Hirano body in the E60K-EGFP cells persisted even after drug treatment as evidenced by the co-localization of E60K-EGFP and TRITC-phalloidin (Fig. 2.8G, H). The decrease in F-actin after LatB treatment for both 34 kDa-EGFP and E60K-EGFP cells was measured by the change in TRITC-phalloidin fluorescence levels of untreated cells and LatB-treated cells using ImageJ software. The 34 kDa-EGFP cells had a 77% decrease in F-actin content when treated with LatB (Table 2.1). Similarly, LatB treated E60K-EGFP cells that contained no Hirano bodies had a reduction in F-actin levels of 81% (Table 2.1). LatB treatment of E60K-EGFP cells that contained at least one Hirano body showed a less severe reduction of F-actin (43%). The higher F-actin levels measured in these cells is due to the persistence of the F-actin contained within the Hirano body; cytoplasmic F-actin levels of these cells appears to decrease similarly as cells without Hirano bodies (Fig. 2.8B vs. F). Measurements of TRITC-phalloidin fluorescence levels contained within the Hirano bodies plus and minus LatB treatment revealed that a small portion of the F-actin in Hirano bodies was susceptible to depolymerization by LatB (31% reduction; Table 2.1). However, even this modest reduction in F-actin within the Hirano bodies was not sufficient to completely disassemble a large Hirano body as evidenced by the large numbers of E60K-EGFP cells with Hirano bodies after LatB treatment (Fig. 2H). Similar Hirano body persistence was observed for longer LatB exposure times but is not shown here because of rising levels of cell death associated with longer LatB treatment. These results show that F-actin within

Hirano bodies is less susceptible to disassembly by LatB, indicating a decreased rate constant for monomer leaving the filament.

Discussion

The actin cytoskeleton has many diverse roles within a cell that continue to be the focus of most research on this topic. However, abnormalities associated with the F-actin cytoskeleton leading to formation of F-actin inclusion bodies are associated with a number of neurodegenerative diseases, and remain poorly understood (Bamburg, 2009). Since the actin cytoskeleton has many diverse roles, components, and regulatory networks within cells, these F-actin inclusion bodies could result from abnormalities in a variety of cellular pathways. Furthermore, the function of these F-actin structures in disease progression is also unknown.

Hirano bodies are F-actin-rich aggregates that accumulate in association with a number of conditions including neurodegenerative disease, aging, and chronic alcoholism (Hirano, 1994). They are identified by a paracrystalline organization, distinctive morphology, and highly ordered filament arrays. Yet, the changes in cytoskeletal regulation and dynamics that trigger formation of Hirano bodies are incompletely understood, and the physiological function and roles of Hirano bodies in disease progression are completely unknown. Therefore, the characterization of potential biological mechanisms leading to F-actin inclusion body formation will be useful in understanding possible pathological or protective roles of the actin cytoskeleton. In the present study, we used a mutant form of the 34 kDa actin-bundling protein (E60K) from *Dictyostelium discoideum* to examine the structural and dynamic changes leading to formation of Hirano bodies in *Dictyostelium*.

The E60K mutant of the *Dictyostelium* 34 kDa actin bundling protein contains a single amino acid substitution at position 60 that results in a change of glutamate (E) to lysine (K) (Fig. 2.1). The glutamate at codon 60 resides within the N-terminal region of 34 kDa protein that was identified as an inhibitory region, since truncation of this domain activates actin binding and abrogates calcium regulation of F-actin binding (Lim, 1999a). Consequently, it was proposed that the N-terminal portion of 34 kDa protein (residues 1-70) interacted with the strong actin-binding site (residues 193-254) in the presence of micromolar calcium, and prevented its interaction with F-actin (Lim, 1999a). Our study of the interaction of the E60K protein with F-actin *in vitro* and *in vivo* was designed to illuminate the structural and biochemical importance of the N-terminal inhibitory region and the requirements for the formation of Hirano bodies.

High-speed F-actin co-sedimentation assays were used to determine the calcium-sensitive binding of E60K protein. Using equimolar amounts of actin and either 34 kDa or E60K protein we showed that E60K and 34 kDa protein had similar reductions (50% vs. 40%, respectively) in F-actin binding in the presence of micromolar calcium (Fig. 2.2A). However, it is important to note that in the absence of calcium, 1.74 μM E60K protein co-sedimented with 3 μM F-actin compared to only 0.74 μM 34 kDa protein. This is significant because although E60K protein is calcium-sensitive, the observed 50% reduction in E60K protein bound to F-actin means that 0.88 μM remains bound and this concentration of E60K protein is higher than the total amount of 34 kDa protein bound to F-actin in the absence of any calcium (0.74 μM) (Fig. 2.2A). Furthermore, increasing the F-actin to 34 kDa protein/E60K protein molar ratio to 2:1 was sufficient to bind almost 90% of E60K protein while only 25% of 34 kDa was bound to F-actin (Fig. 2.2B). Therefore, the E60K protein has a higher affinity for F-actin, but a similar calcium sensitivity as compared to the wild-type protein. Thus, the E60K protein differs from previously characterized

truncated forms such as CT (residues 124–295) (Maselli, 2002) and 34 kDa ΔEF1 (Maselli, 2003) that both show activated F-actin binding and loss of calcium sensitivity. This could have profound consequences in a cellular environment, because E60K protein's higher affinity for F-actin could lead to altered F-actin dynamics. Further, our prior study of a 34 kDa ΔEF2 protein with a normal level of F-actin binding, but lacking calcium sensitivity, showed that calcium regulation of F-actin crosslinking is required to restore the normal function of the 34 kDa protein to strains lacking one or more F-actin crosslinking proteins (Furukawa, 2003).

It has been established previously that the wild-type 34 kDa protein inhibits F-actin depolymerization in a concentration-dependent manner with half-maximal inhibition of the rate of F-actin depolymerization *in vitro* at a 34 kDa:F-actin ratio of 1:25 (Zigmond, 1992). Therefore, we decided to examine if E60K protein also affected F-actin depolymerization. Using F-actin co-sedimentation assays and the F-actin depolymerizing drug, LatB, we showed that both 34 kDa protein and E60K protein inhibited depolymerization of F-actin induced by LatB. Significantly, the E60K protein was able to completely inhibit any LatB-induced depolymerization of F-actin, because F-actin concentrations remained unchanged in both the 2 hour and 24 hour drug incubations (Fig. 2.7). LatB drives F-actin depolymerization by binding to and sequestering G-actin (Yarmola, 2000). The fact that E60K protein bound F-actin did not depolymerize suggests that the F-actin contained in the E60K-actin filaments was not "treadmilling" and thus was not generating a pool of G-actin that would then be accessible to sequestration by LatB. This stabilization of actin monomers within the filament seems likely to be the consequence of a decreased dissociation rate of E60K protein which is also consistent with the higher affinity of the E60K protein for F-actin that was measured directly. Our recent chemical crosslinking and mass spectrometry studies of the molecular interactions

between 34 kDa protein and F-actin *in vitro* provide a molecular explanation for the ability of the 34 kDa protein to stabilize actin filaments. Chemical crosslinking of mixtures of the 34 kDa protein and F-actin followed by analysis by tandem mass spectrometry shows that 34 kDa protein contacts regions on successive actin monomers that are directly juxtaposed in the proposed actin filament structure, so that the 34 kDa protein would essentially stabilize this contact along the filament axis (Griffin, Hoffman, Furukawa, Amster, and Fechheimer, unpublished data).

We also examined the actin structures in *Dictyostelium* cells expressing 34 kDa protein or the E60K variant to determine whether the actin structures were also less dynamic and resistant to disassembly *in vivo*. E60K-EGFP-expressing *Dictyostelium* cells were incubated with 10 μM LatB for 2 hours resulting in a decrease in cytoplasmic F-actin and comparable to what was observed in 34 kDa-EGFP control cells (Fig. 2.8D, H). However, it was striking that the F-actin contained within the Hirano bodies was more resistant to depolymerization (Fig. 2.8H). LatB treatment failed to completely disassemble large Hirano bodies, suggesting that the F-actin contained within them was stabilized and thus resistant to LatB treatment. This observation agrees well with our *in vitro* LatB co-sedimentation assays reported earlier. It is important to note that although large Hirano bodies persisted after LatB treatment, there did seem to be a change in the overall morphology of the Hirano bodies. Figure 2.8F and H show that prior to LatB treatment, large Hirano bodies appear round with tight margins. However, after LatB treatment they appear less defined, and the characteristic round shape is lost (Fig. 2.8F vs. H). The resulting LatB-treated large Hirano bodies therefore may be undergoing some F-actin depolymerization along the periphery of the Hirano body.

We next examined the crosslinking and bundling of actin filaments. The 34 kDa protein crosslinks and bundles actin filaments (Fig. 2.3B) (Fechheimer, 1987; Fechheimer, 1984). Negative staining of 34 kDa-actin bundles reveals that they are predominantly composed of parallel actin filaments that have a filament center to center spacing of 10-12 nm (Fig. 2.3D). These bundles of 34 kDa protein and actin have a thin sheet-like appearance similar to that observed in actin bundles induced by other bundling proteins such as talin (Zhang, 1996) and α-actinin (Meyer, 1990). E60K protein also crosslinks and bundles actin filaments (Fig. 2.3C). However, the morphology of E60K-actin bundles appears different from that of typical 34 kDa-actin bundles (Fig. 2.3D). Although occasionally thin sheet-like bundles can be found in E60K preparations, filaments in these E60K-actin bundles appear to have less longitudinal periodicity than those typically observed in the presence of 34 kDa protein. Bundles of E60K-actin also appear more decorated because of the high affinity binding of E60K protein, making it difficult to resolve individual filaments within the bundle (Fig. 2.3D). Under conditions used for the preparation of actin bundles for TEM (5 μM actin; 2.5 μM E60K or 34 kDa protein), our co-sedimentation results would predict that 90% of the E60K protein should be bound to F-actin. This would result in actin filaments that have many molecules of E60K bound to them, causing them to appear decorated and hard to resolve. The E60K bundle also appears to have actin filaments that are twisted, giving the appearance of an irregular, braided pattern (Fig. 2.3C, E). This unique appearance could be attributed to increased lateral contacts made possible by the high amount of E60K protein bound to each filament. Increasing the number of lateral contacts between actin filaments would most likely result in filament arrangements that do not favor the thin sheet-like arrangement most commonly observed in 34 kDa-actin bundles. Instead, filament arrangement would be dependent on available crosslinks, and in the highly decorated E60K-actin

bundles, filament packing would likely be less regular because of the large number of E60K crosslinks that presumably are available around the entire helical twist of an actin filament. Low magnification views of 34 kDa- and E60K-actin bundles reveal the effect that the increased F-actin affinity of E60K protein has on bundle length (Fig. 2.4A, B). Measurements of random bundle length for E60K protein and 34 kDa protein reveals that E60K-actin bundles are almost twice the average length of 34 kDa-actin bundles (Fig. 2.4C). In agreement with data already discussed here, this increase in average bundle length is likely due to the increased affinity of E60K protein for F-actin. This increase in bundle length could be the result of either a reduced dissociation rate for E60K protein and/or an increased stabilization of actin filaments caused by the presence of many more lateral contacts between filaments contained within an E60K-actin bundle. Additionally, the observed increase in bundle length for E60K-actin bundles may arise from a difference in structural strength. E60K-actin bundles may be more resistant to breakage because of the increased structural integrity that results from the increased number of filament-filament lateral contacts that E60K is able to provide in contrast to the number of 34 kDa lateral contacts.

What then is the key element required for induction of the formation of Hirano bodies? Previous studies using either a mutant form of 34 kDa protein (34 kDa ΔEF1) or a C-terminally truncated form of 34 kDa protein (CT) have been shown to have increased F-actin affinity and loss of calcium sensitivity, and when expressed in *Dictyostelium* or mammalian cells they induce the formation of Hirano bodies (Davis, 2008; Maselli, 2002; Maselli, 2003). The E60K protein is also able to induce the formation of Hirano bodies *in vivo* (Fig. 2.5). These observations of E60K-induced Hirano bodies are consistent with previous studies of Hirano bodies formed with altered forms of 34 kDa protein (Davis, 2008; Maselli, 2002; Maselli, 2003) and studies done

with human brain sections (Hirano, 1994). Higher magnification views of E60K-induced Hirano bodies (Fig. 2.6) show that the ultrastructure of the actin filaments contained within the inclusions is consistent with what has been previously described to define an actin inclusion body as a Hirano body (Hirano, 1994; Schochet, 1972).

Our findings with a variety of altered forms of the 34 kDa protein are summarized in Table 2.2. Altered forms of 34 kDa protein with loss of calcium sensitivity coupled with activation of F-actin binding (CT and 34 kDa ΔEF1) are competent to induce formation of Hirano bodies (Maselli, 2002; Maselli, 2003). However, a 34 kDa mutant exhibiting loss of calcium sensitivity without activation of actin binding does not induce Hirano bodies (Furukawa, 2003). Our studies of the characteristics of the E60K protein support the proposal that the ability to induce formation of Hirano bodies is due to enhanced actin binding, and show for the first time that this is the key activity. Loss of calcium sensitivity in combination with activated F-actin binding is not required to induce formation of Hirano bodies. Furthermore, our studies with LatB show that the enhanced affinity for actin filaments is coupled to a stabilization of the actin filaments and an inhibition of the rate of filament disassembly both *in vitro* and *in vivo* (Figs. 2.7 and 2.8).

It is important to point out here that F-actin-enriched inclusion bodies can be induced to form by several different methods. For example, the actin filament stabilizing drugs, phalloidin and jasplakinolide, have been shown to induce the formation of large F-actin aggregates in *Dictyostelium* (Lee, 1998). More recently, jasplakinolide was shown to induce the formation of F-actin aggregates in cultured mammalian cells (Lázaro-Diéguez, 2008a; Lázaro-Diéguez, 2008b). It is striking that phalloidin, jasplakinolide, and activated forms of 34 kDa protein all possess the ability to stabilize actin filaments, suggesting that this property is a key feature of the

requirements for induction of these inclusions of the actin cytoskeleton. However, jasplakinolid-induced actin aggregations in *Dictyostelium* are amorphous and lack the regular order of Hirano bodies (personal communication from Dr. Andrew Maselli). Furthermore, the ultrastructure of the F-actin aggregates in mammalian cells also do not display the regular actin filament arrangement that is observed in Hirano bodies (Lázaro-Diéguez, 2008a; Lázaro-Diéguez, 2008b). Thus, we conclude that the formation of Hirano bodies requires an activity to stabilize actin filaments but that a second activity, filament crosslinking, is required to bring the filaments into ordered arrays. More recently, Schmauch *et al.* reported the formation of large F-actin aggregates in *Dictyostelium* using the *Dictyostelium* homolog of VASP, which they mistargetted to the surface of the endosome (Schmauch, 2009). When viewed by fluorescence microscopy, these F-actin aggregates appear very similar to Hirano bodies induced by altered forms of 34 kDa protein. However, thin sections of VASP-induced F-actin aggregates by TEM revealed an intermediate actin filament arrangement that is more organized than aggregates formed with drug treatment, but which still lacks the highly ordered actin filament arrangement characteristic of a Hirano body. It seems likely that tethering to the membrane led to a stabilization of actin filaments or at least to a high local concentration of actin filaments. However, in the absence of a crosslinking activity to order the array, a Hirano body-like structure was not observed. Neither jasplakinolide nor targeting of VASP to endosomes faithfully mimics all of the characteristics of Hirano bodies in brain. Thus, the actin filament arrangement observed in Hirano bodies likely arises from a combination of factors including inhibition of actin filament disassembly, a high local actin concentration, and specific crosslinking to induce alignment of filaments. Continued study of the structure, dynamics, and physiological function of Hirano bodies will help us to understand the role of these structures in normal cells, and in disease.

Acknowledgements

This work was supported by awards to RF and MF from NSF (MCB 98-08748), the Alzheimer's Association (IIRG-00-2436), and NIH (1R01-NS04645101).

References

Bamburg, J. R., and Bloom, G. S. (2009). Cytoskeletal pathologies of Alzheimer disease. *Cell Motil. Cytoskeleton* **66**, 635-649.

Blusch, J., Morandini, P. and Nellen, W. (1992). Transcriptional regulation by folate: Inducible gene expression in *Dictyostelium* transformants during growth and early development. *Nucl. Acids Res.* **20**, 6235-6238.

Davis, R. C., Furukawa, R. and Fechheimer, M. (2008). A cell culture model for investigation of Hirano bodies. *Acta Neuropathol.* **115**, 205-217.

dos Remedios, C. G., Chhabra, D., Kekic, M., Dedova, I. V., Tsubakihara, M., Berry, D. A. and Noswort, N. J. (2003). Actin binding proteins: regulation of cytoskeletal microfilaments. *Physiol. Rev.* **83**, 433-73.

Drengk, A., Fritsch, J., Schmauch, C., Rühling,H. and Maniak, M. (2003). A coat of filamentous actin prevents clustering of late-endosomal vacuoles *in vivo*. *Curr. Biol.* **13**, 1814-9.

Fechheimer, M. (1987). The *Dictyostelium discoideum* 30,000-dalton protein is an actin filament-bundling protein that is selectively present in filopodia. *J. Cell Biol.* **104**, 1539-51.

Fechheimer, M., and Furukawa, R. (1993). A 27,000 dalton core of the *Dictyostelium* 34,000 dalton protein retains Ca+2-regulated actin cross-linking but lacks bundling activity. *J. Cell Biol.* **120**, 1169-76.

Fechheimer, M., and Taylor, D. L. (1984). Isolation and characterization of a 30,000-dalton calcium-sensitive actin cross-linking protein from *Dictyostelium discoideum*. *J. Biol. Chem.* **259**, 4514-20.

Fechheimer, M., Ingalls, H. M., Furukawa, R. and Luna, E. J. (1994). Association of the *Dictyostelium* 30,000 dalton actin bundling protein with contact regions. *J. Cell Sci.* **107**, 2393-401.

Furukawa, R., and Fechheimer, M. (1997). The structure, function, and assembly of actin filament bundles. *Int. Rev. of Cytol.* **175**, 29-90.

Furukawa, R., Maselli, A. G., Thomson, S. A. M., Lim, R. W.-L., Stokes, J. V. and Fechheimer, M. (2003). Calcium regulation of actin cross-linking is important for function of the actin cytoskeleton in *Dictyostelium*. *J. Cell Sci.* **116**, 187-96.

Galloway, P. G., Perry, G. and Gambetti, P. (1987). Hirano body filaments contain actin and actin-associated proteins. *J. Neuropathol. Exp. Neurol.* **46**, 185-99.

Gerisch, G., Bretschneider, T., Müller-Taubenberger, A., Simmeth, E., Ecke, M., Diez, S. and Anderson, K. (2004). Mobile actin clusters and traveling waves in cells recovering from actin depolymerization. *Biophys. J.* **87**, 3493-503.

Gibson, P. H., and Tomlinson, B. E. (1977). Numbers of Hirano bodies in the hippocampus of normal and demented people with Alzheimer's disease. *J. Neurol. Sci.* **33**, 199-206.

Goldman, J. E. (1983). The association of actin with Hirano bodies. *J. Neuropathol. Exp. Neurol.* **42**, 146-52.

Hirano, A. (1994). Hirano bodies and related neuronal inclusions. *Neuropathol. Appl. Neurobiol.* **20**, 3-11.

Hirano, A., Dembitzer, H. M., Kurland, L. T. and Zimmerman, H. M. (1968). The fine structure of some intraganglionic alterations. *J. Neuropathol. Exp. Neurol.* **27**, 167-82.

Kim, D.-H., Davis, R. C., Furukawa, R. and Fechheimer, M. (2009). Autophagy contributes to the degradation of hirano bodies. *Autophagy* **5**, 1-8.

Lass, R., and Hagel, C. (1994). Hirano bodies and chronic alcoholism. *Neuropathol. Appl. Neurobiol.* **20**, 12-21.

Lázaro-Diéguez, F., Aguado, C., Mato, E., Sánchez-Ruíz, Y., Esteban, I., Alberch, J., Knecht, E. and Egea, G. (2008a). Dynamics of an F-actin aggresome generated by the actin-stabilizing toxin jasplakinolide. *J. Cell Sci.* **121**, 1415-25.

Lázaro-Diéguez, F., Knecht, E. and Egea, G. (2008b). Clearance of a Hirano body-like F-actin aggresome generated by jasplakinolide. *Autophagy* **4**, 717-20.

Lee, E., Shelden, E. A. and Knecht, D. A. (1998). Formation of F-actin aggregates in cells treated with actin stabilizing drugs. *Cell Motil. Cytoskel.* **39**, 122-33.

Lim, R. W. L., and Fechheimer, M. (1997). Overexpression, purification, and characterization of recombinant *Dictyostelium discoideum* calcium regulated 34,000 dalton F-actin bundling protein from *Escherichia coli*. *Protein Expr. Purif.* **9**, 182-90.

Lim, R. W. L., Furukawa, R. and Fechheimer, M. (1999a). Evidence of intramolecular regulation of the *Dictyostelium discoideum* 34,000 dalton F-actin bundling protein. *Biochemistry* **38**, 16323-32.

Lim, R. W. L., Furukawa, R., Eagle, S., Cartwright, R. C. and Fechheimer, M. (1999b). Three distinct F-actin binding sites in the *Dictyostelium discoideum* 34,000 dalton actin bundling protein. *Biochemistry* **38**, 800-12.

Loomis, W. F. (1971). Sensitivity of *Dictyostelium discoideum* to nucleic acid analogues. *Exp. Cell Res.* **64**, 484-86.

MacLean-Fletcher, S. D., and Pollard, T. D. (1980). Identification of a factor in conventional muscle actin preparations which inhibits actin filament self-association. *Biochem. Biophys. Res. Commun.* **96**, 18-27.

Malchow, D., Lusche, D. F., Schlatterer, C. F., De Lozanne, A. and Müller-Taubenberger, A. (2006). The contractile vacuole in Ca2+-regulation in *Dictyostelium*: its essential function for cAMP-induced Ca2+-influx. *BMC Dev. Biol.* **6**, 31-9.

Mann, S. K. O., Devreotes, P. N., Eliott, S., Jermyn,K., Kuspa, A., Fechheimer, M., Furukawa, R., Parent, C. A., Segall, J., Shaulsky, G., Vardy, P. H., Williams, J., Williams, K. and Firtel, R. A. (1998). Cell biological, molecular genetic, and biochemical methods to examine *Dictyostelium*. In *Cell biology: a laboratory handbook*, vol. 1 (ed. J. E. Celis), pp. 431-465. San Diego: Academic Press, Inc.

Maselli, A. G., Davis, R., Furukawa, R. and Fechheimer, M. (2002). Formation of Hirano bodies in *Dictyostelium* and mammalian cells induced by expression of a modified form of an actin cross-linking protein. *J. Cell Sci.* **115**, 1939-52.

Maselli, A. G., Furukawa, R., Thomson, S. A. M., Davis, R. C. and Fechheimer, M. (2003). Formation of Hirano bodies induced by the expression of an actin cross-linking protein with a gain of function mutation. *Eucaryot. Cell* **2**, 778-87.

Meyer, R. K., and Aebi, U. (1990). Bundling of actin filaments by alpha-actinin depends on its molecular length. *J. Cell Biol.* **110**, 2013-24.

Mitake, S., Ojika, K. and Hirano, A. (1997). Hirano bodies and Alzheimer's disease. *Kao-Hsiung I Hseuh K'o Tsa Chih* **13**, 10-8.

Novak, K. D., Peterson, M. D., Reedy, M. C. and Titus, M. A. (1995). *Dictyostelium* myosin I double mutants exhibit conditional defects in pinocytosis. *J. Cell Biol.* **131**, 1205-21.

Rewcastle, N. B., and Ball, M. J. (1968). Electron microscopic structure of the "inclusion bodies" in Pick's disease. *Neurology* **18**, 1205-13.

Rivero, F., Furukawa, R., Noegel, A. A. and Fechheimer, M. (1996). *Dictyostelium discoideum* cells lacking the 34,000 dalton actin binding protein can grow, locomote, and develop, but exhibit defects in regulation of cell structure and movement: a case of partial redundancy. *J. Cell Biol.* **135**, 965-80.

Schmauch, C., Claussner, S., Zöltzer, H. and Maniak, M. (2009). Targeting the actin-binding protein VASP to late endosomes induces the formation of giant actin aggregates. *Eur. J. Cell Biol.* **88**, 385-96.

Schmidt, M. L., V. M. Lee, J. Q. Trojanowski. (1989). Analysis of epitopes shared by Hirano bodies and neurofilament proteins in normal and Alzheimer's disease hippocampus. *Lab. Investig.* **60**, 513-522.

Schochet, S. S. J., and McCormick, W. F. (1972). Ultrastructure of Hirano bodies. *Acta Neuropathol.* **21**, 50-60.

Schochet, S. S. J., Lampert, P. W. and Lindenburg, R. (1968). Fine structure of the Pick and Hirano bodies in a case of Pick's disease. *Acta Neuropathol. (Berlin)* **11**, 330-7.

Smith, P. K., Krohn, R. I., Hermanson, G. T., Mallia, A. K., Gartner, F. H., Provenzano, M. D., Fujimoto, E. K., Goeke, N. M., Olson, B. J. and Klenk, D. C. (1985). Measurement of protein using bicinchoninic acid. *Anal. Biochem.* **150**, 76-85.

Spudich, J. A., and Watt, S. (1971). The regulation of rabbit skeletal muscle contraction. *J. Biol. Chem.* **246**, 4866-71.

Wiśniewski, H., Terry, R. D. and Hirano, A. (1970). Neurofibrillary pathology. *J. Neuropathol. Exp. Neurol.* **29**, 163-76.

Yarmola, E. G., Somasundaram, T., Boring, T. A., Spector, I. and Bubb, M. R. (2000). Actin-latrunculin A structure and function. Differential modulation of actin-binding protein function by latrunculin A. *J. Biol. Chem.* **275**, 28120-7.

Zhang, J., Robson, R. M., Schmidt, J. M. and Stromer, M. H. (1996). Talin can crosslink actin filaments into both networks and bundles. *Biochem. Biophys. Res. Commun.* **218**, 530-7.

Zigmond, S. H., Furukawa, R. and Fechheimer, M. (1992). Inhibition of actin filament depolymerization by the *Dictyostelium* 30,000-D actin-bundling protein. *J. Cell Biol.* **119**, 559-67.

Figure 2.1. Nucleotide and amino acid sequence for wild-type 34 kDa and E60K flanking the position 60 site. The site of mutation at position 60 is marked with an asterisk with the corresponding codon and amino acid for wild-type 34 kDa and E60K highlighted in bold type.

	53							60*							67
WT 34 kDa	Y	W	A	Q	V	S	K	**E**	A	E	F	I	Y	S	V
	TAT	TGG	GCT	GAA	GTT	AGC	AAA	**GAA**	GCT	GAA	TTC	ATC	TAT	TCC	GTT
E60K	Y	W	A	Q	V	S	K	**K**	A	E	F	I	Y	S	V
	TAT	TGG	GCT	GAA	GTT	AGC	AAA	**AAA**	GCT	GAA	TTC	ATC	TAT	TCC	GTT

Figure 2.2. F-actin binding for 34 kDa and E60K proteins assayed by co-sedimentation. (A) Determination of calcium-sensitive F-actin binding for 34 kDa and E60K proteins. Equimolar concentrations (3 μM) of actin and either 34 kDa protein or E60K protein were compared in the presence of low or high calcium. The E60K protein had similar calcium sensitive F-actin binding to 34 kDa protein. Error bars represent SEM. (B) Saturation binding for E60K protein and 34 kDa protein was assayed by increasing the total actin concentration. E60K protein was saturated by a 2:1 molar ratio (actin:E60K), while 34 kDa protein never achieved saturation even at 20:1 molar ratio (actin:34 kDa).

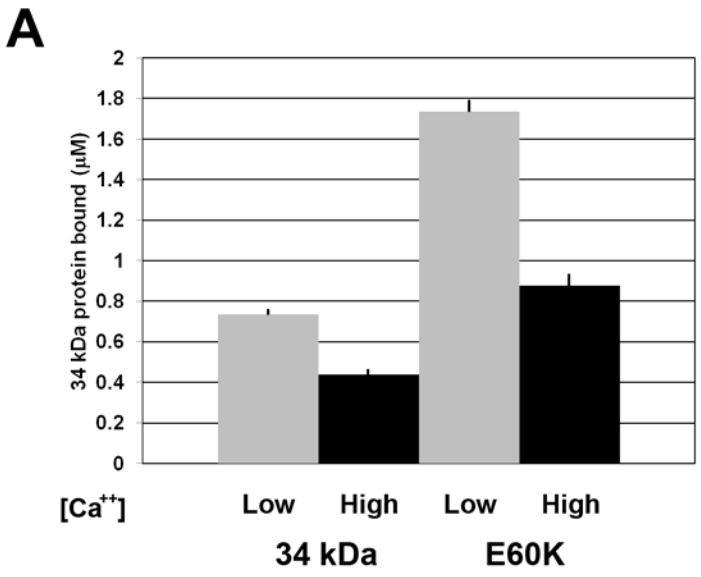
A
34 kDa protein bound (μM)
2
1.8
1.6
1.4
1.2
1
0.8
0.6
0.4
0.2
0
[Ca++]
Low
High
Low
High
34 kDa
E60K

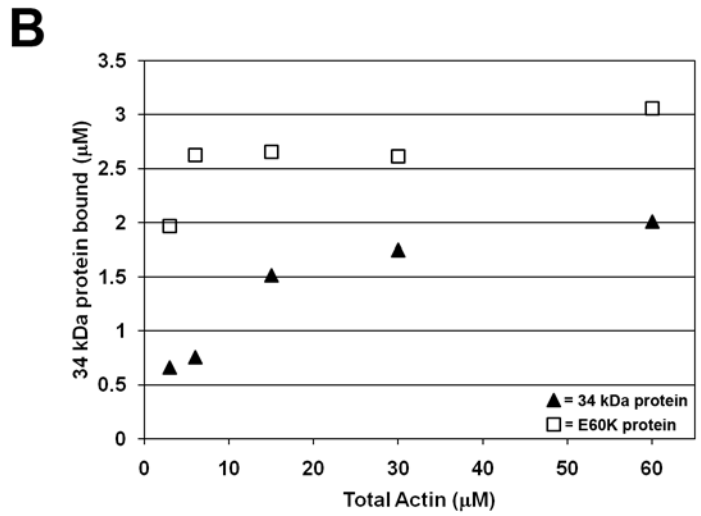
B
34 kDa protein bound (μM)
3.5
3
2.5
2
1.5
1
0.5
0
0
10
20
30
40
50
60
Total Actin (μM)
▲ = 34 kDa protein
□ = E60K protein

Figure 2.3. Electron micrographs of 5 μM actin polymerized overnight in the absence or presence of either 2.5 μM 34 kDa protein or E60K protein. (A) Control actin polymerized in the absence of crosslinking protein. (B) Actin polymerized in the presence of 34 kDa protein. (C) Actin polymerized in the presence of E60K protein. Scale bar = 250 nm. (D) and (E) Higher magnification electron micrographs of actin bundles formed as a result of crosslinking by 34 kDa protein or E60K protein. (D) 34 kDa protein-induced actin bundles. Filament arrangement in bundles is well-ordered and parallel. Most filaments are evenly spaced along the length of the bundle into 2-dimensional thin sheets. (E) E60K protein-induced actin bundles. Bundles formed in the presence of E60K have varied filament arrangements. Some bundles have filament areas that are thin sheet-like arrangements, but often this periodicity did not extend very far. However, most bundles show mixed periodicity and appear to be decorated, making it hard to resolve individual filaments. Scale bar = 100 nm.

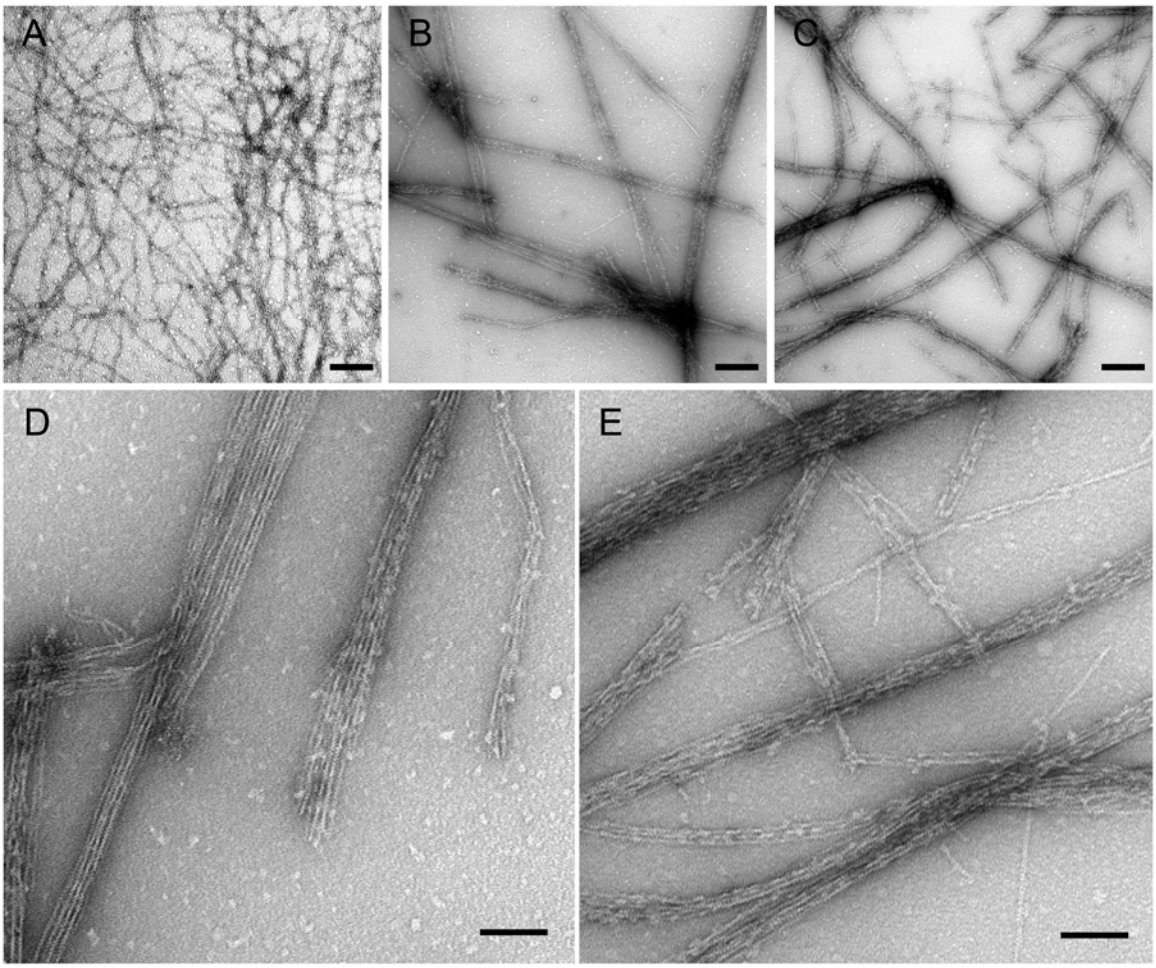
A
B
C
D
E

Figure 2.4. Low magnification electron micrographs of actin bundles formed in the presence of either 34 kDa protein or E60K protein. (A) 34 kDa protein-induced actin bundles. The bundles formed in the presence of 34 kDa protein appear much shorter than those observed in the presence of the E60K protein (B). (C) Summary graph of the average bundle lengths measured for F-actin polymerized overnight in the presence of 34 kDa protein or E60K protein. Average bundle length was calculated by measuring the lengths of only those bundles having both ends in the field of view. The average length of E60K F-actin bundles was almost twice that observed for 34 kDa F-actin bundles (3.98 ± 0.34 μm (SEM) vs. 2.25 ± 0.14 μm (SEM) respectively). The high-affinity binding of the E60K protein may help stabilize F-actin, thereby resulting in increased bundle length. (N=86 for 34 kDa bundles; N=62 for E60K bundles). Scale bar = 1 micron.

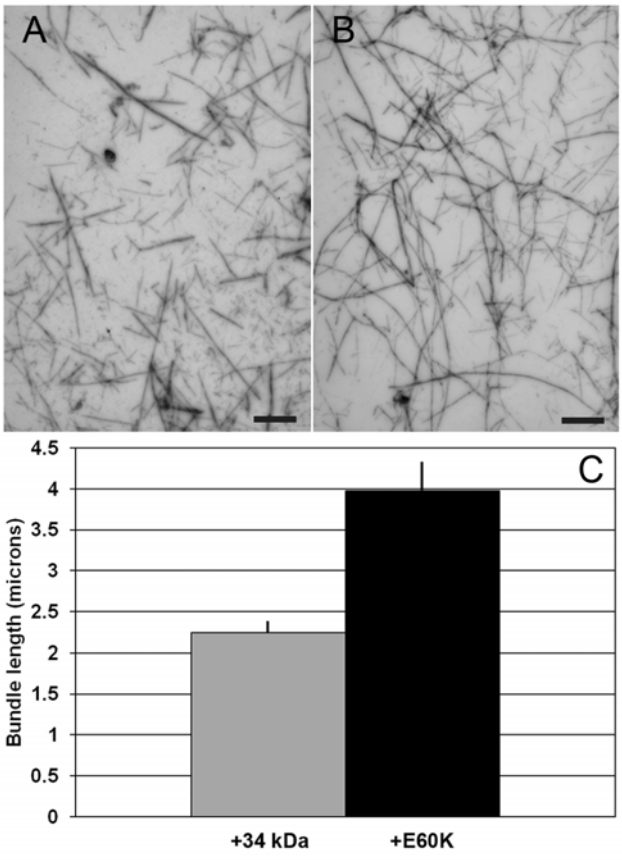
A
B
C
Bundle length (microns)
4.5
4
3.5
3
2.5
2
1.5
1
0.5
0
+34 kDa
+E60K

Figure 2.5. Expression of E60K protein in *Dictyostelium* cells leads to the formation of Hirano bodies. pEVII-transformed *Dictyostelium* cells were examined by differential interference contrast (DIC) microscopy (panel 1) and by fluorescence microscopy using either GFP (panel 2) or TRITC-phalloidin (panel 3). (A) Control cells expressing 34 kDa-EGFP do not contain Hirano bodies while (B) E60K-EGFP-expressing cells contain large Hirano bodies. Scale bar = 10 microns.

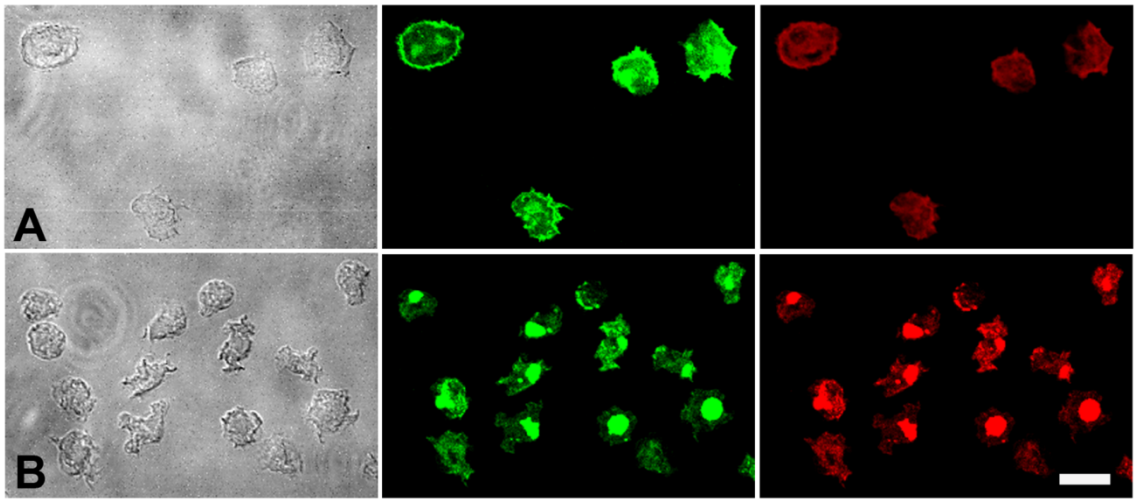
A
B

Figure 2.6. Transmission electron micrographs of E60K-EGFP-expressing *Dictyostelium* cells with Hirano bodies. (A) A thin section of a cell with Hirano bodies. The presence of two electron dense inclusions that are not membrane-bound are indicated by the label "HB". These inclusions are distinct from the electron dense nuclear material that is clearly contained in the nuclear membrane (labeled as "Nuc"). Scale bar = 1 micron. (B) and (C) are corresponding higher magnification views of the "HB" structures in (A). Arrows are used to indicate the cytoplasmic origin of (B and C). Note the presence of many membrane-bound organelles surrounding the "HB" in both (B) and (C), while no membrane is observed surrounding either "HB". Scale bar = 250 nm. High magnification (TEM) images showing the morphology and actin filament arrangement of randomly selected Hirano bodies observed in E60K-EGFP-expressing *Dictyostelium* cells. (D) and (E) show actin filaments arranged parallel to one another. (F) and (G) Hirano bodies that display the "cross-hatched" appearance believed to arise from the simultaneous view of two parallel actin filament layers arranged at oblique angles. Note that the cross-hatched appearance differs from (F) and (G) and is the result of the angle at which the layers of each are arranged. Scale bar = 50 nm.

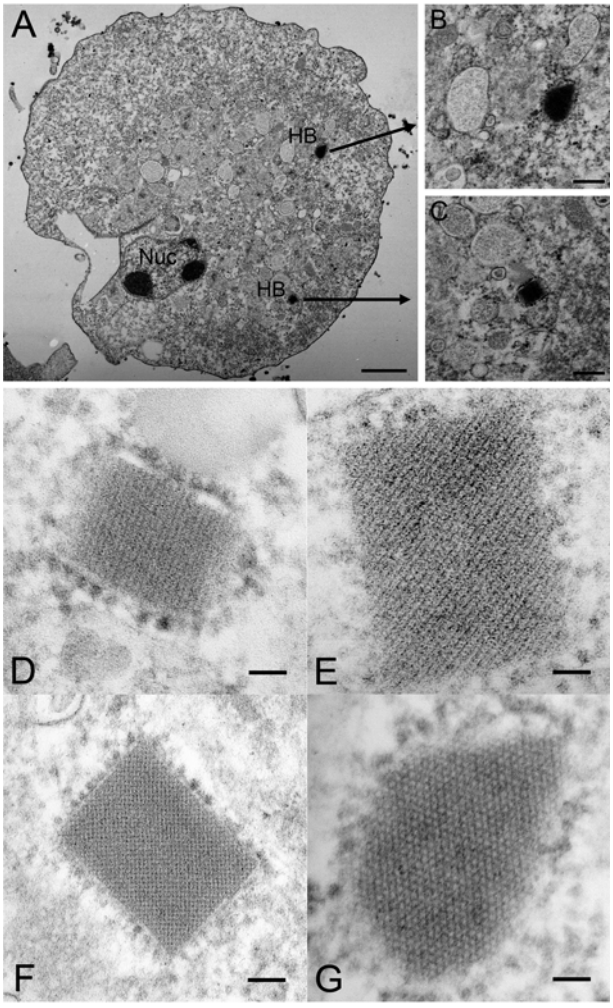
A
HB
Nuc
HB
B
C
D
E
F
G

Figure 2.7. E60K protein and 34 kDa protein inhibit F-actin depolymerization induced by LatB *in vitro*. F-actin co-sedimentation assays were used to determine the effect that 34 kDa and E60K proteins have on the depolymerization of F-actin in the absence and presence of LatB. 3 μM actin either alone or with 3μM 34 kDa or E60K protein were co-polymerized overnight and then incubated with or without 6μM latrunculin B for 2 hours at room temperature. LatB treatment of F-actin only samples resulted in a 76% reduction in F-actin concentration (2.34 ± 0.21 vs. 0.53 ± 0.24 μM (SD)). The presence of 34 kDa protein partially inhibited LatB depolymerization resulting in a 36% reduction in F-actin concentration (2.38 ± 0.11 vs. 1.53 ± 0.06 μM (SD)). In contrast, E60K protein completely inhibited depolymerization showing no significant change in F-actin concentrations in the no LatB and LatB samples (2.51 ± 0.1 vs. 2.6 ± 0.22 μM (SD)).

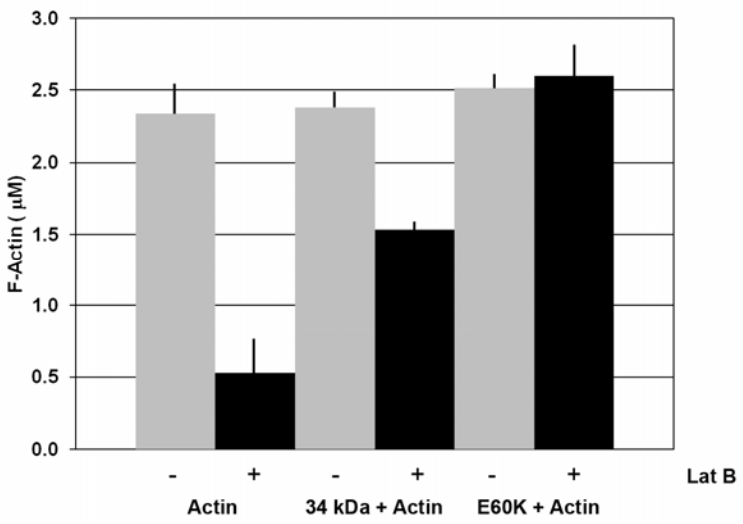
3.0
2.5
2.0
1.5
1.0
0.5
0.0
F-Actin (µM)
-
+
-
+
-
+
Lat B
Actin
34 kDa + Actin
E60K + Actin

Figure 2.8. Hirano bodies are resistant to depolymerization induced by LatB. *Dictyostelium* cells expressing either 34 kDa-EGFP or E60K-EGFP were incubated with 10 μM LatB for 2 hours at 19^{o}C and then fixed and stained for observation by fluorescence microscopy. (A) 34 kDa-EGFP-expressing cells showing the normal cellular localization of 34 kDa protein by GFP and (B) the actin cytoskeleton stained with TRITC-phalloidin. LatB treatment results in redistribution of 34 kDa protein (C) coupled to the depolymerization of the actin cytoskeleton as displayed by loss of TRITC-phalloidin staining (D). (E) E60K-EGFP-expressing *Dictyostelium* cells with Hirano bodies have E60K protein localized to cellular locations consistent with 34 kDa protein (A) but additionally have E60K protein enrichment contained within the Hirano body as evidenced by GFP fluorescence (E). The corresponding F-actin content of the actin cytoskeleton and Hirano body is shown in (F). Incubation of E60K-EGFP Hirano body-containing cells with LatB results in a modest change in E60K protein localization (G) and depolymerization of the actin cytoskeleton (H). However, F-actin contained within the Hirano bodies appear to be resistant to depolymerization by LatB as evidenced by the high intensity of TRITC-phalloidin staining that persists within the Hirano bodies. Scale bar = 5 microns.

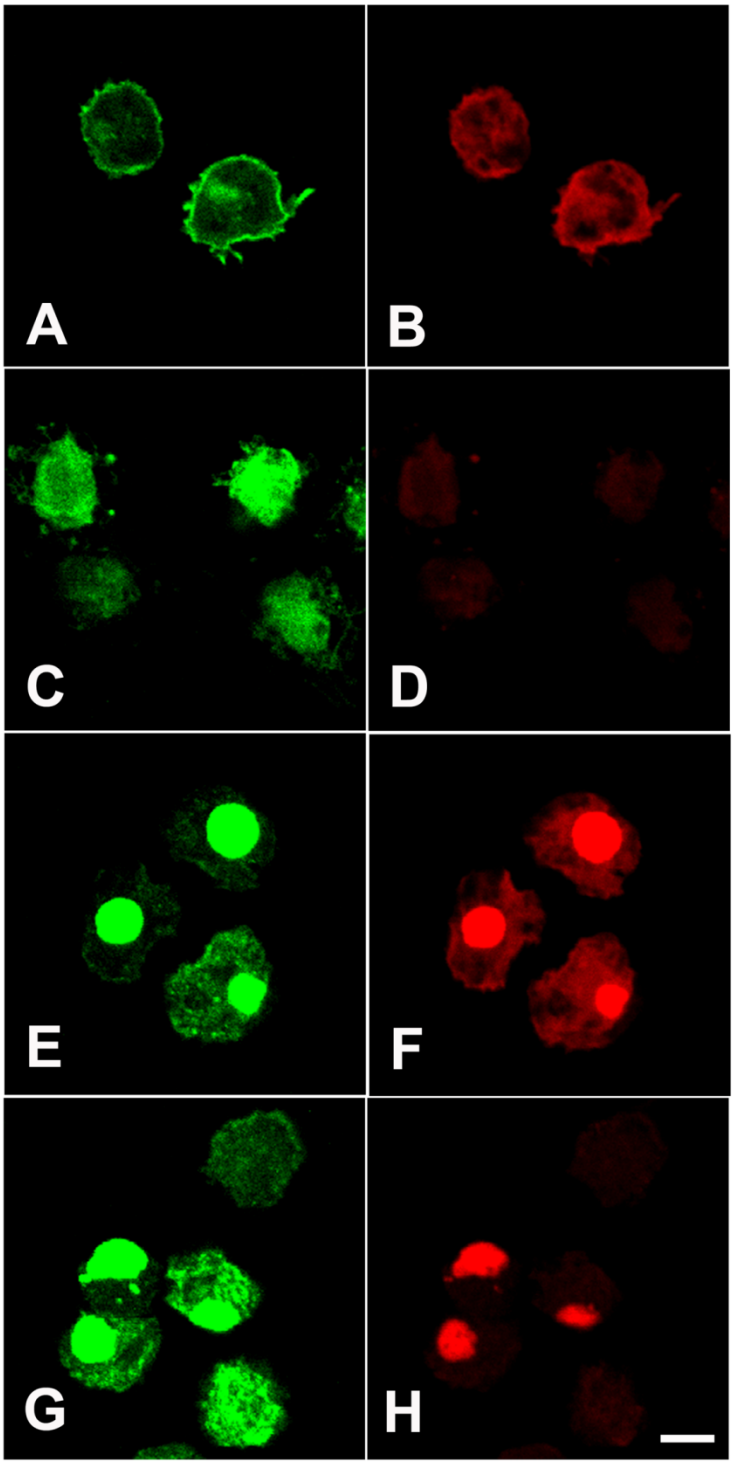
A
B
C
D
E
F
G
H

Table 2.1. Summary table of the average mean intensities for TRITC fluorescence measured in E60K-EGFP- and 34 kDa-EGFP-expressing cells in the presence and absence of latrunculin B. LatB treatment of 34 kDa-EGFP *Dictyostelium* cells results in a 77% reduction in total F-actin (top panel). Similarly, LatB treatment of E60K-EGFP *Dictyostelium* cells without Hirano bodies show an 81% reduction in total F-actin (middle panel). E60K-EGFP cells with Hirano bodies have reductions in total F-actin (43%) however, measurements of the F-actin content of the Hirano bodies shows only a modest 31% reduction with LatB treatment. Although our results suggest that the F-actin within a Hirano body is slightly sensitive to depolymerization, it is important to note that cell death resulting from increasing duration of LatB precludes a significant loss of Hirano body size (data not shown).

	TRITC Fluorescence Mean Intensity (Relative units ± s.d.)	F-actin decrease (%)
34 kDa-EGFP	45.3±14.3	
34 kDa-EGFP + LatB	10.4± 2.4	77
E60K-EGFP (No Hirano body)	34.5± 9.2	
E60K-EGFP (No Hirano body) + LatB	6.4± 2.0	81
E60K-EGFP (with Hirano body)	39.4± 5.5	
E60K-EGFP (with Hirano body) + LatB	22.3± 8.8	43
Hirano body only	89.2± 0.8	
Hirano body only + LatB	57.2±17.2	31

Table 2.2. *In vitro* and *in vivo* properties of 34 kDa protein and altered 34 kDa protein forms

Protein	F-actin binding affinity	Calcium sensitivity	Induces formation of Hirano bodies	References
Wild-type 34 kDa	Normal	Yes	No	(Maselli, 2002; Maselli, 2003; Davis, 2008; Ha, 2010; Kim, 2009; Current study)
CT (residues 124-295)	Activated	No	Yes	(Maselli, 2002; Davis, 2008; Davis 2010)
ΔEF2	Normal	No	No	(Furukawa, 2003)
ΔEF1	Activated	No	Yes	(Maselli, 2003; Kim, 2009)
E60K	Activated	Yes	Yes	Current study

Chapter 3

IDENTIFICATION OF 34 KDA PROTEIN AND F-ACTIN BINDING INTERFACES BY CHEMICAL CROSSLINKING AND MASS SPECTROMETRY[1]

[1] Paul Griffin, Lisabeth Hoffman, Ruth Furukawa, Jon Amster and Marcus Fechheimer. To be submitted to Biochemistry (Spring 2010)

Abstract

The *Dictyostelium* 34 kDa protein is a calcium-sensitive F-actin-bundling protein. Molecular dissection of 34 kDa protein identified three distinct actin binding regions in 34 kDa protein at residues 1-123, 193-254, and 279-295. However, the specific residues involved in binding to F-actin within each of the three actin binding regions of 34 kDa protein have not been identified. Additionally, it is unknown where the 34 kDa protein binding site(s) are on F-actin. In this study, we used chemical cross-linking and mass spectrometry analysis to identify the intermolecular interaction sites involved at the 34 kDa protein-actin binding interface. Chemical crosslinking of 34 kDa protein in the presence of F-actin yielded a 78 kDa product that corresponded to a 1:1 34 kDa protein-actin complex in the reaction mixtures of three different crosslinking reagents. LC-MS/MS analysis of the proteolytic fragments of the 78 kDa complex identified two potential 34 kDa protein binding sites on actin (localized at Lys213, Lys326, Lys61 and Asp179, Lys191) and the actin contact sites in all three actin-binding regions of 34 kDa protein.

Introduction

The actin cytoskeleton is a complex and dynamic structure. The actin cytoskeleton is built from a pool of monomeric actin (G-actin) that assembles into actin filaments (F-actin) that remain in a complex dynamic equilibrium with unpolymerized species. The actin cytoskeleton plays an important part in many cellular functions such as muscle contraction, cell motility, cell morphology, cell adhesion, intracellular transport and localization of organelles, and cytokinesis. In order for actin to participate in so many diverse roles it requires a large number of actin binding proteins (*1, 2*). One important group of actin binding proteins, the actin crosslinking

proteins, promote assembly of actin filaments into the 3-dimensional macrostructures that are needed for each specific cellular function. Amino acid sequence analysis and biochemical assays of proteins that bind and crosslink F-actin have shown they share some common basic structural elements. For example, it has been proposed that proteins that bind F-actin must do so by interacting with at least two adjacent actin protomers along the length of an actin filament (*3*). Additionally, proteins that crosslink and/or bundle F-actin into these distinct structures display a basic modular structure (*4*). The crosslinking of two actin filaments requires a minimum of two actin-binding sites. The simplest modular form is a monomeric protein containing two actin-binding sites located along the length of its polypeptide chain. Other modular arrangements can be achieved by the oligomerization of proteins each containing one actin binding site (*4*). The F-actin binding interface(s) for actin crosslinking proteins has been the focus of many studies. Key to these efforts was the crystallization of G-actin (*5*) and the subsequent building of an atomic model of F-actin (*6, 7*). The atomic model of F-actin has enabled several 3-dimensional reconstructions of F-actin and actin crosslinking proteins built through the combination of structural data obtained from x-ray crystallography and nuclear magnetic resonance (NMR) spectroscopy coupled with electron density maps generated by cryoelectron microscopy. This combinatorial approach has been successfully applied to determine the F-actin binding interfaces for crosslinking proteins fimbrin (*8-10*), α-actinin (*11-13*), dystrophin/utrophin (*14-16*), gelsolin (*17*), scruin (*18-21*), villin (*22*), and talin (*23*). Comparison of the F-actin binding interfaces of these crosslinking proteins has revealed that although many of them share common F-actin binding domains, the sites and mode of interaction of these proteins with F-actin is not universal (*8, 22, 24*). Therefore, in order to fully understand the function of any F-actin crosslinking protein, it is important to characterize its specific interactions at the F-actin binding interface.

The *Dictyostelium* 34 kDa actin-bundling protein is a calcium-regulated protein that crosslinks and bundles actin filaments and is involved in locomotion, phagocytosis, and development (*25-28*). Biochemical characterization of purified 34 kDa protein has shown that it is monomeric in solution (*25, 29, 30*), and its interaction with F-actin is inhibited by the presence of micromolar calcium (*25, 31*). Mutagenesis and molecular dissection of recombinant forms of 34 kDa protein have identified the site of calcium binding (*32*), and three F-actin binding regions were mapped to residues 1-123, 193-254, and 279-295 in an intensive study of fragments and truncated molecules (*33*). The strongest F-actin binding site on 34 kDa protein is located in the 62 amino acid peptide stretch comprised of residues 193-254 (*33*). Using high speed F-actin cosedimentation assays, Lim *et al.* also found that N-terminal truncated forms of 34 kDa displayed increased F-actin affinity (*33, 34*). Further biochemical characterization of 34 kDa truncations using intramolecular interaction assays lead to the development of a model for the actin binding activity of 34 kDa protein (*34*). Briefly, the model proposes that the presence of a bound calcium ion induces a conformational change in the local structure of 34 kDa protein that places the N-terminal inhibitory region (residues 1-70) in an interaction with the strong site (residues 193-254) that inhibits the ability of the strong site to interact with F-actin. Dissociation of the calcium ion from the 34 kDa protein induces another conformational change that removes the N-terminal inhibitory domain from the strong site and exposes the strong site enabling it to interact with F-actin (*34*). In addition, binding of 34 kDa protein to the side of an actin filament leads to a decrease in the rate of filament disassembly with no change in the critical concentration for assembly (*35*). Importantly, recent *in vivo* studies using modified forms of 34 kDa protein that have increased F-actin affinity show that they are able to induce the formation of Hirano bodies (*36-38*). This is an exciting observation because Hirano bodies are actin-

enriched cytoplasmic inclusions that that have been found to be associated with a number of human diseases such as Alzheimer's disease (*39-41*), amyotrophic lateral sclerosis (ALS), and Parkinson's disease (*42*). The observation that increased F-actin affinity of an actin crosslinking protein was sufficient to induce the formation of Hirano bodies in cells stresses the importance of understanding the molecular interactions involved at the F-actin binding interface of actin crosslinking proteins. In order to determine how 34 kDa protein interacts with F-actin, several attempts were made to crystallize either full length and truncated forms of 34 kDa protein (data not shown). However, these attempts were unsuccessful in yielding crystals that diffract to high resolution. Accordingly, we chose to employ chemical crosslinking and mass spectrometry (MS) to identify the molecular interactions between 34 kDa protein and F-actin.

Chemical crosslinking of proteins and subsequent analysis by mass spectrometry is a powerful strategy used to study protein-protein interactions (*43-45*) and protein topology (*46, 47*). However, identification of crosslinked peptides in mixtures of proteolytic digestion products remains a major obstacle for complete mapping of the intermolecular and intramolecular interactions of proteins. This is primarily due to the high amounts of "unwanted" peptide products inherent to proteolytic digests of chemically cross-linked proteins. The identification of specific crosslinked peptide species from proteolytic digests must be done in the presence of a high concentration of uncrosslinked peptide fragments, singly modified peptides that contain a hydrolyzed crosslinker (dead ends), and a mixed population of intramolecular and intermolecular crosslinked peptides (*48, 49*). In order to overcome this problem, much focus has been applied to the development of alternative strategies for improving the chances of identifying rare crosslinked species. One promising strategy is the development of rapidly identifiable novel chemical crosslinking agents that are designed to incorporate unique chemical

labels that increase the probability of detection. In 2005, Tang *et al.* developed a new mass spectrometry identifiable-crosslinking strategy using a novel reagent they synthesized called protein interaction reporter (PIR) crosslinker (*50*). More recently, another novel crosslinker was developed and described that contains a bromine mass defect that enables rapid identification of crosslinked peptides from proteolytic reaction mixtures by tandem MS (*51*). Another improvement has been the development of high-throughput capable software analysis programs that use automated algorithms to search datasets obtained by MS (*46*) and MS/MS (*48*).

The goal of this study was to identify the interaction sites on 34 kDa protein and actin that are involved in the F-actin-34 kDa protein binding interface and to use the information to gain insight into how mutations in 34 kDa protein can lead to increased F-actin binding, and how the binding of the 34 kDa protein to actin inhibits the rate of filament disassembly. We used three chemical crosslinking reagents, 1-Ethyl-3-(3-dimethylaminopropyl-carbodimide hydrochloride (EDC), bis-sulfosuccinimide suberate (BS^3), and dibromo-aniline-dipropionic acid N-succinimydyl ester (DiBMADPS) to crosslink 34 kDa protein to F-actin, and employed mass spectrometry analysis to identify crosslinked interpeptides that are sites of interaction between 34 kDa protein and actin. The DiBMADPS crosslinker was chosen to improve our chances of detecting and identifying crosslinked interpeptides (Hoffman, 2010). Our results show that 34 kDa protein contacts F-actin through all three previously described 34 kDa actin binding sites (*33, 34*), and we identified specific interacting residues on 34 kDa protein in the strong actin-binding site and carboxyl-terminal weak-actin binding site. In addition, we identified a novel actin binding site on 34 kDa protein at residue Lys184. We also show that although 34 kDa protein binds to F-actin at sites characterized for other actin crosslinking proteins, the F-actin

binding interfaces are unique to 34 kDa protein. The results also provide a molecular explanation of the ability of 34 kDa protein to inhibit disassembly of actin filaments.

Experimental procedures

Reagents

1-Ethyl-3-(3-dimethylaminopropyl)-carbodiimide hydrochloride (EDC) a zero length, bifunctional crosslinking reagent and the supporting chemical modification reagent, N-hydroxysulfosuccinimide (Sulfo-NHS) were purchased from Pierce (Rockford, IL). The 11.4 Å spacer arm length homobifunctional crosslinker bis-sulfosuccinimide suberate (BS^3) was obtained from ThermoScientific (Waltham, MA). A novel, amino group-specific, homobifunctional cross-linker dibromo-aniline-dipropionic acid N-succinimydyl ester (DiBMADPS) was synthesized by UVic-GBC Proteomics Centre, Victoria, BC (*51*). The spacer arm length of DiBMADPS is 12.1 Å. Trypsin Gold Mass spectroscopy grade trypsin was purchased from Promega (Madison, WI).

Expression and purification of recombinant proteins

34 kDa protein was expressed in the E. *coli* expression strain BL21(DE3) using the pET-15b vector system (Novagen EMD), and purification of recombinant protein was done as previously described (*29, 52*). Protein concentrations were determined by the BCA method (*53*) and protein samples were dialyzed against 2 mM PIPES pH 7.0, 50 mM KCl, 0.2 mM DTT, 0.02% NaN_3 and stored at –80^{o}C.

Actin

Rabbit skeletal muscle actin was prepared from acetone powder (*54, 55*). The Sephadex G-150 actin fraction was maintained for up to one week in 2 mM Tris-HCl pH 8.0, 0.2 mM

$CaCl_2$, 0.2 mM ATP, 0.2 mM DTT at 4°C with daily buffer changes. G-actin used for chemical crosslinking was exchanged into 20 mM imidazole pH 7.5, 0.2 mM $CaCl_2$, 0.2mM ATP, 24 hours prior to use.

Chemical crosslinking reactions

18 μM actin alone or with 6 μM 34 kDa protein was polymerized at 4°C overnight in 20 mM PIPES pH 7.0, 50 mM KCl, 1 mM $MgCl_2$, 1 mM ATP, and 5 mM EGTA. Freshly prepared stocks of either BS^3 (10 mM in H_2O), EDC/NHS (5 mM each in DMSO), or DiBMADPS (10 mM in DMSO) were used for chemical crosslinking. Final concentrations of each crosslinker were dependent on the total molar concentration of protein to be crosslinked. The final crosslinker to protein concentrations used were: BS^3 20:1; EDC/NHS 25:1; and DiBMADPS 10:1. All crosslinking reactions were incubated at room temperature for 60 minutes and stopped by quenching with 1 M Tris-HCl pH 8.0 to a final concentration of 10 mM. After quenching, all samples were prepared for SDS-PAGE by dilution with 4X reducing Laemmli sample buffer and boiled for 5 minutes. Samples were subjected to SDS-PAGE (*56*) and stained with Coomassie blue.

Western blot analysis of crosslinked species

Identification of components present in novel species generated by chemical crosslinking was achieved by Western blot analysis (*57*) using either an anti-34 kDa monoclonal antibody (B2C) (*26*) or an anti-actin monoclonal antibody (MAbGEa; a kind gift from Dr. Rich Meagher, UGA) (*58*) and a horseradish peroxidase-conjugated goat anti-mouse antibody. Visualization of immunoreactive bands was accomplished by chemiluminescence (Pierce Biotechnology, Rockford, IL).

In-gel trypsin digestion

Gel bands to be subjected to analysis by mass spectrometry were excised, reduced, and alkylated (*59*) with slight modifications. Gels bands were excised using a clean razor blade, cut into 1 mm^3 pieces and placed in a methanol-cleaned eppendorf tube. Gel pieces were further destained using several changes in 50 mM NH_4HCO_3 and 50% methanol. After complete destaining, the final solution was removed, and the gel pieces were dehydrated in 75% acetonitrile for 20 minutes at room temperature. The acetonitrile solution was removed, and the gel pieces were dried at 40^oC. Disulfide bonds were reduced by incubating the dried gel pieces in 10 mM DTT, 20 mM NH_4HCO_3 for 45 minutes at 56^oC. Reducing solution was removed, and the gel pieces were alkylated in 100 mM iodoacetamide, 20 mM NH_4HCO_3 for 30 minutes at room temperature in the dark. Gel pieces were then washed with 50% methanol in 50 mM NH_4HCO_3 for 20 minutes at room temperature. After removal of wash solution, gel pieces were incubated in 75% acetonitrile for 20 minutes at room temperature. The acetonitrile solution was removed, and the gel pieces were dried at 40^oC. Dried gel pieces were in-gel digested using 20 μg/ml trypsin in 20 mM NH_4HCO_3 at 37^oC for 12 hours. Trypsin-digested peptides were extracted from gel pieces by incubation in 50% acetonitrile/0.1% TFA at room temperature for 20 minutes, then centrifuged for 30 seconds at low speed, and the resulting supernatant was removed and saved in a clean eppendorf tube. Gel pieces were subjected to a second extraction, and the supernatants from both extractions were pooled and dried in vacuo to < 5 μl. Extracted peptide solutions were volume-adjusted to 10-15 μl in 50% acetonitrile/0.1% TFA and stored at -80^oC.

Mass spectrometry

Experiments were performed on a 9.4 T Bruker Apex IV QeFTMS (Billerica, MA) fitted with an Apollo II dual source, and a Synrad 75W maximum power continuous wavelength CO_2 laser (model J48-2) for infrared multiphoton dissociation (IRMPD) experiments. Solutions of each crosslinked compound were analyzed at concentrations of 1-10 μM in 100 mM ammonium bicarbonate solutions and were analyzed using electrospray ionization. Samples were run through a PepMap 100 C18 column (Dionex) with varying gradients and a flow rate of 0.4 ml/minute prior to mass spectrometric analysis. For MS^2 experiments, collisionally activated dissociation (CAD) was used for ion dissociation. Precursor ions were automatically mass selected in the external quadrupole and stored for 2 to 4 seconds before fragmentation, using argon as a collision gas, followed by their injection into the ion cyclotron resonance (ICR) analyzer cell. Mass spectroscopy software was configured to autoselect the 8 most abundant peaks from each HPLC window, and to perform CAD MS^2 on the fly. In some cases, peptides to be analyzed were selected using the aid of a "preferred list" or excluded list" generated from MS identified peaks of interest and the known peptides from actin and 34 kDa. Data was then analyzed using Bruker Daltonics Data Analysis software and Links/MS2Links programs (*46, 48*) via the C-MS3D portal (https://ms3d.ca.sandia.gov:11443/cms3d/portal) (*60*).

Sequence analysis

The sequence of 34 kDa actin bundling protein (AAA33144) was analyzed for possible coiled-coil forming regions using the prediction programs Marcoil (*61*) and MultiCoil (*62*) (available on World Wide Web). The secondary structure content of 34 kDa protein was analyzed using the program PSIPRED version 2.6 (*63*) via the protein structure prediction server at University College London (*64*).

Results

Chemical crosslinking of 34 kDa protein and actin

To examine the molecular interfaces between 34 kDa protein and actin, we induced the polymerization of F-actin in the presence of 34 kDa protein and incubated them with different chemical crosslinkers. We used three different chemical crosslinkers to crosslink 34 kDa protein in the presence of F-actin to determine the specific sites of molecular interaction between actin and 34 kDa protein.

The first crosslinker used in this study was the zero-length crosslinker EDC. Reaction products generated by the crosslinking of co-polymerized 34 kDa protein and F-actin in the presence of 5mM EDC/5mM sulfo-NHS were resolved by SDS-PAGE (Fig. 3.1B). Control loads of noncrosslinked actin and 34 kDa protein (Fig. 3.1A) are shown for comparison. The major, resolvable products generated with EDC/sulfo-NHS crosslinking have estimated molecular weights of 191 kDa, 120 kDa, 106 kDa, 87 kDa, and 78 kDa (Fig. 3.1B). In order to identify the protein components of each new complex, western blot analysis was performed using monoclonal antibodies for actin (MAbGEa) and 34 kDa protein (B2C). The 120 kDa band and the 87 kDa band were immunoreactive for actin only (Fig. 3.1C) and likely represent a crosslinked actin trimer and actin dimer, respectively. The 191 kDa and 78 kDa bands were immunoreactive for both 34 kDa protein and actin (Fig. 3.1C). The 78 kDa band is a complex composed of one actin and one 34 kDa protein. The 191 kDa band is most likely a complex of four actin and one 34 kDa protein; however, it could also be made of three actin and two 34 kDa protein. The 106 kDa band gave mixed immunoreactive results on multiple repeat blots and therefore made positive identification difficult (Fig. 3.1C). Therefore, the 106 kDa band was not targeted for further study at this time.

The second crosslinker used was the homobifunctional crosslinker, BS^3, that has a spacer arm length of 11.4 Å. The same reaction conditions were used as described for EDC/sulfo-NHS except that the concentration of BS^3 was 600 μM. The products of the BS^3 reaction mixture were separated by SDS-PAGE (Fig. 3.2A). BS^3 crosslinking of 34 kDa protein and F-actin produced four novel bands of estimated molecular weights of 153 kDa, 118 kDa, 88 kDa, and 78 kDa. Western blot analysis of the BS^3 cross-linking reaction mixture revealed that the 153 kDa, 118 kDa, and 88 kDa bands were immunoreactive for actin only (Fig. 3.2B) and represent actin tetramer, trimer, and dimer species, respectively. Similar to EDC crosslinking results, the BS^3 crosslinking reaction contained a 78 kDa band (Fig. 3.2A) that was immunoreactive for 34 kDa protein (Fig. 3.2B) but gave ambiguous results for actin immunoreacivity. Over-exposure of blots in the presence of anti-actin antibody always resulted in varying but slight immunoreactivity but at the cost of making other bands on blots unresolveable (data not shown). Based on this observation and the similarity to the 78 kDa band in EDC/sulfo-NHS reaction mixtures, it is most likely that the 78 kDa band is composed of one 34 kDa protein and one actin. One possible explanation for the low actin immunoreactivity for the BS^3 crosslinked 78 kDa species is that the epitope on actin recognized by our monoclonal antibody may be compromised by BS^3 crosslinking or masked by 34 kDa.

The final crosslinker used in this study was DiBMADPS, a novel homobifunctional crosslinker that has the same reactive chemistry as BS^3 and a similar spacer arm length (12.04 Å), but has an additional feature designed specifically to aid identification of crosslinked species in subsequent mass spectrometry analysis. The DiBMADPS crosslinker contains a bromine mass defect that changes the mass defect of proteolytic crosslinked peptides in a manner that increases their identification specificity. Briefly, the heavy element bromine, introduces a large

mass defect (-84 mmu) that can be rapidly identified by the characteristic isotopic pattern of the presence of two bromines (*51, 65*). Therefore, the DiBMADPS crosslinker was included in the study to increase our chances of finding rare 34 kDa-actin crosslinked peptide complexes. Crosslinking of 34 kDa protein and F-actin was performed as described for EDC/sulfo-NHS and BS^3 with a concentration of 600 μM DiBMADPS. As anticipated, the DiBMADPS crosslinking reaction mixture separated by SDS-PAGE gave similar results as reaction mixtures with BS^3 crosslinker (Fig. 3.3A vs. 3.2A). Further, the DiBMADPS reaction mixture contained 4 major bands of estimated molecular weights of 153 kDa, 118 kDa, 90 kDa, and 78 kDa similar to those observed with BS^3. However, the DiBMADPS reaction mixture also contained a novel band of 66 kDa that was not found in either the BS^3 or EDC/sulfo-NHS samples (Fig. 3.3A asterisk). Western blot analysis revealed that the 153 kDa, 118 kDa, and 88 kDa bands were immunoreactive for actin only, consistent with the results observed in the BS^3 crosslinker reactions (Fig. 3.3B). The 78 kDa band was immunoreactive for 34 kDa protein (Fig 3.3B), but similar to what was observed for BS^3, the 78 kDa band was only immunoreactive for actin after overexposure (data not shown). Unique to the DiBMADPS reaction mixture was the 66 kDa band which was not immunoreactive for actin (even after over-exposure), but was immunoreactive for 34 kDa protein. Therefore, the 66 kDa band is likely a crosslinked dimer of 34 kDa protein. The possibility of a functional role for a 34 kDa dimer is an exciting result. However, the analysis of 66 kDa band was not included in the present report which is focused on investigation of the crosslinks between actin and 34 kDa. We selected the crosslinked species in the 78 kDa bands containing one molecule each of actin and 34 kDa that were generated with all three crosslinkers.

Identification of actin-34 kDa protein interpeptide crosslinks

Extracted tryptic peptides of the 78 kDa band from all three crosslinkers were subjected to mass spectrometry analysis to identify potential actin-34 kDa protein interpeptide crosslinks as described in *Experimental procedures*. Datasets collected by ESI-MS were analyzed for potential actin-34 kDa protein interpeptides with both Bruker Daltonics Data analysis software and MSLinks software (*46*). Analysis of ESI-MS spectra datasets for actin-34 kDa protein EDC/sulfo-NHS crosslinked tryptic digests yielded the identification of three potential actin-34 kDa protein interpeptide complexes with monoisotopic masses $[M+H]^+$ of 2278.0818 amu (Fig. 3.4A), 3212.7142 amu (Fig. 3.5A), and 2205.0376 amu (Fig. 3.6A). For BS^3 crosslinked actin-34 kDa protein tryptic digests, ESI-MS analysis identified two potential actin-34 kDa protein interpeptide complexes with monoiosotopic masses $[M+H]^+$ of 3398.8893 amu (Fig. 3.7A) and 3376.8861 amu (Fig. 3.8A). Identification of potential actin-34 kDa protein interpeptide complexes from DiBMADPS tryptic digests required manual alteration to the search parameters of the MSLinks software. In order to identify DiBMADPS crosslinked species, we had to input a crosslinker value of 202.0868 amu for DiBMADPS. Using this crosslinker modification to the MSLinks program, we were able to identify three potential actin-34 kDa protein interpeptide complexes of monoisotopic masses $[M+H]^+$ of 2554.1354 amu (Fig. 3.9A), 2037.8988 amu (Fig. 3.10A),and 3488.7271 amu (Fig. 3.11A). Table 3.1 summarizes the results of the crosslinked interpeptide complexes of actin and 34 kDa protein identified by ESI-MS for all three crosslinkers (Table 3.1 under "interpeptide species" heading).

Nano-LC-MS/MS analysis was used to confirm identities of crosslinked species and to map the specific crosslinked residues for all of the actin-34 kDa protein interpeptide complexes. The fragmentation patterns of the EDC/sulfo-NHS actin-34 kDa protein species were analyzed,

and the doubly charged precursor ion 1139.5409 was found to be crosslinked between Lys213 of actin and Glu210 of 34 kDa protein (Fig. 3.4B). The triply charged precursor ion, 1071.5714, was crosslinked between Asp179 of actin and Lys184 of 34 kDa protein (Fig. 3.5B). Lastly, MS/MS analysis of the triply charged precursor ion, 735.6792, identified Lys191 of actin and Glu285 of 34 kDa protein as the site of crosslinking (Fig. 3.6B). For the BS^3 actin-34 kDa crosslinked species, the triply charged precursor ion, 1133.6312, was crosslinked at Lys213 of actin and Lys17 of 34 kDa protein (Fig. 3.7B). The triply charged precursor ion, 1126.2901, did not give a complete fragmentation pattern. We were able to identify Lys326 as the site of crosslink on actin, but it was not possible to identify the specific site of crosslinking on 34 kDa protein (Fig. 3.8B). Both Lys286 and Lys287 of 34 kDa protein are identified as alternative potential crosslinking sites. For the DiBMADPS actin-34 kDa interpeptide complexes, analysis of the resulting fragmentation pattern for the doubly charged precursor ion 1277.5001, showed Lys213 of actin and Lys204 of 34 kDa protein to be crosslinked (Fig. 3.9B). Analysis of the doubly charged precursor ion 1019.4542, identified Lys61 of actin and Lys288 of 34 kDa protein as the specific site of crosslinking with DiBMADPS (Fig. 3.10B). Lastly, the site of crosslinking of the triply charged precursor ion 1163.5823, was determined to be between Lys213 of actin and Lys17 of 34 kDa protein. The results of both MS and MS/MS analysis of all actin-34 kDa interpeptide complexes identified in this study are summarized in Table 3.1.

Discussion

Coupling chemical crosslinking and mass spectrometry has proved to be a successful approach for studying protein interactions. Chemical crosslinkers of different spacer arm lengths and reaction chemistries have enabled researchers to gain structural information on proteins that

have not been characterized by either X-ray crystallography or nuclear magnetic resonance (NMR). Additionally, chemical crosslinking and mass spectrometry allow for the mapping of protein-protein complexes that reflect physiological situations. In this study, we used chemical crosslinking, MS, and tandem MS to identify the intermolecular interactions involved between F-actin and the 34 kDa actin-bundling protein. Using three different chemical crosslinkers we were able to identify specific 34 kDa protein and actin interactions and gain basic structural information about 34 kDa protein while bound to F-actin.

Molecular dissection of 34 kDa protein employing F-actin co-sedimentation, F-actin binding, and disassembly assays identified three actin-binding regions spaced along the 34 kDa protein (*33*, *34*). The site with the strongest F-actin binding affinity was mapped to the region spanning residues 193-254, and the two other "weaker" actin binding regions were mapped to the N-terminal (residues 1-123) and C-terminal (residues 279-295) ends of 34 kDa protein (*33*). However, the specific residues on 34 kDa protein that were involved in binding to F-actin for each of the three binding regions were not identified in those studies. Further, the contributions of these regions to actin binding were inferred from their activity in fragments of the intact protein, and their involvement in the actin binding by the intact protein remained to be critically investigated. Therefore, we chose to use chemical crosslinking coupled with mass spectrometry analysis to identify the 34 kDa protein-F-actin-binding interface and characterize specific intermolecular interactions that may be involved in 34 kDa protein binding to F-actin.

34 kDa protein-F-actin-binding interface

Our mass spectrometry analysis of 34 kDa-actin crosslinked tryptic digests identified chemically crosslinked residues in all three of the 34 kDa protein actin-binding regions, and confirm that 34 kDa protein utilizes all of these binding regions when crosslinking actin

filaments (Table 3.1; Fig. 3.12) (*33*). Additionally, our crosslinking data also identified a novel 34 kDa protein actin-binding site at Lys184 (Fig. 3.12).

Mass spectrometry analysis of the zero-length crosslinker, EDC/sulfo-NHS 34 kDa protein-actin tryptic digests identified three actin interaction sites on 34 kDa protein. Two of these sites, Glu210 and Glu285 lie within previously described 34 kDa protein actin-binding regions; Glu210 is in the strong actin binding region and Glu285 is in the C-terminal weak actin-binding region. The third site, Lys184, does not map to any of the three known actin-binding regions. However, it is near the strong actin-binding site (residues 193-254). It is possible that Lys184 was not identified in earlier studies as an F-actin-binding site because its interaction was dependent on the proper three dimensional structural constraints that could not be represented in expressed truncated forms of 34 kDa protein. Crosslinked sites on 34 kDa protein identified in the tryptic digests of BS^3 and DiBMADPS crosslinked samples also mapped to all three actin binding regions (Fig. 3.12). Because the length of the spacer arms for both BS^3 and DiBMADPS are long, we cannot identify these residues as actual interaction sites. However, they do give us some basic insight into the structural organization of 34 kDa protein bound to F-actin. For example, Lys17 crosslinked to actin was found in both BS^3 and DiBMADPS crosslinked samples (Table 3.1). Therefore, the simplest interpretation is that the N-terminal portion of 34 kDa protein is in close proximity to F-actin, and this supports the observation that the N-terminus of 34 kDa protein is important in F-actin binding (*33, 34*). Additionally, both BS^3 and DiBMADPS crosslinked the C-terminal portion of 34 kDa protein to actin (Lys286/7 and Lys288, respectively) (Table 3.1). This result is also consistent with previous studies (*33, 34*) and provides additional support for our EDC/sulfo-NHS crosslinking data which also places the C-terminus of 34 kDa protein at a 34 kDa protein-F-actin binding interface. Lastly, unlike BS^3, the

DiBMADPS crosslinked tryptic digests contained a unique 34 kDa peptide fragment that was crosslinked to actin at Lys204 (Table 3.1) and is consistent with our EDC/sulfo-NHS results that place the 34 kDa protein strong actin-binding region at the 34 kDa protein-F-actin-binding interface.

34 kDa protein-F-actin-binding interface

When the crosslinked residues we identified in actin are highlighted in the context of the filament structure, there appears to be a patch on one face of F-actin formed by a cluster of three residues that could potentially be a 34 kDa protein binding site. This 34 kDa protein-binding patch is comprised of Lys213 and Lys61 of the lower subunit and Lys326 of the upper subunit and significantly spans two successive actin subunits along one strand of the filament (Fig. 3.13A). The fact that the 34 kDa protein-binding site is comprised of two actin monomers is consistent with observations found at the binding interfaces for many other F-actin-binding proteins and with the proposal that concurrent interaction with at least two successive actin subunits defines F-actin binding specificity (*3*). The putative 34 kDa protein binding patch is also proximal to well characterized ligand-binding "hot spots" on actin, referred to as the "hydrophobic cleft" and "hydrophobic pocket" (*66*). In addition to the 34 kDa protein binding patch, there appears to be a second 34 kDa protein F-actin-binding site that is located proximal to the junction between subdomains 3 and 4 in G-actin involving residues Asp179 and Lys191, respectively. Examination of the spatial locations of Lys191 and Asp179 within the F-actin model structure reveals that this second binding site could enable 34 kDa protein to simultaneously contact three adjacent actin subunits (Fig. 3.13B). Interestingly, in F-actin structural models both Asp179 and Lys191 have been implicated in molecular interactions that are important to filament stability (*6, 7, 67, 68*). Although, it is unclear how 34 kDa protein

interacts with these residues, it is reasonable to believe they are both in direct contact with 34 kDa protein because both Asp179 and Lys191 were crosslinked to 34 kDa protein by EDC/sulfo-NHS (Table 3.1). One possible explanation could be that bundling by 34 kDa protein induces a conformational change in the filament structure that then exposes these residues for 34 kDa protein binding. The F-actin binding proteins scruin and cofilin have been both been shown to alter F-actin structure (*18, 20, 69*). Another possible explanation could be that 34 kDa protein is able to bind G-actin which has both Asp179 and Lys191 exposed for crosslinking. However, all experimental data to date on 34 kDa protein has demonstrated that it exclusively binds F-actin (*25, 29-31, 33, 34*). Lastly, it is possible that 34 kDa protein may remain "attached" to a newly dissociated actin monomer for enough time to become crosslinked.

Previous studies have shown that 34 kDa protein and modified forms of 34 kDa protein inhibit the depolymerization rate of F-actin (*33, 35, 52*). In 1992, Zigmond *et al.* used pyrenyl-labeled actin *in vitro* and showed that 34 kDa protein inhibited the rate of F-actin depolymerization, but not the rate of elongation. Based on their observations, they proposed that *in vivo*, 34 kDa protein may also function to increase actin filament stability (*35*). Recently, Griffin *et al.* used a 34 kDa protein point mutant, E60K, and provided evidence based on *in vitro* and *in vivo* studies that 34 kDa protein promotes actin filament stability (*52*). The results of our crosslinking and mass spectrometry analysis have identified two putative 34 kDa protein-binding sites on F-actin and structural analysis of these sites suggests a possible mechanism by which 34 kDa protein may affect the rate of actin subunit dissociation from an actin filament. Both of the 34 kDa protein F-actin binding sites we identified in this study are located at regions on F-actin that enable 34 kDa protein to interact with more than one actin subunit. We hypothesize that the simultaneous binding of successive actin subunits within the filament by 34 kDa protein may

prevent or slow actin subunit dissociation from filament ends and lead to increased filament stability.

Potential mode for 34 kDa protein F-actin crosslinking

Mass spectrometry analysis on chemically crosslinked 34 kDa protein-actin tryptic digests has identified key residues on both 34 kDa protein and actin that are involved at the 34 kDa protein-F-actin binding interface. Furthermore, combining previous biochemical data on 34 kDa protein and 34 kDa protein truncations with the results of the present study, it is clear that 34 kDa protein interacts with F-actin at at least three actin-binding regions. What remains unanswered, however, is the mode in which 34 kDa protein uses these multiple actin binding sites to crosslink and bundle actin filaments. F-actin crosslinking proteins must contain at least two distinct F-actin binding sites in order to crosslink two actin filaments (*4, 70*). Some proteins crosslink F-actin as a monomer and contain at least two separate F-actin-binding sites along the length of their polypeptide chain while other crosslinking proteins contain only a single F-actin-binding site and therefore require dimerization/oligomerization to be able to crosslink actin filaments.

All biochemical data on 34 kDa protein to date indicates that it is globular and monomeric in solution (*25, 29, 30, 34*). Examination of 34 kDa protein actin bundles by transmission electron microscopy showed a ~ 10 nm center-to-center filament spacing that could be accommodated by a single 34 kDa protein (*30*). Additionally, molecular dissection of 34 kDa protein revealed that it contained three distinct F-actin binding regions which could be used simultaneously to crosslink two actin filaments (*33, 34*) However, it remains a possibility that 34 kDa protein dimerizes or oligomerizes in the presence of F-actin, and this putative "induced" 34 kDa protein interaction is important in filament-filament crosslinking and/or bundling.

Importantly, F-actin-induced dimerization/oligomerization has been observed for the F-actin crosslinking proteins vinculin (*71*) and scruin (*18, 20, 72*). Amino acid sequence analysis of 34 kDa protein by coiled-coil prediction programs Marcoil (*61*) and MultiCoil (*62*) predict a potential coiled-coil forming region in residues 182-210 (probability scores > 80%), suggesting that 34 kDa protein could dimerize using coiled-coil interactions. Additionally, the secondary structure prediction program PSIPRED (*63*) suggests that the region (residues 182-210) has a high α- helical content which is also consistent with coiled-coil forming regions.

Further support for the potential of 34 kDa protein to form dimers/oligomers comes from observations of the solution state of several truncated forms of 34 kDa protein in which three truncated forms (residues 1-240; 71-240; and 77-295) were able to form stable dimers/oligomers in solution (*34*). Significantly, all three of the truncated forms contained the predicted coiled-coil region (residues 182-210).

Although the current study did not focus on this issue directly, some interesting observations can be made based on the results of the chemical crosslinking reactions. For example, SDS-PAGE and Western blot analysis of the EDC/sulfo-NHS and BS^3 crosslinked reaction samples failed to detect the presence of an "induced" 34 kDa protein dimer species (Fig. 3.1B, C and Fig. 3.2A, B). However, in the DiBMADPS crosslinking reaction sample, a faint 66 kDa band can be observed by Coomassie staining (Fig. 3.3A) and is immunoreactive for 34 kDa protein only (Fig. 3.3B). Interestingly, all of the three crosslinker samples contained large molecular weight species that were immunoreactive for both 34 kDa protein and actin (Fig. 3.1C; Fig. 3.2B; Fig. 3.3B). It is possible that these large molecular weight species may contain a 34 kDa protein dimer that is crosslinked to actin(s). Knowledge of the interface of the 34 kDa protein with actin will aid future studies designed specifically to elucidate the mechanism by

which the 34 kDa protein can crosslink two actin filaments to make a network or bundled structure.

Acknowledgements

This work was supported by awards to RF and MF from NSF (MCB 98-08748), the Alzheimer's Association (IIRG-00-2436), and NIH (1R01-NS04645101).

References

1. dos Remedios, C. G., Chhabra, D., Kekic, M., Dedova, I. V., Tsubakihara, M., Berry, D. A. and Noswort, N. J. (2003) Actin binding proteins: regulation of cytoskeletal microfilaments, *Physiol. Rev. 83*, 433-473.
2. Ayscough, K. R. (1998) *In vivo* functions of actin-binding proteins, *Curr. Opin. Cell Biol. 10*, 102-111.
3. McGough, A. (1998) F-actin binding proteins, *Curr. Opin. Struct. Biol. 8*, 166-176.
4. Puius, Y. A., Mahoney, N. M. and Almo, S. C. (1998) The modular structure of actin-regulatory proteins, *Curr. Opin. Cell Biol. 10*, 23-34.
5. Kabsch, W., Mannherz, H. G., Suck, D., Pai, E. and Holmes, K. C. (1990) Atomic structure of the actin:DNAse I complex, *Nature (London) 347*, 37-44.
6. Holmes, K. C., Popp, D., Gebhard, W. and Kabsch, W. (1990) Atomic model of the actin filament, *Nature (London) 347*, 44-49.
7. Lorenz, M., Popp, D. and Holmes, K. C. (1993) Refinement of the F-actin model against X-ray fiber diffraction data by the use of a directed mutation algorithm, *J. Mol. Biol. 234*, 826-836.
8. Galkin, V. E., Orlova, A., Cherepanova, O., Lebart, M. C. and Egelman, E. H. (2008) High-resolution cryo-EM structure of the F-actin-fimbrin/plastin ABD2 complex, *Proc. Natl. Acad. Sci. USA 105*, 1494-1498.
9. Hanein, D., Volkmann, N., Goldsmith, S., Michon, A. M., Lehman, W., Craig, R., DeRosier, D., Almo, S. and Matsudaira, P. (1998) An atomic model of fimbrin binding to F-actin and its implications for filament crosslinking and regulation, *Nat. Struct. Biol. 5*, 787-792.
10. Volkmann, N., DeRosier, D., Matsudaira, P. and Hanein, D. (2001) An atomic model of actin filaments cross-linked by fimbrin and its implications for bundle assembly and function, *J. Cell Biol. 153*, 947-956.
11. McGough, A., Way, M. and DeRosier, D. (1994) Determination of the alpha-actinin-binding site on actin filaments by cryoelectron microscopy and image analysis, *J. Cell Biol. 126*, 433-443.

12. Tang, J., Taylor, D. W. and Taylor, K. A. (2001) The three-dimensional structure of alpha-actinin obtained by cryoelectron microscopy suggests a model for Ca(2+)-dependent actin binding, *J. Mol. Biol. 10*, 845-858.
13. Liu, J., Taylor, D. W. and Taylor, K. A. (2004) A 3-D reconstruction of smooth muscle alpha-actinin by CryoEm reveals two different conformations at the actin-binding region, *J. Mol. Biol. 338*, 115-125.
14. Galkin, V. E., Orlova, A., VanLoock, M. S., Rybakova, I. N., Ervasti, J. M. and Egelman, E. H. (2002) The utrophin actin-binding domain binds F-actin in two different modes: implications for the spectrin superfamily of proteins, *J. Cell Biol. 157*, 243-251.
15. Sutherland-Smith, A. J., Moores, C. A., Norwood, F. L., Hatch, V., Craig, R., Kendrick-Jones, J. and Lehman, W. (2003) An atomic model for actin binding by the CH domains and spectrin-repeat modules of utrophin and dystrophin, *J. Mol. Biol. 329*, 15-33.
16. Moores CA, K. N., Kendrick-Jones J. . (2000) Structure of the utrophin actin-binding domain bound to F-actin reveals binding by an induced fit mechanism, *J Mol Biol. 297*, 465-480.
17. McGough, A., Chiu, W. and Way, M. (1998) Determination of the gelsolin binding site on F-actin: implications for severing and capping, *Biophys. J. 74*, 764-772.
18. Schmid, M. F., Sherman, M. B., Matsudaira, P. and Chiu, W. (2004) Structure of the acrosomal bundle, *Nature 431*, 104-107.
19. Owen C, D. D. A. (1993) A 13-A map of the actin-scruin filament from the limulus acrosomal process, *J Cell Biol. 123*, 337-344.
20. Schmid MF, A. J., Jakana J, Matsudaira P, Chiu W. (1994) Three-dimensional structure of a single filament in the Limulus acrosomal bundle: scruin binds to homologous helix-loop-beta motifs in actin, *J Cell Biol. 124*, 341-350.
21. Cong Y, T. M., Sali A, Matsudaira P, Dougherty M, Chiu W, Schmid MF. (2008) Crystallographic conformers of actin in a biologically active bundle of filaments, *J Mol Biol. 375*, 331-336.
22. Hampton, C. M., Liu, J., Taylor, D. W., DeRosier, D. J. and Taylor, K. A. (2008) The 3D structure of villin as an unusual F-Actin crosslinker, *Structure 16*, 1882-1891.
23. Gingras, A. R., Bate, N., Goult, B. T., Hazelwood, L., Canestrelli, I., Grossmann, J. G., Liu, H., Putz, N. S., Roberts, G. C., Volkmann, N., Hanein, D., Barsukov, I. L. and Critchley, D. R. (2008) The structure of the C-terminal actin-binding domain of talin, *EMBO J. 27*, 458-469.
24. Galkin, V. E., Orlova, A., Fattoum, A., Walsh, M. P. and Egelman, E. H. (2006) The CH-domain of calponin does not determine the modes of calponin binding to F-actin, *J. Mol. Biol. 359*, 478-485.
25. Fechheimer, M. (1987) The *Dictyostelium discoideum* 30,000-dalton protein is an actin filament-bundling protein that is selectively present in filopodia, *J. Cell Biol. 104*, 1539-1551.
26. Furukawa, R., Butz, S., Fleishmann, E. and Fechheimer, M. (1992) The *Dictyostelium discoideum* 30,000 dalton protein contributes to phagocytosis, *Protoplasma 169*, 18-27.
27. Furukawa, R., and Fechheimer, M. (1994) Differential localization of alpha-actinin and the 30 kDa actin-bundling protein in the cleavage furrow, phagocytic cup, and contractile vacuole of *Dictyostelium discoideum*, *Cell Motil. Cytoskel. 29*, 46-56.

28. Fechheimer, M., Ingalls, H. M., Furukawa, R. and Luna, E. J. (1994) Association of the *Dictyostelium* 30,000 dalton actin bundling protein with contact regions, *J. Cell Sci. 107*, 2393-2401.
29. Lim, R. W. L., and Fechheimer, M. (1997) Overexpression, purification, and characterization of recombinant *Dictyostelium discoideum* calcium regulated 34,000 dalton F-actin bundling protein from *Escherichia coli*, *Protein Expr. Purif. 9*, 182-190.
30. Furukawa, R., and Fechheimer, M. (1990) Localization, expression, evolutionary conservation, and structure of the 30,000 dalton actin bundling protein of *Dictyostelium discoideum*, *Dev. Genetics 11*, 362-368.
31. Fechheimer, M., and Taylor, D. L. (1984) Isolation and characterization of a 30,000-dalton calcium-sensitive actin cross-linking protein from *Dictyostelium discoideum*, *J. Biol. Chem. 259*, 4514-4520.
32. Furukawa, R., Maselli, A. G., Thomson, S. A. M., Lim, R. W.-L., Stokes, J. V. and Fechheimer, M. (2003) Calcium regulation of actin cross-linking is important for function of the actin cytoskeleton in *Dictyostelium*, *J. Cell Sci. 116*, 187-196.
33. Lim, R. W. L., Furukawa, R., Eagle, S., Cartwright, R. C. and Fechheimer, M. (1999) Three distinct F-actin binding sites in the *Dictyostelium discoideum* 34,000 dalton actin bundling protein, *Biochemistry 38*, 800-812.
34. Lim, R. W. L., Furukawa, R. and Fechheimer, M. (1999) Evidence of intramolecular regulation of the *Dictyostelium discoideum* 34,000 dalton F-actin bundling protein, *Biochemistry 38*, 16323-16332.
35. Zigmond, S. H., Furukawa, R. and Fechheimer, M. (1992) Inhibition of actin filament depolymerization by the *Dictyostelium* 30,000-D actin-bundling protein, *J. Cell Biol. 119*, 559-567.
36. Maselli, A. G., Davis, R., Furukawa, R. and Fechheimer, M. (2002) Formation of Hirano bodies in *Dictyostelium* and mammalian cells induced by expression of a modified form of an actin cross-linking protein, *J. Cell Sci. 115*, 1939-1952.
37. Maselli, A. G., Furukawa, R., Thomson, S. A. M., Davis, R. C. and Fechheimer, M. (2003) Formation of Hirano bodies induced by the expression of an actin cross-linking protein with a gain of function mutation, *Eucaryot. Cell 2*, 778-787.
38. Davis, R. C., Furukawa, R. and Fechheimer, M. (2008) A cell culture model for investigation of Hirano bodies, *Acta Neuropathol. 115*, 205-217.
39. Gibson, P. H., and Tomlinson, B. E. (1977) Numbers of Hirano bodies in the hippocampus of normal and demented people with Alzheimer's disease, *J. Neurol. Sci. 33*, 199-206.
40. Mitake, S., Ojika, K. and Hirano, A. (1997) Hirano bodies and Alzheimer's disease, *Kao-Hsiung I Hseuh K'o Tsa Chih 13*, 10-18.
41. Schmidt, M. L., Lee, V. M. and Trojanowski, J. Q. (1989) Analysis of epitopes shared by Hirano bodies and neurofilament proteins in normal and Alzheimer's disease hippocampus, *Lab. Invest. 60*, 513-522.
42. Hirano, A., Dembitzer, H. M., Kurland, L. T. and Zimmerman, H. M. (1968) The fine structure of some intraganglionic alterations, *J. Neuropathol. Exp. Neurol. 27*, 167-182.
43. Trester-Zedlitz, M., Kamada, K., Burley, S. K., Fenyö, D., Chait, B. T. and Muir, T. W. (2003) A modular cross-linking approach for exploring protein interactions, *J. Am. Chem. Soc. 125*, 2416-2425.

44. Rappsilber, J., Siniossoglou, S., Hurt, E. C. and Mann, M. (2000) A generic strategy to analyze the spatial organization of multi-protein complexes by cross-linking and mass spectrometry, *Anal. Chem. 72*, 267-275.
45. Lanman, J., Lam, T. T., Barnes, S., Sakalian, M., Emmett, M. R., Marshall, A. G. and Prevelige, P. E. Jr (2003) Identification of novel interactions in HIV-1 capsid protein assembly by high-resolution mass spectrometry, *J. Mol. Biol. 325*, 759-772.
46. Young, M. M., Tang, N., Hempel, J. C., Oshiro, C. M., Taylor, E. W., Kuntz, I. D., Gibson, B. W. and Dollinger, G. (2000) High throughput protein fold identification by using experimental constraints derived from intramolecular cross-links and mass spectrometry, *Proc. Natl. Acad. Sci. USA 97*, 5802-5806.
47. Novak P, H. W., Ayson MJ, Jacobsen RB, Schoeniger JS, Leavell MD, Young MM, Kruppa GH. (2005) Unambiguous assignment of intramolecular chemical cross-links in modified mammalian membrane proteins by Fourier transform-tandem mass spectrometry, *Anal Chem. 77*, 5101-5106.
48. Schilling, B., Row, R. H., Gibson, B. W., Guo, X. and Young, M. M. (2003) MS2Assign, automated assignment and nomenclature of tandem mass spectra of chemically crosslinked peptides, *J. Am. Soc. Mass Spectrom. 14*, 834-850.
49. Sinz, A. (2006) Chemical cross-linking and mass spectrometry to map three-dimensional protein structures and protein-protein interactions, *Mass Spectrom. Rev. 25*, 663-682.
50. Tang, X., Munske, G. R., Siems, W. F. and Bruce, J. E. (2005) Mass spectrometry identifiable cross-linking strategy for studying protein-protein interactions, *Anal. Chem. 77*, 311-318.
51. Hoffman, L., Griffin, P. A., Furukawa, R., Fechheimer, M., Petrotchenko, E., Borchers, C. and Amster, I. J. (2010) Novel mass defect-labeled mass-spectrometry identifiable cross-linker applied to the 34kDa-Actin protein system, *To be submitted to J. Am. Soc. Mass Spectrom.*
52. Griffin, P. A., Kim, D-H., Furukawa, R. and Fechheimer, M. (2010) The formation of Hirano bodies requires both stabilization of actin filaments and cross-linking to produce an ordered array, *to be submitted to Journal of Cell Science*.
53. Smith, P. K., Krohn, R. I., Hermanson, G. T., Mallia, A. K., Gartner, F. H., Provenzano, M. D., Fujimoto, E. K., Goeke, N. M., Olson, B. J. and Klenk, D. C. (1985) Measurement of protein using bicinchoninic acid, *Anal. Biochem. 150*, 76-85.
54. Spudich, J. A., and Watt, S. (1971) The regulation of rabbit skeletal muscle contraction, *J. Biol. Chem. 246*, 4866-4871.
55. MacLean-Fletcher, S. D., and Pollard, T. D. (1980) Identification of a factor in conventional muscle actin preparations which inhibits actin filament self-association, *Biochem. Biophys. Res. Commun. 96*, 18-27.
56. Laemmli, U. K. (1970) Cleavage of structural proteins during the assembly of the head of bacteriophage T4, *Nature (London) 227*, 680-685.
57. Towbin, H., Staehelin, T. and Gordon, J. (1979) Electrophoretic transfer of proteins from polyacrylamide gels to nitrocellulose sheets: procedure and some applications, *Proc. Natl. Acad. Sci. USA 76*, 4350-4354.
58. Kandasamy, M. K., McKinney, E. and Meagher, R. B. (1999) The pollen-specific actins in angiosperms. , *Plant J. 18*, 681-691.

59. Shevchenko, A., Wilm, M., Vorm, O. and Mann, M. (1996) Mass spectrometric sequencing of proteins silver-stained polyacrylamide gels, *Anal. Chem. 68*, 850-858.
60. Yu, E. T., Hawkins, A., Kuntz, I. D., Rahn, L. A., Rothfuss, A., Sale, K., Young, M. M., Yang, C. L., Pancerella, C. M. and Fabris, D (2008) The collaboratory for MS3D: a new cyberinfrastructure for the structural elucidation of biological macromolecules and their assemblies using mass spectrometry-based approaches, *J. Proteome Res. 7*, 4848-4857.
61. Delorenzi, M., and Speed, T. (2002) An HMM model for coiled-coil domains and a comparison with PSSM-based predictions, *Bioinformatics 18*, 617-625.
62. Wolf E, K. P., Berger B. (1997) MultiCoil: a program for predicting two- and three-stranded coiled coils. Protein Sci. 1997 Jun;6(6):1179-89, *Protein Sci. 6*, 1179-1189.
63. Jones, D. T. (1999) Protein structure prediction based on position-specific scoring matrices, *J. Mol. Biol. 292*, 195-202.
64. Bryson, K., McGuffin, L. J., Marsden, R. L., Ward, J. J., Sodhi, J. S. and Jones, D. T. (2005) Protein structure prediction servers at University College London, *Nucl. Acids Res. 33*, W36-38.
65. Hernandez H, N. S., Boltz SA, Gawandi V, Phillips RS, Amster IJ. (2006) Mass defect labeling of cysteine for improving peptide assignment in shotgun proteomic analyses, *Anal Chem. 78*, 3417-3423.
66. Dominguez, R. (2004) Actin-binding proteins--a unifying hypothesis, *Trends Biochem. Sci. 29*, 572-578.
67. Holmes, K. C., Angert, I., Kull, F. J., Jahn, W. and Schröder, R. R. (2003) Electron cryo-microscopy shows how strong binding of myosin to actin releases nucleotide, *Nature 425*, 423-427.
68. Oda, T., Iwasa, M., Aihara, T., Maéda, Y. and Narita, A. (2009) The nature of the globular- to fibrous-actin transition, *Nature 457*, 441-445.
69. McGough, A., Pope, B., Chiu, W. and Weeds, A. (1997) Cofilin changes the twist of F-actin: implications for actin filament dynamics and cellular function, *J. Cell Biol. 138*, 771-781.
70. Matsudaira, P. (1991) Modular organization of actin crosslinking proteins, *Trends Biochem. Sci. 16*, 87-92.
71. Johnson RP, C. S. (2000) Actin activates a cryptic dimerization potential of the vinculin tail domain. J Biol Chem. 2000 Jan 7;275(1):95-105, *J Biol Chem. 275*, 95-105.
72. Sherman MB, J. J., Sun S, Matsudaira P, Chiu W, Schmid MF. (1999) The three-dimensional structure of the Limulus acrosomal process: a dynamic actin bundle. J Mol Biol. 1999 Nov 19;294(1):139-49, *J Mol Biol. 294*, 139-149.
73. Roepstrorff, P., and Fohlman, J. (1984) Proposal for a common nomenclature for sequence ions in mass-spectra of peptides, *Biomed. Mass Spectrom. 11*, 601.
74. Biemann, K. (1988) Contributions of mass spectrometry to peptide and protein structure, *Biol. Mass Spectrom. 16*, 99-111.
75. Biemann, K. (1990) Nomenclature for peptide fragment ions (positive ions), *Methods Enzymol. 193*, 886-887.

Figure 3.1. EDC/sulfo-NHS reaction products for 34 kDa protein crosslinked F-actin. (A) SDS-PAGE analysis of control sample loads for actin and 34 kDa protein. (B) SDS-PAGE and (C) Western blot analysis of resulting products generated by EDC/sulfo-NHS chemical cross-linking of 34 kDa protein co-polymerized with F-actin. In (B) the Coomassie-resolvable crosslinked species are indicated with an arrow and corresponding estimated molecular weight (kDa). For (C) the 34 kDa and actin immunoreactivity of the major crosslinked species are indicated by a directed arrow.

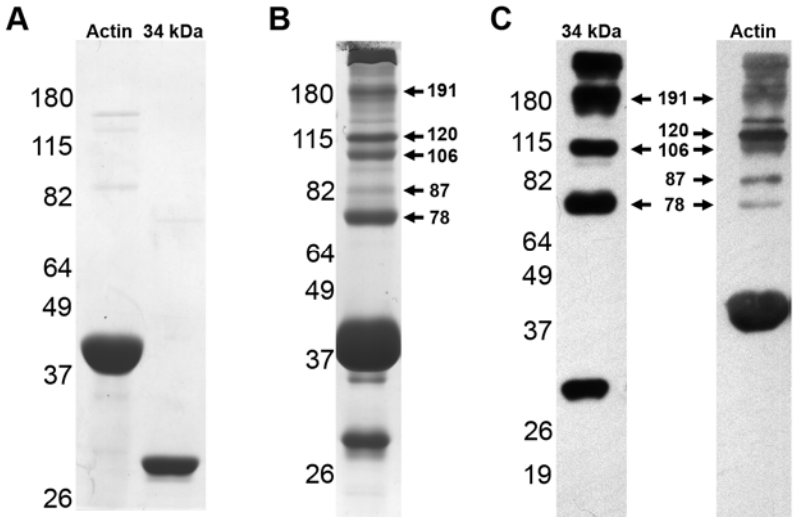
A
Actin
34 kDa
180
115
82
64
49
37
26
B
180
115
82
64
49
37
26
191
120
106
87
78
C
34 kDa
Actin
180
115
82
64
49
37
26
19
191
120
106
87
78

Figure 3.2. BS^3 reaction products for 34 kDa protein crosslinked F-actin. (A) SDS-PAGE and (B) Western blot analysis of resulting products generated by BS^3 chemical crosslinking of 34 kDa protein co-polymerized with F-actin. In (A) the Coomassie-resolvable crosslinked species are indicated with an arrow and corresponding estimated molecular weight (kDa). For (B) the 34 kDa and actin immunoreactivity of the major crosslinked species are indicated by a directed arrow.

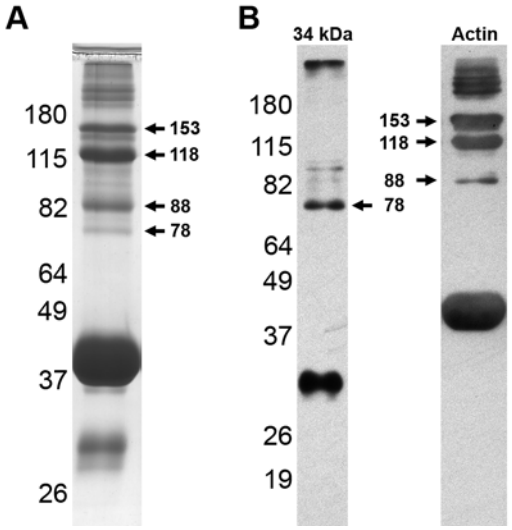
A
180
115
82
64
49
37
26
153
118
88
78
B
34 kDa
Actin
180
115
82
64
49
37
26
19
153
118
88
78

Figure 3.3. DiBMADPS reaction products for 34 kDa protein crosslinked F-actin. (A) SDS-PAGE and (B) Western blot analysis of resulting products generated by DiBMADPS chemical crosslinking of 34 kDa protein co-polymerized with F-actin. In (A) the Coomassie-resolvable crosslinked species are indicated with an arrow and corresponding estimated molecular weight (kDa). For (B) the 34 kDa and actin immunoreactivity of the major crosslinked species are indicated by a directed arrow. In both (A) and (B) the unique 66 kDa band is highlighted with an asterisk.

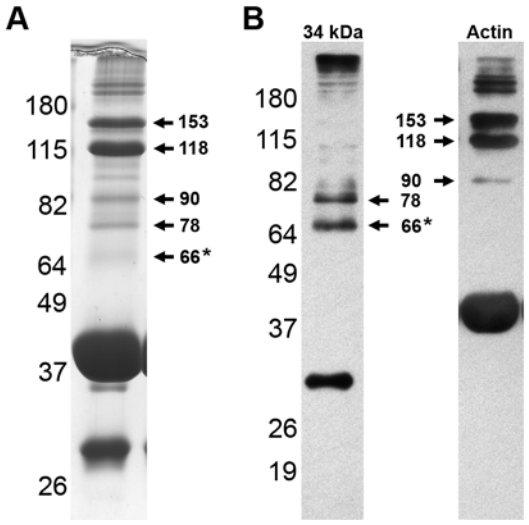
A
180
115
82
64
49
37
26
153
118
90
78
66*
B
34 kDa
Actin
180
115
82
64
49
37
26
19
153
118
90
78
66*

Figure 3.4. Mass spectra set for EDC/sulfo-NHS monoisotopic mass 2278.0818. (A) ESI mass spectrum for EDC/sulfo-NHS crosslinked interpeptide species of monoisotopic mass 2278.0818. (B) MS/MS spectrum of ions at *m/z* 1139.54^{2+}, which is labeled with a diamond. Peptide (α) is actin and peptide (β) is 34 kDa protein. The sequence of each peptide and the identified b (N-terminally derived fragment ions) and y (C-terminally derived fragment ions) ions are shown, corresponding to the masses indicated in the spectra. The results show that Lys213 of actin is crosslinked to Glu210 of 34 kDa protein. Peptide fragments are denoted following the nomenclature for fragmentation of crosslinked oligopeptides (*73-75*).

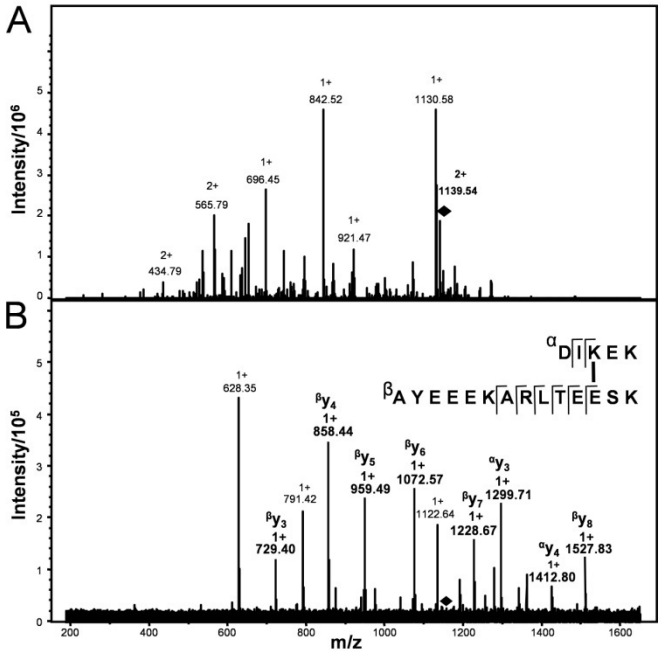
A
Intensity/10^6
1+
842.52
1+
1130.58
2+
1139.54
1+
696.45
2+
565.79
1+
921.47
2+
434.79
B
Intensity/10^5
αDIKEK
βAYEEEKARLTEESK
1+
628.35
βy4
1+
858.44
βy5
1+
959.49
βy6
1+
1072.57
αy3
1+
1299.71
1+
791.42
βy3
1+
729.40
1+
1122.64
βy7
1+
1228.67
βy8
1+
1527.83
αy4
1+
1412.80
m/z

Figure 3.5. Mass spectra set for EDC/sulfo-NHS monoisotopic mass 3212.7142. (A) ESI mass spectrum for EDC/sulfo-NHS crosslinked interpeptide species of monoisotopic mass 3212.7142. (B) MS/MS spectrum of ions at *m/z* 1071.57^{3+}, which is labeled with a diamond. Peptide (α) is actin and peptide (β) is 34 kDa protein. The sequence of each peptide and the identified b (N-terminally derived fragment ions) and y (C-terminally derived fragment ions) ions are shown, corresponding to the masses indicated in the spectra. The results show that Asp179 of actin is crosslinked to Lys184 of 34 kDa protein. Peptide fragments are denoted following the nomenclature for fragmentation of crosslinked oligopeptides (*73-75*).

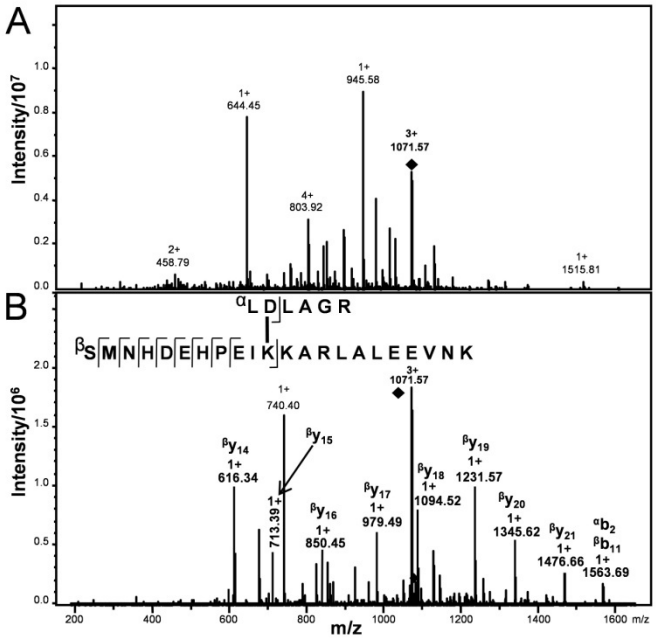
A
Intensity/10^7
1+
644.45
1+
945.58
3+
1071.57
4+
803.92
2+
458.79
1+
1515.81
B
αL D L A G R
βS M N H D E H P E I K K A R L A L E E V N K
Intensity/10^6
1+
740.40
3+
1071.57
βy14
1+
616.34
βy15
1+
713.39
βy16
1+
850.45
βy17
1+
979.49
βy18
1+
1094.52
βy19
1+
1231.57
βy20
1+
1345.62
βy21
1+
1476.66
αb2
βb11
1+
1563.69
m/z

Figure 3.6. Mass spectra set for EDC/sulfo-NHS monoisotopic mass 2205.0376. (A) ESI mass spectrum for EDC/sulfo-NHS crosslinked interpeptide species of monoisotopic mass 2205.0376. (B) MS/MS spectrum of ions at *m/z* 735.69^{3+}, which is labeled with a diamond. Peptide (α) is 34 kDa protein and peptide (β) is actin. The sequence of each peptide and the identified b (N-terminally derived fragment ions) and y (C-terminally derived fragment ions) ions are shown, corresponding to the masses indicated in the spectra. The results show that Lys191 of actin is crosslinked to Glu285 of 34 kDa protein. Peptide fragments are denoted following the nomenclature for fragmentation of crosslinked oligopeptides (*73-75*).

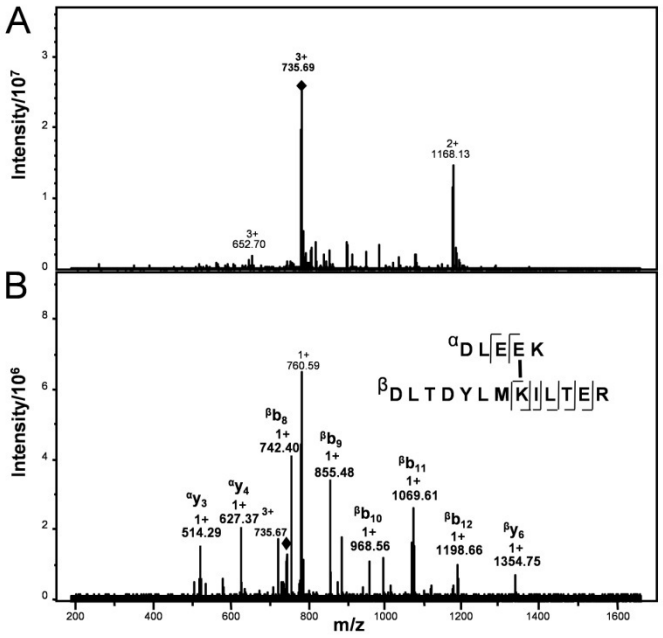
A
Intensity/10^7
3+
735.69
2+
1168.13
3+
652.70
B
Intensity/10^6
αD L E E K
βD L T D Y L M K I L T E R
1+
760.59
βb8
1+
742.40
βb9
1+
855.48
βb11
1+
1069.61
αy3
1+
514.29
αy4
1+
627.37
3+
735.67
βb10
1+
968.56
βb12
1+
1198.66
βy6
1+
1354.75
m/z

Figure 3.7. Mass spectra set for BS^3 monoisotopic mass 3398.8893. (A) ESI mass spectrum for BS^3 crosslinked interpeptide species of monoisotopic mass 3398.8893. (B) MS/MS spectrum of ions at *m/z* 1133.63^{3+}, which is labeled with a diamond. Peptide (α) is actin and peptide (β) is 34 kDa protein. The sequence of each peptide and the identified b (N-terminally derived fragment ions) and y (C-terminally derived fragment ions) ions are shown, corresponding to the masses indicated in the spectra. The results show that Lys213 of actin is crosslinked to Lys17 of 34 kDa protein. Peptide fragments are denoted following the nomenclature for fragmentation of crosslinked oligopeptides (*73-75*).

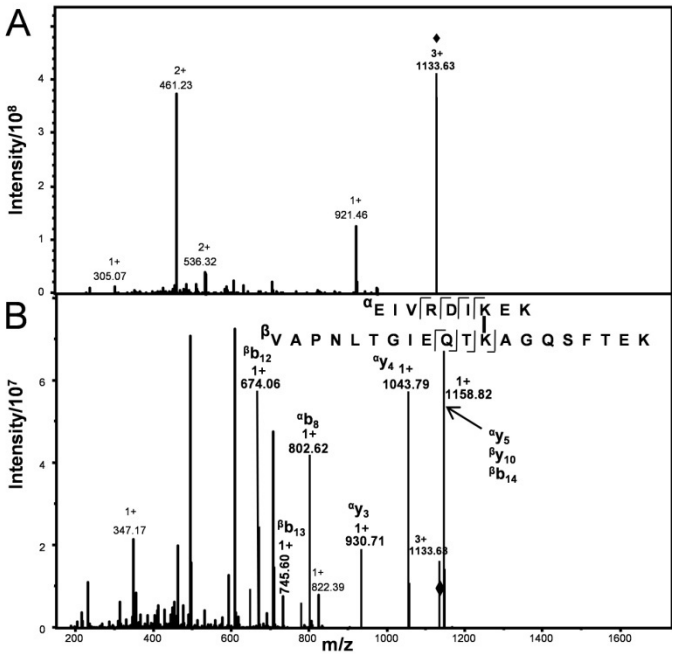
A
Intensity/10^8
3+
1133.63
2+
461.23
1+
921.46
2+
536.32
1+
305.07
B
αE I V R D I K E K
βV A P N L T G I E Q T K A G Q S F T E K
Intensity/10^7
βb12
1+
674.06
αy4 1+
1043.79
1+
1158.82
αb8
1+
802.62
αy5
βy10
βb14
αy3
1+
930.71
βb13
1+
745.60
1+
347.17
3+
1133.63
1+
822.39
200
400
600
800
1000
1200
1400
1600
m/z

Figure 3.8. Mass spectra set for BS^3 monoisotopic mass 3376.8661. (A) ESI mass spectrum for BS^3 crosslinked interpeptide species of monoisotopic mass 3376.8661. (B) MS/MS spectrum of ions at *m/z* 1126.29^{3+}, which is labeled with a diamond. Peptide (α) is actin and peptide (β) is 34 kDa protein. The sequence of each peptide and the identified b (N-terminally derived fragment ions) and y (C-terminally derived fragment ions) ions are shown, corresponding to the masses indicated in the spectra. The results show that Lys326 of actin is crosslinked to Lys286/7 of 34 kDa protein. Peptide fragments are denoted following the nomenclature for fragmentation of crosslinked oligopeptides (*73-75*).

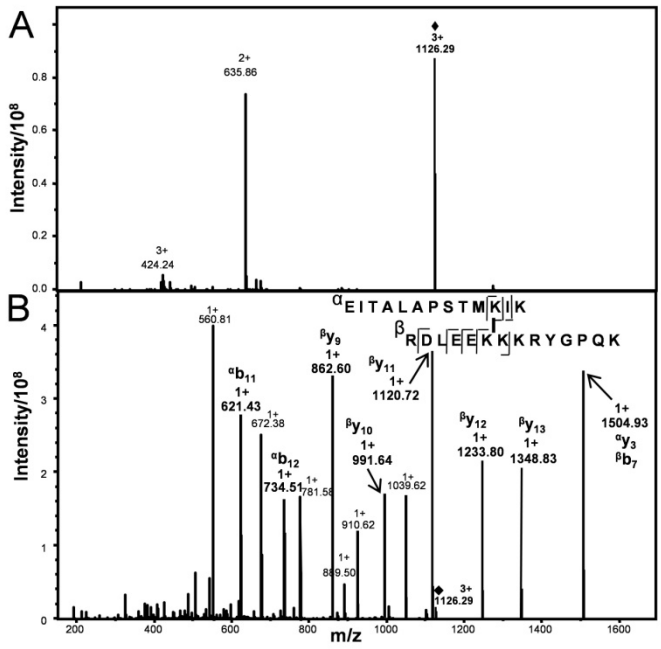
A
3+
1126.29
2+
635.86
3+
424.24
Intensity/10^8
B
αEITALAPSTMKIK
βRDLEEKKKRYGPQK
1+
560.81
βy9
1+
862.60
βy11
1+
1120.72
αb11
1+
621.43
1+
672.38
βy10
1+
991.64
αb12
1+
734.51
1+
781.58
1+
1039.62
βy12
1+
1233.80
βy13
1+
1348.83
1+
1504.93
αy3
βb7
1+
910.62
1+
889.50
3+
1126.29
m/z

Figure 3.9. Mass spectra set for DiBMADPS monoisotopic mass 2554.1354. (A) ESI mass spectrum for DiBMADPS crosslinked interpeptide species of monoisotopic mass 2554.1354. (B) MS/MS spectrum of ions at *m/z* 1277.49^{2+}, which is labeled with a diamond. Peptide (α) is 34 kDa protein and peptide (β) is actin. The sequence of each peptide and the identified b (N-terminally derived fragment ions) and y (C-terminally derived fragment ions) ions are shown, corresponding to the masses indicated in the spectra. The results show that Lys213 of actin is crosslinked to Lys204 of 34 kDa protein. Peptide fragments are denoted following the nomenclature for fragmentation of crosslinked oligopeptides (*73-75*).

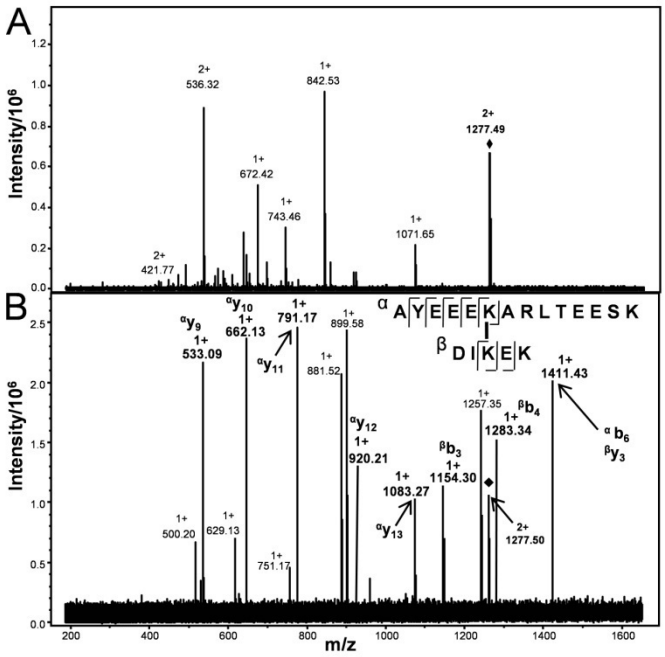
A
Intensity/10^6
2+ 536.32
1+ 842.53
2+ 1277.49
1+ 672.42
1+ 743.46
1+ 1071.65
2+ 421.77
B
α AYEEEEKARLTEESK
β DIKEK
αy10 1+ 662.13
αy9 1+ 533.09
αy11
1+ 791.17
1+ 899.58
1+ 881.52
αy12 1+ 920.21
βb3 1+ 1154.30
1+ 1083.27
αy13
1+ 1257.35
βb4 1+ 1283.34
1+ 1411.43
α b6
βy3
2+ 1277.50
1+ 500.20
1+ 629.13
1+ 751.17
m/z

Figure 3.10. Mass spectra set for DiBMADPS monoisotopic mass 2037.8988. (A) ESI mass spectrum for DiBMADPS crosslinked interpeptide species of monoisotopic mass 2037.8988. (B) MS/MS spectrum of ions at *m/z* 1019.45^{2+}, which is labeled with a diamond. Peptide (α) is actin and peptide (β) is 34 kDa protein. The sequence of each peptide and the identified b (N-terminally derived fragment ions) and y (C-terminally derived fragment ions) ions are shown, corresponding to the masses indicated in the spectra. The results show that Lys61 of actin is crosslinked to Lys288 of 34 kDa protein. Peptide fragments are denoted following the nomenclature for fragmentation of cross-linked oligopeptides (*73-75*).

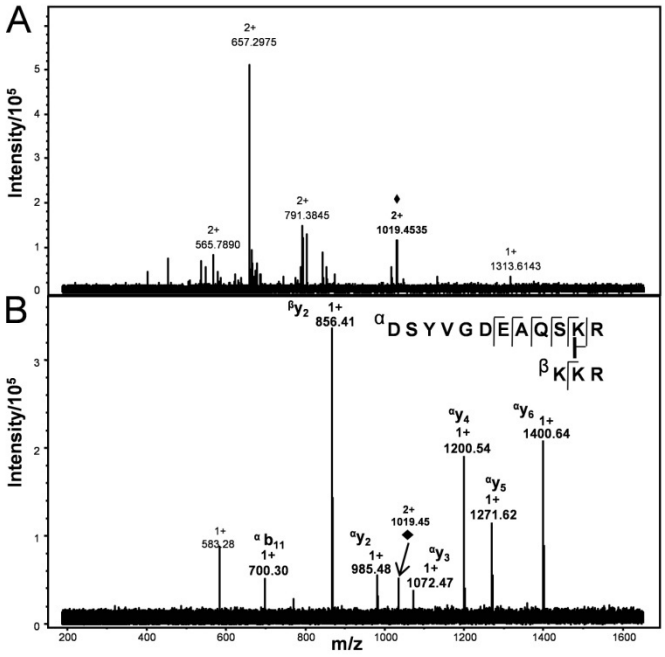
A
2+
657.2975
2+
565.7890
2+
791.3845
2+
1019.4535
1+
1313.6143
Intensity/10^5
B
βy2 1+
856.41
α D S Y V G D E A Q S K R
β K K R
αy4 1+
1200.54
αy6 1+
1400.64
αy5 1+
1271.62
2+
1019.45
1+
583.28
αb11 1+
700.30
αy2 1+
985.48
αy3 1+
1072.47
Intensity/10^5
m/z

Figure 3.11. Mass spectra set for DiBMADPS monoisotopic mass 3488.7271. (A) ESI mass spectrum for DiBMADPS crosslinked interpeptide species of monoisotopic mass 3488.7271. (B) MS/MS spectrum of ions at *m/z* 1163.58^{3+}, which is labeled with a diamond. Peptide (α) is actin and peptide (β) is 34 kDa protein. The sequence of each peptide and the identified b (N-terminally derived fragment ions) and y (C-terminally derived fragment ions) ions are shown, corresponding to the masses indicated in the spectra. The results show that Lys213 of actin is crosslinked to Lys17 of 34 kDa protein. Peptide fragments are denoted following the nomenclature for fragmentation of crosslinked oligopeptides (*73-75*).

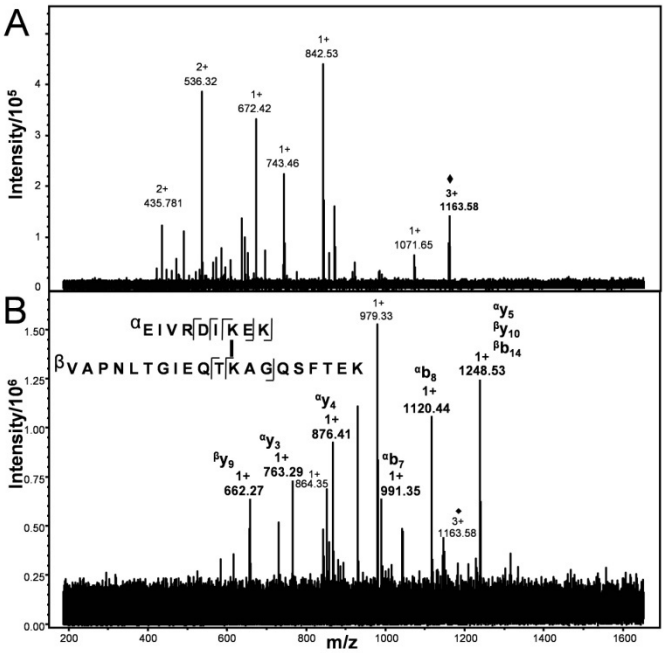
A
Intensity/10^5
2+
435.781
2+
536.32
1+
672.42
1+
743.46
1+
842.53
1+
1071.65
3+
1163.58
B
Intensity/10^6
αEIVRDIKEK
βVAPNLTGIEQTKAGQSFTEK
1+
979.33
αy5
βy10
βb14
1+
1248.53
αb8
1+
1120.44
αy4
1+
876.41
αy3
1+
763.29
βy9
1+
662.27
1+
864.35
αb7
1+
991.35
3+
1163.58
m/z

Table 3.1. Summary of crosslinked species and crosslinked residues identified by mass spectrometry.

$[M+H]^+$ observed	$[M+H]^+$ theoretical	Error (ppm)	Interpeptide species		Crosslinked residues		Crosslinker
			Actin	34 kDa	Actin	34 kDa	
2278.0818	2278.2394	0.1516	211-215	199-212	Lys213	Glu210	EDC/NHS
3212.7142	3212.6724	- 0.0418	178-183	174-195	Asp179	Lys184	EDC/NHS
2205.0376	2205.1113	0.0737	184-196	282-286	Lys191	Glu285	EDC/NHS
3398.8893	3398.9936	0.1043	207-215	6-25	Lys213	Lys17	BS^3
3376.8861	3376.8912	0.0015	316-328	281-294	Lys326	Lys286/7	BS^3
2554.1354	2554.1645	0.0286	211-215	199-212	Lys213	Lys204	DiBMADPS
2037.8988	2037.8993	0.0005	51-62	287-289	Lys61	Lys288	DiBMADPS
3488.7271	3488.7640	- 0.0631	207-215	6-25	Lys213	Lys17	DiBMADPS

Figure 3.12. Schematic model of the important functional regions of 34 kDa protein and sites identified to be crosslinked to actin. The asterisks above the model indicate the approximate location of each crosslinked residue identified in 34 kDa protein. The three F-actin-binding regions in 34 kDa protein (*33*) are colored blue and the calcium-binding EF hand is red.

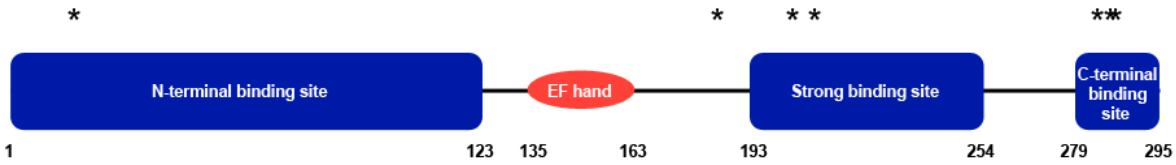
*
*
* *
**
N-terminal binding site
EF hand
Strong binding site
C-terminal binding site
1
123
135
163
193
254
279
295

Figure 3.13. Space-filling F-actin models highlighting putative 34 kDa binding sites. The filament models are oriented with the pointed end on top and the barbed end on the bottom. Lysine residues are colored red and aspartate is colored yellow. Three actin subunits within the actin filament are colored magenta, blue, and cyan. (A) The 34 kDa binding patch on F-actin is comprised of Lys326, Lys61, and Lys213 and spans two successive actin subunits. (B) The second 34 kDa protein binding site is comprised of Lys191 and Asp179 on the same actin subunit (blue). Note that Lys191 and Asp179 are located at sites of contact with different actin subunits. Thus 34 kDa protein binding at this location on F-actin likely involves simultaneous contact on all three actin subunits. The F-actin filament figure was generated using RasMol and was modified from Liu *et al.* (PDB ID code 1JSS) (*13*).

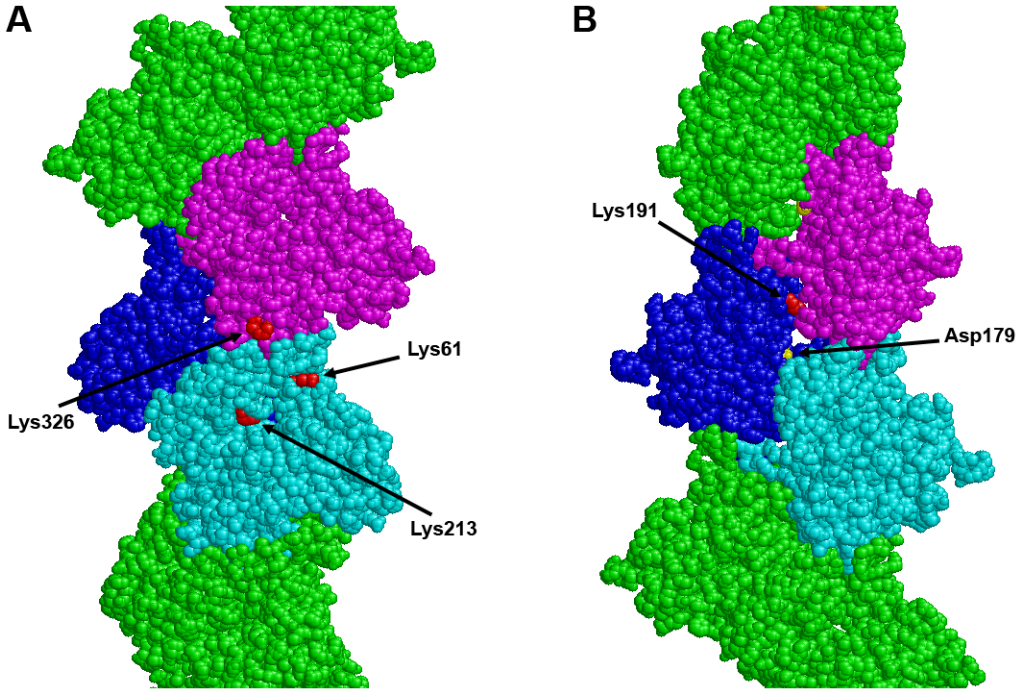
A
Lys61
Lys326
Lys213
B
Lys191
Asp179

Chapter 4

CONCLUSION

Hirano bodies are eosinophilic rod-like structures that were first described in post mortem brain tissue samples taken from patients affected by a familial form of either Parkinson's disease or Amyotrophic Lateral Sclerosis (ALS) in Guam (Hirano 1968). Hirano bodies contain parallel filaments arranged in orthogonal sheets that vary in appearance depending on the plane of sectioning through an individual Hirano body (Schochet 1972; Tomonaga 1974). Since most work done on Hirano bodies has been performed on post mortem tissue, very little is known about the formation, fate, and consequences Hirano bodies may have on cell physiology. Fortunately, a cell model system was developed in *Dictyostelium* that accurately recapitulates the formation of Hirano bodies (Maselli 2002; Maselli 2003). Maselli *et al.* found that expression of either a truncated (CT) or mutated (34 kDa ΔEF1) form of the *Dictyostelium* 34 kDa actin-bundling protein induced the formation of F-actin enriched structures that were ultrastructurally equivalent to those found in Hirano bodies. Expression of CT also induced Hirano body formation in mammalian tissue culture cells and in a transgenic mouse model, illustrating that this model for Hirano body formation is a probe for a highly conserved cellular response, and can be utilized in a wide variety of eukaryotic cell types (Maselli 2002).

The first goal of my dissertation was to use a novel 34 kDa actin-bundling protein point mutant, E60K, to investigate the biochemical and structural features required for the formation of Hirano bodies. Using F-actin cosedimentation assays I showed that E60K protein has activated

F-actin binding and is regulated by calcium indicating that the increased F-actin-binding affinity of E60K protein is not the result of loss of regulation by calcium. This result is consistent with a previous study done in our lab using a mutated form of 34 kDa protein (34 kDa ΔEF2) that was constructed by site-directed mutagenesis to ablate the calcium binding EF hand of 34 kDa protein. The 34 kDa ΔEF2 protein was not calcium sensitive but had normal F-actin binding affinity (Furukawa 2003)

Examination of negative stained actin filaments in the presence of E60K protein by transmission electron microscopy revealed that E60K protein was able to crosslink and bundle F-actin. However, the morphology of the E60K-F-actin bundles had a "ragged", less ordered appearance that lacked the longitudinal periodicity of the 34 kDa-actin bundles. It is likely that the observed difference in bundle morphology is the result of an increase in available lateral contacts, a consequence of the higher F-actin-binding affinity of E60K protein. Lastly, the actin filaments contained within the E60K-F-actin bundles appeared to be "twisted" in comparison to actin filaments in 34 kDa-F-actin bundles which were organized into parallel, thin sheet-like bundles. It is possible that the filaments are indeed twisted as a result of the binding of the 34 kDa protein. Alternatively, the twisted appearance may arise from the binding of the 34 kDa protein on subunit interfaces bridging individual monomers in the filament. Discrimination among these possibilities could be approaches using high resolution electron microscopy, tomography, and reconstruction.

The 34 kDa protein and truncated forms of 34 kDa protein have been shown to inhibit the rate of F-actin depolymerization (Zigmond 1992; Lim 1999). Therefore, to determine if E60K protein also had an effect on F-actin depolymerization, I used F-actin cosedimentation assays and the drug latrunculin B (LatB) that induces F-actin depolymerization by sequestering actin

monomers. The results revealed that both 34 kDa protein and E60K protein inhibit F-actin depolymerization. Thus, it can be inferred that E60K protein prevents the dissociation of actin monomers from both ends of the actin filament.

In vivo studies of E60K protein expression in *Dictyostelium* revealed that it induced the formation of F-actin enriched inclusion bodies. Ultrastructural characterization of E60K protein induced F-actin inclusions by transmission electron microscopy confirmed that they were analogous in actin filament arrangement to what has been observed in Hirano bodies. E60K protein induced Hirano body formation was consistent with previous studies done in our lab with other mutant forms of 34 kDa protein that also have increased F-actin affinities (Maselli 2002; Maselli 2003; Davis 2008; Kim 2009). LatB treatment of E60K protein expressing *Dictyostelium* cells with Hirano bodies showed that the F-actin contained within the Hirano body structure was resistant to depolymerization. Thus, it is likely that E60K protein stabilizes actin filaments and affects normal cellular actin turnover which then could lead to an accumulation of F-actin *in vivo*. However, stabilization of actin filaments alone is not the only feature important to form Hirano bodies. It is important to note that not all intracytoplasmic F-actin aggregates are necessarily Hirano bodies. Hirano bodies are highly ordered F-actin structures and this degree of order is what distinguishes them from other F-actin aggregations. Since inhibition of actin disassembly by F-actin stabilizing drugs induces the formation of disordered F-actin aggregations (Lee 1998; Lázaro-Diéguez 2008), it can be concluded that actin filament stabilization alone is not sufficient to induce the formation of Hirano bodies. Additionally, a recent study reported that the mistargeting of VASP protein to endosomes induced the formation of large F-actin aggregations in *Dictyostelium* cells that were intermediate in the actin filament ordering (Schmauch 2009). Based on these independent reports and the results of my

investigations, I propose that the additional feature required for the formation of Hirano bodies is the ability to crosslink and/or bundle F-actin into higher ordered structures.

The second goal of my dissertation was to identify the site(s) on 34 kDa protein and actin that are involved at the F-actin-34 kDa protein binding interface. Although there is a large body of literature describing the occurrence of Hirano bodies, the mechanism by which they form and their relationship to disease is still unknown. The Hirano body cell model system developed in our lab uses the expression of altered forms of 34 kDa protein that have activated actin binding to induce the formation of Hirano bodies. Therefore, in order to understand the role activated actin binding has in the formation of Hirano bodies in cells, we need to identify the sites on 34 kDa protein that are involved in binding to F-actin. Using chemical crosslinking and mass spectrometry I showed that all three of the actin binding regions of full length 34 kDa protein make contact with actin and identified two residues within the strong site (Lys-204 and Glu-210) that bind to F-actin. I also identified two 34 kDa protein binding sites on actin. The first 34 kDa binding site on F-actin is comprised of a localized cluster of three residues that form a "34 kDa protein binding patch". The "patch" spans two successive actin monomers and involves residues Lys213 and Lys61 on one actin subunit and Lys326 on the successive actin subunit. The putative "34 kDa binding patch" we identified on F-actin is located proximal to the "hydrophobic cleft" on actin that is the binding site for many other actin binding proteins and ligands (Dominguez 2004) I also indentified a second 34 kDa protein binding site on F-actin that involved residues Asp179 and Lys191. Importantly, this second 34 kDa protein binding site is located at molecular interfaces of three actin subunits on the actin filament. Mapping of the binding sites of the 34 kDa protein on the actin filament provides a molecular explanation for the stabilization of actin filaments by the 34 kDa protein to LatB induced disassembly. This finding

is a most satisfying synergy between the structural and cellular approaches employed in this dissertation.

The results of the current study enable us to ask new questions. For example, although we have identified the residues in 34 kDa protein that are important in binding to actin, it remains unclear how the 34 kDa protein crosslinks and bundles actin filaments. In order to understand how 34 kDa protein crosslinks F-actin, we need to determine the structure of the 34 kDa. One approach would be to obtain an NMR structure for the T193 fragment (residues 193-254). The T193 fragment is a good choice for study because it is small (only 62 amino acids) and retains the ability to crosslink F-actin (Lim *et al*. unpublished data). We could then use the T193 fragment NMR structure and high resolution electron microscopy to reconstruct a 3 dimensional structure of the T193 fragment crosslinked actin filaments. Another approach to gain basic 34 kDa protein structural information is to extend our chemical crosslinking and mass spectroscopy studies to identify 34 kDa protein intramolecular interactions. We are currently pursuing this approach.

Another interesting question to be addressed is to further define the molecular requirements of Hirano body formation. Our current hypothesis is that Hirano body formation requires both increased filament stabilization and filament crosslinking. However, it is unclear as to what contribution filament crosslinking and/or bundling plays in Hirano body formation. For example, does crosslinking/bundling only stabilize actin filaments or does it also organize the actin filaments into the characteristic paracrystalline filament arrays found in Hirano bodies? In order to address this question, one approach would be to express the 34 kDa T193 fragment in *Dictyostelium* cells and see if it is able to induce the formation of Hirano bodies. The T193 fragment is a 62 amino acid peptide that corresponds to the strong actin binding site of 34 kDa

protein (residues 193-254). The T193 fragment can crosslink F-actin filaments *in vitro* (Lim *et al*. unpublished data) but it is unlikely to be able to bundle actin filaments since it was shown that a 27 kDa chymotryptic fragment of 34 kDa protein (residues 40-241; Griffin *et al.* unpublished data) could crosslink but not bundle actin filaments (Fechheimer 1993). High resolution electron microscopy tomography could be used to reconstruct the individual filaments within Hirano bodies, to elucidate the structural organization of the actin filaments in Hirano bodies, and to discern if the ability to bundle actin filaments is a required feature for the formation of Hirano bodies.

References

Davis, R. C., Furukawa, R. and Fechheimer, M (2008). "A cell culture model for investigation of Hirano bodies." Acta Neuropathol. **115**: 205-217.

Dominguez, R. (2004). "Actin-binding proteins--a unifying hypothesis." Trends Biochem. Sci. **29**(11): 572-8.

Fechheimer, M., and Furukawa, R (1993). "A 27,000 dalton core of the *Dictyostelium* 34,000 dalton protein retains Ca+2-regulated actin cross-linking but lacks bundling activity." J. Cell Biol. **120**: 1169-76.

Furukawa, R., Maselli, A. G., Thomson, S. A. M., Lim, R. W.-L., Stokes, J. V. and Fechheimer, M (2003). "Calcium regulation of actin cross-linking is important for function of the actin cytoskeleton in *Dictyostelium*." J. Cell Sci. **116**: 187-96.

Hirano, A., Dembitzer, H. M., Kurland, L. T. and Zimmerman, H. M (1968). "The fine structure of some intraganglionic alterations." J. Neuropathol. Exp. Neurol. **27**: 167-82.

Kim, D.-H., Davis, R. C., Furukawa, R. and Fechheimer, M (2009). "Autophagy contributes to the degradation of hirano bodies." Autophagy **5**(1): 1-8.

Lázaro-Diéguez, F., Aguado, C., Mato, E., Sánchez-Ruíz, Y., Esteban, I., Alberch, J., Knecht, E. and Egea, G (2008). "Dynamics of an F-actin aggresome generated by the actin-stabilizing toxin jasplakinolide." J. Cell Sci. **121**: 1415-25.

Lee, E., Shelden, E. A. and Knecht, D. A (1998). "Formation of F-actin aggregates in cells treated with actin stabilizing drugs." Cell Motil. Cytoskel. **39**(2): 122-33.

Lim, R. W. L., Furukawa, R., Eagle, S., Cartwright, R. C. and Fechheimer, M (1999). "Three distinct F-actin binding sites in the *Dictyostelium discoideum* 34,000 dalton actin bundling protein." Biochemistry **38**: 800-12.

Maselli, A. G., Davis, R., Furukawa, R. and Fechheimer, M (2002). "Formation of Hirano bodies in *Dictyostelium* and mammalian cells induced by expression of a modified form of an actin cross-linking protein." J. Cell Sci. **115**: 1939-52.

Maselli, A. G., Furukawa, R., Thomson, S. A. M., Davis, R. C. and Fechheimer, M (2003). "Formation of Hirano bodies induced by the expression of an actin cross-linking protein with a gain of function mutation." Eucaryot. Cell **2**: 778-87.

Schmauch, C., Claussner, S., Zöltzer, H. and Maniak, M (2009). "Targeting the actin-binding protein VASP to late endosomes induces the formation of giant actin aggregates." Eur. J. Cell Biol. **88**(7): 385-96.

Schochet, S. S. J., and McCormick, W. F (1972). "Ultrastructure of Hirano bodies." Acta Neuropathol. **21**: 50-60.

Tomonaga, M. (1974). "Ultratructure of Hirano bodies." Acta Neuropathol. **28**: 365-6.

Zigmond, S. H., Furukawa, R. and Fechheimer, M (1992). "Inhibition of actin filament depolymerization by the *Dictyostelium* 30,000-D actin-bundling protein." J. Cell Biol. **119**(3): 559-67.